International Journal for Numerical Methods in Fluids

WILEY

RESEARCH ARTICLE OPEN ACCESS

Advection-Pressure Splitting Schemes Applied to a Non-Conservative 1D Blood Flow Model With Transport for Arteries and Veins

Alessandra Spilimbergo[1] | Eleuterio F. Toro[2] | Annunziato Siviglia[2] | Lucas O. Müller[1]

[1]Department of Mathematics, University of Trento, Trento, Italy | [2]Laboratory of Applied Mathematics, DICAM, University of Trento, Trento, Italy

Correspondence: Alessandra Spilimbergo (alessandra.spilimbergo@uniroma1.it)

Received: 17 March 2025 | **Revised:** 22 September 2025 | **Accepted:** 21 October 2025

Funding: This work was supported by Università degli Studi di Trento and Next Generation EU (European Union) (CUP: E53D23005920006).

Keywords: 1D blood flow models | hyperbolic systems of PDEs | path-conservative schemes | TV splitting

ABSTRACT

We introduce new first order, splitting-based numerical schemes for the non-conservative one-dimensional (1D) blood flow equations with a general constant momentum correction coefficient that describe blood flow, for different velocity profiles, in arteries and veins with discontinuous mechanical and geometrical properties. In this model an advection equation for a passive scalar transport is also considered. Our schemes are inspired by the original flux vector splitting approach of Toro and Vázquez-Cendón (2012) designed for the Euler equations. They also represent an improvement of the work proposed by Toro et al. (2024) regarding non-conservative blood flow models, which considered a tube law describing only arteries, a momentum correction coefficient equal to one, no passive scalar transport and included a smaller number of discontinuous mechanical and geometrical parameters. The considered framework separates advection terms and pressure terms, generating two different systems of PDEs: the advection system in conservative form, and the pressure system in non-conservative form, both of which have a very simple eigenstructure compared to that of the full system. Our schemes involve approximate Riemann solvers and present a modification of the path-conservative framework that renders unnecessary the use of a path. They are systematically assessed on a carefully designed suite of test problems with exact solution and compared with several existing mainstream methods. A detailed efficiency analysis is performed in order to showcase the advantages of the proposed methodology in comparison with standard approaches.

1 | Introduction

Blood flow models are essential tools used in medical research and healthcare to study and understand the complex dynamics of blood circulation in the human body. These models are designed to simulate the flow of blood through various parts of the body and can be used to study diseases, develop new treatments, and improve medical technologies [1–3]. The three-dimensional (3D) incompressible Navier-Stokes equations are commonly utilized as a preferred model to examine the blood flow in a specific region of the cardiovascular system. In addition, in certain situations, it is important to consider the mechanical reaction of vessel or organ walls when simulating the cardiovascular system. 3D fluid models combined with a description of the interaction between fluid and vessel walls result in 3D Fluid-Structure-Interaction (FSI) solvers. These models take into account the 3D geometry of blood vessels, and thus provide a three-dimensional description of pressure and velocity fields [4, 5]. While 3D blood flow models

provide a high level of detail and accuracy, they are computationally expensive and often require high-performance computing resources to run simulations. Consequentially these models can be time-consuming and expensive to implement, resulting to be less practical for routine clinical use.

One-dimensional (1D) blood flow models (Hughes and Lubliner [6]) are simplified models derived from 3D FSI models. They are more computationally efficient than the 3D FSI models [7], and therefore more suitable for clinical applications [8]. These schemes use simplified representations of blood vessels as interconnected 1D segments, and they focus on modeling blood flow in a more macroscopic manner: while 1D blood flow models may lack the fine-grained detail of their 3D counterparts, they can be readily integrated into clinical workflow and can provide rapid assessments of haemodynamic parameters, making them valuable for diagnostic and treatment planning purposes. Moreover, these models can be used to study large-scale physiological phenomena and simulate the effects of various cardiovascular pathologies on blood circulation. They are in fact valuable for studying various aspects of blood flow, including pressure and flow waveforms [9]. They have been extensively used to study wave propagation phenomena in arteries [10–15]. More recently, their use has been extended to the venous circulation [16–18]. Moreover, when combined with zero-dimensional (0D) models, 1D blood flow models have enabled the development of comprehensive models of the entire human circulation [17–22]. Additionally, 1D models have proven to be valuable in their ability to be coupled with 3D models, thereby providing realistic boundary conditions necessary for the analysis of detailed 3D problems that focus on the investigation of spatially localized pathological conditions [23–26].

In particular the application of 1D blood flow models with discontinuous mechanical and geometrical parameters becomes relevant in medical contexts where these attributes exhibit spatial variations. These changes can occur due to the insertion of stents in arteries or veins after a surgical procedure, with the aim of restoring the vessel lumen to its original shape. For example atherosclerotic plaques, which are a common pathology in the circulatory system, can cause restrictions in the arterial lumen known as stenoses. In severe cases, stenoses can obstruct or completely block the blood flow. To address this issue, the implantation of a stent, which is an expandable metal mesh, is often performed to restore the artery lumen. This procedure is preferred over more invasive methods like surgical bypass. However, the presence of a stent can lead to a sudden change in the elastic properties of the vessel wall, as the stent is typically different from the soft arterial tissue [9, 27]. This change can disrupt the blood flow pattern and cause variations in wall displacement, resulting in the emergence of reflected waves and abrupt jumps in mechanical and geometrical properties. Due to the spatial variability of these parameters, the 1D mathematical model will incorporate supplementary source terms that involve parameter derivatives. These source terms, known as geometric source terms, necessitate cautious handling during the discretization of the equations otherwise they may lead to the occurrence of spurious oscillations in the approximated solutions, rendering numerical schemes incapable of accurately resolving steady or stationary solutions [28, 29]. Numerical schemes able to appropriately solve steady state solutions are said to be well-balanced (Parés [30]). While in this article, we deal with an extreme case of discontinuous parameters (introduced in the next paragraph), it is worth noting that many have addressed the smooth case. The influence of varying mechanical properties resulting from stent placement was examined in Sherwin et al. [9], where smooth variations were taken into account, but no attention was given to the well-balanced properties of the resulting schemes. Well-balanced schemes for smooth variations of parameters were designed in [31–35].

Analytically the 1D blood flow equations are a nonlinear system of two partial differential equations with source term. These equations represent conservation of mass and balance of momentum and are obtained by cross-sectional averaging the 3D Navier-Stokes equations, and including a tube law describing the interaction between vessel wall and fluid [6, 36]. The space- and time-dependent unknowns are the cross-sectional area, flow rate and pressure. To close the system, elastic tube laws have been proposed, which distinguish between arteries and veins. In Bernard et al. [37], the 1D blood flow equations were derived for the first time from the 3D incompressible Navier-Stokes equations. During the derivation of the 1D blood flow equations the velocity profile of the axial component of velocity has to be prescribed. This in turn determines a couple of coefficients appearing in the momentum balance equation, one related to the dissipation due to the friction between blood and the vessel wall and a second one, called momentum correction coefficient, which is related to the convective term of the equation. Toro and Siviglia [38] formulated a complete mathematical model for physiological flows in compliant vessels with discontinuous material properties with in addition an advection equation for a passive scalar transport, for a momentum correction coefficient describing an inviscid fluid. This model suggests an efficient handling of the aforementioned geometric source terms. In this article, we refer to this model taking into account a general constant momentum correction coefficient.

From the mathematical as well as the numerical point of view, a basic problem to be solved is the special Cauchy problem called the Riemann problem [39–41]. Toro and Siviglia [38] presented the complete exact solution of the Riemann problem for the aforementioned 1D blood flow equations, for initial conditions resulting in subcritical flow regimes. This topic was enriched in Spilimbergo et al. [42] with a novel approach to calculate wave relations for superimposed contact waves. This exact solution was obtained for a momentum correction coefficient equal to one (i.e., corresponding to a flat blood velocity profile describing an inviscid fluid). In Spilimbergo et al. [43] this analysis was extended to a general constant momentum correction coefficient describing, among others, velocity profiles that include the parabolic and the blunt one.

The model presented in Toro and Siviglia [38] can not be expressed in a conservative form with respect to the conserved variables. Numerical approximations of this type of problems are found resorting in generalizations of well-known results for conservative problems [44] and are obtained with the so-called path-conservative numerical schemes (Parés [30]). In this context, Dumbser and Toro [45, 46] extended the Osher-Solomon Riemann solver [47] to non-conservative systems, presenting a path-conservative, finite volume-type, first order scheme and a high-order extension. Subsequently, Müller and Toro [48]

enhanced this approach by constructing well-balanced fluctuations for a first order non-oscillatory scheme, and further extending it to achieve higher order of accuracy in both space and time. An alternative methodology, based on the Generalized Hydrostatic Reconstruction [49] was adopted in [50, 51], where an exactly well-balanced scheme for non-stationary steady state solutions was designed.

In the context of describing the flow of blood in extensive networks of vessels, the computational cost holds paramount importance. Therefore, it is essential to focus on studying numerical methods that are increasingly efficient. In this regard, a particular approach involves the utilization of splitting techniques, which partition the initial system into two subsystems of PDEs. These subsystems present a simpler eigenstructure compared to the one of the entire system, thereby contributing to improve the computational efficiency [52–56]. In the present study, our attention is focused on this approach.

Our analysis involves a two-step framework that incorporates flux splitting at the level of partial differential equations (PDEs) and numerical methods for discretizing the resulting problems. We expand upon the flux vector splitting approach introduced by Toro and Vázquez [54], referred to as the TV splitting, which was originally designed for the conservative Euler equations of compressible gas dynamics. In this approach the flux vector is split into advection and pressure terms, resulting in two separate systems of partial differential equations: the advection system and the pressure one. The TV splitting approach offers several valuable properties that can be applied to simulate blood flow in complex vessels networks. By separating the original system into the two resulting subsystems, the wave relations that need to be enforced when using a Riemann solver are simplified. In more general blood flow models, wave relations can be highly complex and require the solution of nonlinear ordinary differential equations, which may not always have a closed form solution (Spilimbergo et al. [43]). Simplifying the wave relations not only benefits the numerical method used to solve the blood flow equations within vessels, but also aids in determining the coupling conditions between one-dimensional domains, which are determined by the wave relations themselves [12, 15]. The TV splitting approach has already been adapted for a 1D blood flow model in conservative and non-conservative form for a tube law describing arteries in Toro et. al. [57] and extended to veins for the conservative counterpart in Spilimbergo et al. [58]. In this article, we apply the TV splitting methodology to the non-conservative 1D blood flow model presented in Toro and Siviglia [38], for both arteries and veins and considered with a general momentum correction coefficient accounting for uniform and parabolic velocity profiles.

In detail, the complete system of non-conservative 1D blood flow equations is split into the advection subsystem in conservative form, and the pressure one in non-conservative form. At PDEs level the modification with respect to the original TV-splitting approach (Toro and Vázquez [54]) introduced in Toro and al. [57], is maintaned: the flux of the continuity equation is assigned to the pressure system instead of assigning it to the advection one. This choice is determined by both the consistency with zero-dimensional models and the loss of hyperbolicity of the resulting subsystems of PDEs, otherwise. Regarding the advection equation for a passive scalar transport, at PDEs level its conservative flux is assigned to the advection system (the passive scalar is advected by the blood flow). At the numerical level, on the other hand, we propose simple, finite volume-type, first order, numerical schemes, derived from a conservative form of the path-conservative schemes for the pressure system, obviating the use of any path necessary for the path-conservative methods. Regarding the advection numerical flux a modification with respect to the one described in [57, 58] is presented, to adequately address a larger number of discontinuous parameters. These schemes incorporate approximate Riemann problem solvers as a constitutive component. An approximate two rarefaction Riemann solver for the pressure system describing arteries and veins with discontinuous mechanical and geometrical properties is thus introduced, and furthermore, a linearized version of it is also described. These approximate solvers lead to the description of two different final numerical methods. The proposed numerical schemes are first order accurate, but they can be integrated into higher-order methods (for more details see Siviglia et al. [59]).

The manuscript is organized as follows: we start with a brief review of the mathematical model, that is, the 1D blood flow equations with discontinuous parameters and an advection equation for the passive scalar, giving some theoretical notions and addressing the wave relations (Section 2). In Section 3 we describe the proposed advection-pressure splitting at the level of the PDEs. In Section 4 we present the pressure system resulting after the aforementioned splitting, briefly reviewing some theoretical aspects and introducing the Riemann problem for it. In Section 5 we present two approximate Riemann solvers for the above-mentioned pressure system. The numerical splitting schemes are presented in Section 6. The numerical results are given in Section 7, with an efficiency analysis performed in Section 7.2. Finally the conclusions are drawn in Section 8.

2 | Non-Conservative 1D Blood Flow Model With Transport

2.1 | Governing Equations

Assuming a deformable axially symmetric vessel configuration in three space dimensions at time t, and one-dimensional flow in the axial direction x, the 1D blood flow model with spatially varying mechanical and geometrical parameters and an advection equation for the passive scalar transport added, reads

$$\begin{cases} \partial_t A + \partial_x(Au) = 0, \\ \partial_t(Au) + \partial_x(\alpha Au^2) + \frac{A}{\rho}\partial_x p = 0, \\ \partial_t(A\phi) + \partial_x(Au\phi) = 0. \end{cases} \tag{1}$$

The first equation in (1) represents the mass conservation, the second implies the momentum balance and the third is the advection equation for a passive scalar transport. $A(x,t)$ is the cross-sectional area of the vessel or tube at position x and time t, with the assumption that $A \in \mathbb{R}^+$, $u(x,t) \in \mathbb{R}$ is the averaged velocity of blood at a cross section, $p(x,t) \in \mathbb{R}$ is the pressure, $\rho \in \mathbb{R}^+$ is the density of blood, assumed constant, $\phi(x,t) \in \mathbb{R}_0^+$

is the concentration of the passive scalar, α is the momentum correction coefficient (assumed constant) that in the 1D blood flow equations is related to the assumed velocity profile. Here we consider the velocity profile function proposed in Smith et al. [60] and given by

$$s(r) = \frac{\xi+2}{\xi}\left[1-\left(\frac{r}{R}\right)^{\xi}\right], \tag{2}$$

where $r = [0, R]$ is the radial coordinate and $\xi \in \mathbb{R}^+$ determines the shape of the velocity profile. Then, the momentum correction coefficient α can be defined as

$$\alpha = \frac{\int_{\mathfrak{S}} s^2 d\sigma}{A}, \tag{3}$$

where $\mathfrak{S}$ is the cross section of the vessel and $A = \int_{\mathfrak{S}} d\sigma$ is the cross-sectional area of the vessel. Inserting (2) into (3), we obtain

$$\alpha = \alpha(\xi) = \frac{2+\xi}{1+\xi},$$

that has the following property

$$\frac{d\alpha}{d\xi} < 0, \quad \forall \xi > 0.$$

Clearly

$$\lim_{\xi\to+\infty} \alpha(\xi) = 1, \qquad \lim_{\xi\to 0^+} \alpha(\xi) = 2,$$

consequently $\alpha \in [1, 2]$. In particular in this article, we consider $\xi = 2$ (that is, $\alpha = \frac{4}{3}$) which is related to a parabolic velocity profile, and $\xi \to +\infty$ (that is, $\alpha \to 1$) related to a uniform (flat) velocity profile obtained for inviscid fluid.

To close the system (1), we adopt a tube law of the form

$$p = p_e + \psi(A, K, A_0), \tag{4}$$

where $p_e(x)$ is the external pressure and $\psi(A, K, A_0)$ is the *transmural pressure*, assumed of the form

$$\psi(A, K, A_0) = K\left[\left(\frac{A}{A_0}\right)^m - \left(\frac{A}{A_0}\right)^n\right], \tag{5}$$

with

$$K(x) = \begin{cases} \frac{E(x)}{(1-\nu^2)}\left(\frac{h_0(x)}{R_0(x)}\right) & \text{for arteries,} \\ \frac{E(x)}{12(1-\nu^2)}\left(\frac{h_0(x)}{R_0(x)}\right)^3 & \text{for veins,} \end{cases} \tag{6}$$

$$m = \begin{cases} 1/2 & \text{for arteries,} \\ 10 & \text{for veins,} \end{cases} \qquad n = \begin{cases} 0 & \text{for arteries,} \\ -3/2 & \text{for veins.} \end{cases} \tag{7}$$

Here $h_0(x)$ is the vessel wall thickness; $A_0(x)$ and $R_0(x)$ are the cross-sectional area of the vessel and the radius at equilibrium, that is, $p = p_e$, or in other words $\psi(A, K, A_0) = 0$; $E(x)$ is the Young's modulus; ν is the Poisson ratio taken as $\nu = 0.5$; m and n are real numbers and are generally taken $m > 0$ and $-2 \le n \le 0$ (see for example Colombo et al. [61]); $K(x) \in \mathbb{R}^+$; $A_0(x) \in \mathbb{R}^+$; $R_0(x) \in \mathbb{R}^+$; $p_e(x) \in \mathbb{R}$; $E(x) \in \mathbb{R}^+$; $h_0(x) \in \mathbb{R}^+$.

Developing the partial derivative of the pressure, we have

$$\begin{cases} \partial_t A + \partial_x(Au) = 0, \\ \partial_t(Au) + \alpha\partial_x(Au^2) + \frac{A}{\rho}\psi_A\partial_x A = \\ \qquad = -\frac{A}{\rho}\psi_K\partial_x K - \frac{A}{\rho}\psi_{A_0}\partial_x A_0 - \frac{A}{\rho}\partial_x p_e, \\ \partial_t(A\phi) + \partial_x(Au\phi) = 0, \end{cases} \tag{8}$$

where

$$\begin{aligned} \psi_A &= \frac{\partial\psi}{\partial A} = \frac{K}{A}\left[m\left(\frac{A}{A_0}\right)^m - n\left(\frac{A}{A_0}\right)^n\right], \\ \psi_K &= \frac{\partial\psi}{\partial K} = \left[\left(\frac{A}{A_0}\right)^m - \left(\frac{A}{A_0}\right)^n\right], \\ \psi_{A_0} &= \frac{\partial\psi}{\partial A_0} = -\frac{K}{A_0}\left[m\left(\frac{A}{A_0}\right)^m - n\left(\frac{A}{A_0}\right)^n\right]. \end{aligned} \tag{9}$$

We note that the right hand side of equation (8) has terms involving unknowns and spatial gradients of parameters. Such terms are usually called *geometric source terms*. Following the approach presented in Toro and Siviglia [38], we rewrite system (8) in the form of the augmented system

$$\begin{cases} \partial_t A + \partial_x(Au) = 0, \\ \partial_t(Au) + \alpha\partial_x(Au^2) + \frac{A}{\rho}\psi_A\partial_x A + \\ \qquad + \frac{A}{\rho}\psi_K\partial_x K + \frac{A}{\rho}\psi_{A_0}\partial_x A_0 + \frac{A}{\rho}\partial_x p_e = 0, \\ \partial_t K = 0, \\ \partial_t A_0 = 0, \\ \partial_t p_e = 0, \\ \partial_t(A\phi) + \partial_x(Au\phi) = 0, \end{cases} \tag{10}$$

that in quasi-linear form reads

$$\partial_t \mathbf{Q} + \mathbf{M}(\mathbf{Q})\partial_x \mathbf{Q} = \mathbf{0}, \tag{11}$$

where

$$\mathbf{Q} = \begin{bmatrix} A(x,t) \\ A(x,t)u(x,t) \\ K(x) \\ A_0(x) \\ p_e(x) \\ A(x,t)\phi(x,t) \end{bmatrix},$$

$$\mathbf{M}(\mathbf{Q}) = \begin{bmatrix} 0 & 1 & 0 & 0 & 0 & 0 \\ c^2 - \alpha u^2 & 2\alpha u & \frac{A}{\rho}\psi_K & \frac{A}{\rho}\psi_{A_0} & \frac{A}{\rho} & 0 \\ 0 & 0 & 0 & 0 & 0 & 0 \\ 0 & 0 & 0 & 0 & 0 & 0 \\ 0 & 0 & 0 & 0 & 0 & 0 \\ -u\phi & \phi & 0 & 0 & 0 & u \end{bmatrix}. \tag{12}$$

Here c is the *wave speed*

$$c(A,K,A_0)=\sqrt{\frac{A}{\rho}\frac{\partial p}{\partial A}}=\sqrt{\frac{A}{\rho}\psi_A}=$$
$$=\sqrt{\frac{K}{\rho}\left[m\left(\frac{A}{A_0}\right)^m-n\left(\frac{A}{A_0}\right)^n\right]}, \tag{13}$$

which is always real, being $\psi_A\in\mathbb{R}^+$ for the choices of m and n given in (7). The eigenvalues of $\mathbf{M}(\mathbf{Q})$ in (12) are given by

$$\lambda_1=\alpha u-c_\alpha,\quad \lambda_2=\lambda_3=\lambda_4=0,\quad \lambda_5=u,\quad \lambda_6=\alpha u+c_\alpha, \tag{14}$$

with

$$c_\alpha(\mathbf{Q})=\sqrt{c^2+\alpha(\alpha-1)u^2}. \tag{15}$$

A possible choice of right eigenvectors of $\mathbf{M}(\mathbf{Q})$ corresponding to eigenvalues (14) is

$$\mathbf{R}_1=\begin{bmatrix}1\\ \alpha u-c_\alpha\\ 0\\ 0\\ 0\\ \phi\end{bmatrix},\quad \mathbf{R}_2=\begin{bmatrix}0\\ 0\\ 1\\ 0\\ -\psi_K\\ 0\end{bmatrix},\quad \mathbf{R}_3=\begin{bmatrix}0\\ 0\\ 0\\ 1\\ -\psi_{A_0}\\ 0\end{bmatrix},$$
$$\mathbf{R}_4=\begin{bmatrix}1\\ 0\\ 0\\ 0\\ \frac{\rho}{A}(\alpha u^2-c^2)\\ \phi\end{bmatrix},\ \mathbf{R}_5=\begin{bmatrix}0\\ 0\\ 0\\ 0\\ 0\\ 1\end{bmatrix},\ \mathbf{R}_6=\begin{bmatrix}1\\ \alpha u+c_\alpha\\ 0\\ 0\\ 0\\ \phi\end{bmatrix}. \tag{16}$$

Remark 1. Note that in this article we refer to the flow rate as Au or $q=Au$ without distinction, and also refer to c in (13) in this way: for example, we write c_L for $c(A_L,K_L,A_{0L})$, c_R for $c(A_R,K_R,A_{0R})$, and so on.

Being the considered domain $\Omega_d=[\mathbb{R}^+\times\mathbb{R}\times\Omega_\pi\times\mathbb{R}_0^+]\subset\mathbb{R}^6$, with $\Omega_\pi\subseteq\mathbb{R}^+\times\mathbb{R}^+\times\mathbb{R}$, we will consider only subcritical states, that is, situations in which $\alpha|u|<c_\alpha$, and we define the new domain

$$\overline{\Omega}_d=\left\{\mathbf{Q}\in\Omega_d\quad|\quad \alpha|u|<c_\alpha\right\}.$$

Proposition 1 (Hyperbolicity). *The system defined in (11) and (12) is hyperbolic under the following hypotheses*:

1. *the set of admissible solutions is restricted to* $\mathbf{Q}\in\overline{\Omega}_d$,
2. $\alpha\in[1,2]$,
3. *the pressure function (4) is a monotonically increasing function of the cross-sectional area* A, *that is,* $\dfrac{\partial p}{\partial A}>0$.

Proof. Since $\alpha\in[1,2]$ and for pressure functions that satisfy the last hypothesis, it can be easily verified that $c_\alpha\in\mathbb{R}^+$ and thus eigenvalues (14) are always real. □

Remark 2. It is worth noting that since there are three repeated eigenvalues $\lambda_2=\lambda_3=\lambda_4=0$ strict hyperbolicity is lost $\forall\mathbf{Q}\in\overline{\Omega}_d$.

Corollary 1. *Condition 1 of Proposition 1 is necessary for hyperbolicity only for* $\alpha=1$. *For* $\alpha>1$, *hyperbolicity is never lost.*

Proof. If, for example, $\alpha|u|=c_\alpha$ with $u>0$, having $c_\alpha>0$,

$$\alpha u-c_\alpha=0. \tag{17}$$

For $\alpha=1$, $c_\alpha=c$ in (13), so in this case the first and the fourth eigenvectors become

$$\mathbf{R}_1=\mathbf{R}_4=\begin{bmatrix}1\\0\\0\\0\\0\\\phi\end{bmatrix},$$

that leads to a loss of hyperbolicity, in fact the eigenvectors are not linearly independent anymore. The same issue arises with $u<0$. For $\alpha>1$ this possibility never occurs. □

Proposition 2 (Nature of the characteristic fields). *Under the hypotheses of Proposition 1, the* λ_1- *and* λ_6-*characteristic fields for system (11) are genuinely nonlinear for* $\mathbf{Q}\in\overline{\Omega}_d$. *Moreover the* λ_2-, λ_3-, λ_4-, λ_5-*characteristic fields, are linearly degenerate. In particular provided* $m>0$, $-2\le n\le 0$ *we have*

$$\nabla\lambda_1(\mathbf{Q})\cdot\mathbf{R}_1(\mathbf{Q})<0,\qquad \nabla\lambda_6(\mathbf{Q})\cdot\mathbf{R}_6(\mathbf{Q})>0\quad\forall\mathbf{Q}\in\overline{\Omega}_d.$$

Proof. The proof is presented in detail in Appendix A. In short: regarding the λ_1- and λ_6-characteristic fields a proof is similar to the one for the analogous characteristic fields in Spilimbergo et al. [43]. For the λ_k-fields with $k=2,\dots,5$, it is sufficient to check that

$$\nabla\lambda_k(\mathbf{Q})\cdot\mathbf{R}_k(\mathbf{Q})=0,\qquad\forall\mathbf{Q}\in\overline{\Omega}_d.$$ □

2.2 | Riemann Problem for the Full System

The Riemann problem for system (11) is:

$$\begin{cases}\partial_t\mathbf{Q}+\mathbf{M}(\mathbf{Q})\partial_x\mathbf{Q}=\mathbf{0}, & x\in\mathbb{R},\quad t\in\mathbb{R}_0^+,\\ \mathbf{Q}(x,0)=\begin{cases}\mathbf{Q}_L & \text{if}\quad x<x_d,\\ \mathbf{Q}_R & \text{if}\quad x>x_d,\end{cases}\end{cases} \tag{18}$$

being $x_d\in\mathbb{R}$ the spatial coordinate of the discontinuity at $t=0$. For the purposes of this article, we always consider $x,x_d\in\mathbb{R}_0^+$. The initial conditions are given by the two constant states

$$\mathbf{Q}_L=\begin{bmatrix}A_L\\ A_Lu_L\\ K_L\\ A_{0L}\\ p_{eL}\\ A_L\phi_L\end{bmatrix},\qquad \mathbf{Q}_R=\begin{bmatrix}A_R\\ A_Ru_R\\ K_R\\ A_{0R}\\ p_{eR}\\ A_R\phi_R\end{bmatrix}. \tag{19}$$

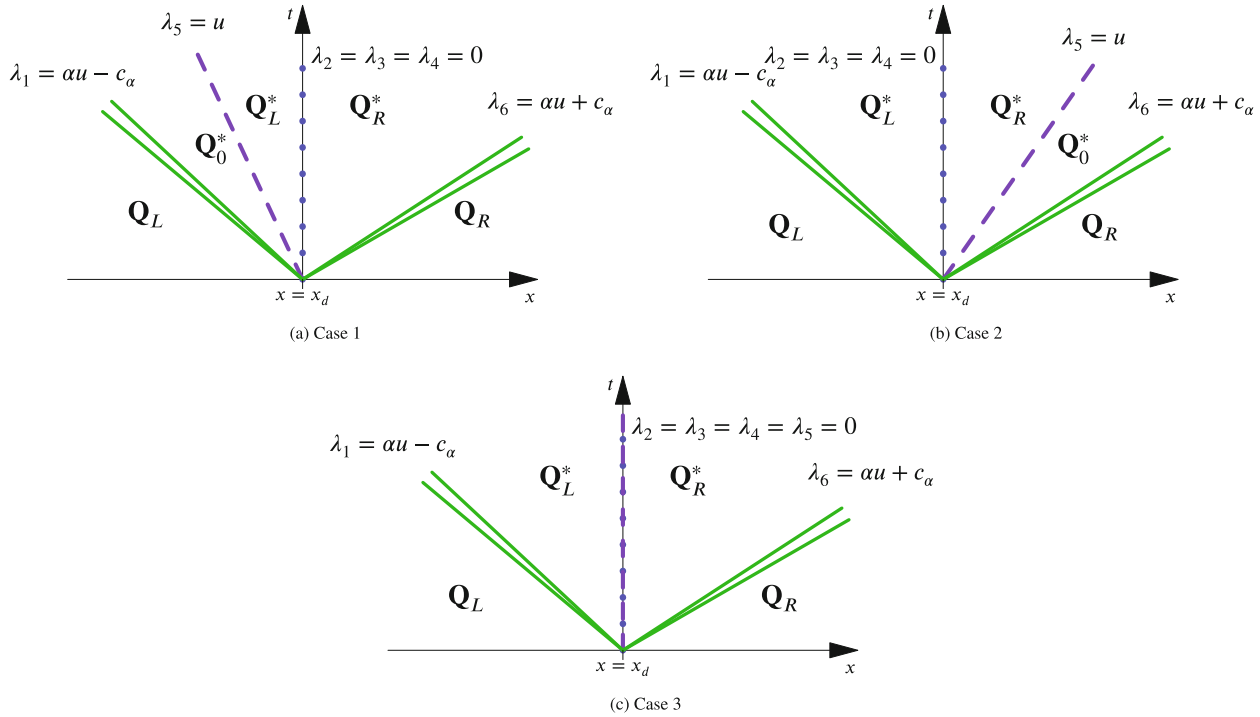

FIGURE 1 | The three possible configurations of the solution of the Riemann problem for the complete system of 1D blood flow equations with discontinuous mechanical and geometrical parameters (18) within the subcritical regime. Green solid lines represent waves associated with genuinely nonlinear fields that can be either shocks or rarefactions, while the dotted blue line and the dashed purple one depict contact discontinuities and are associated with linearly degenerate fields. In this article, the λ_1-wave will be sometimes called left wave, while the λ_6-one, right wave. It follows that the related wave patterns will be called left rarefaction/left shock or right rarefaction/right shock. The generalized Riemann invariants related to the characteristic fields and the jump relations across the superimposed contact discontinuities are presented in Appendix B. The relations across the waves in cases of shocks and the complete exact solution of the Riemann problem, however, are not explicitly provided in this article. The interested reader can refer to Spilimbergo [62] for further details, or to [38, 42, 43] for the exact solution of the Riemann problem for the same equations but with some modifications. [Colour figure can be viewed at wileyonlinelibrary.com]

The unknowns are $\mathbf{Q}_L^*$, $\mathbf{Q}_R^*$ and $\mathbf{Q}_0^*$ where this latter exists (cases 1 and 2 in Figure 1) defined

$$\mathbf{Q}_L^* = \begin{bmatrix} A_L^* \\ A_L^* u_L^* \\ K_L^* \\ A_{0L}^* \\ p_{eL}^* \\ A_L^* \phi_L^* \end{bmatrix}, \quad \mathbf{Q}_R^* = \begin{bmatrix} A_R^* \\ A_R^* u_R^* \\ K_R^* \\ A_{0R}^* \\ p_{eR}^* \\ A_R^* \phi_R^* \end{bmatrix}, \quad \mathbf{Q}_0^* = \begin{bmatrix} A_z^* \\ A_z^* u_z^* \\ K_z^* \\ A_{0z}^* \\ p_{ez}^* \\ A_z^* \phi_z^* \end{bmatrix}. \tag{20}$$

The stationary contact discontinuities associated with $\lambda_2 = \lambda_3 = \lambda_4 = 0$ are the only discontinuities for the parameters K, A_0 and p_e, while the λ_5-contact wave is the only discontinuity for the passive scalar ϕ (see Appendix B for further details). It follows that the unknowns (20) become

- Case 1 of Figure 1

$$\mathbf{Q}_L^* = \begin{bmatrix} A_L^* \\ A_L^* u_L^* \\ K_L \\ A_{0L} \\ p_{eL} \\ A_L^* \phi_R \end{bmatrix}, \quad \mathbf{Q}_R^* = \begin{bmatrix} A_R^* \\ A_R^* u_R^* \\ K_R \\ A_{0R} \\ p_{eR} \\ A_R^* \phi_R \end{bmatrix}, \quad \mathbf{Q}_0^* = \begin{bmatrix} A_L^* \\ A_L^* u_L^* \\ K_L \\ A_{0L} \\ p_{eL} \\ A_L^* \phi_L \end{bmatrix},$$

- Case 2 of Figure 1

$$\mathbf{Q}_L^* = \begin{bmatrix} A_L^* \\ A_L^* u_L^* \\ K_L \\ A_{0L} \\ p_{eL} \\ A_L^* \phi_L \end{bmatrix}, \quad \mathbf{Q}_R^* = \begin{bmatrix} A_R^* \\ A_R^* u_R^* \\ K_R \\ A_{0R} \\ p_{eR} \\ A_R^* \phi_L \end{bmatrix}, \quad \mathbf{Q}_0^* = \begin{bmatrix} A_R^* \\ A_R^* u_R^* \\ K_R \\ A_{0R} \\ p_{eR} \\ A_R^* \phi_R \end{bmatrix},$$

- Case 3 of Figure 1

$$\mathbf{Q}_L^* = \begin{bmatrix} A_L^* \\ A_L^* u_L^* \\ K_L \\ A_{0L} \\ p_{eL} \\ A_L^* \phi_L \end{bmatrix}, \quad \mathbf{Q}_R^* = \begin{bmatrix} A_R^* \\ A_R^* u_R^* \\ K_R \\ A_{0R} \\ p_{eR} \\ A_R^* \phi_R \end{bmatrix}.$$

The complete exact solution of the Riemann problem (18) is not explicitly provided in this article. The interested reader can consult Spilimbergo [62] for further details. Alternatively, we direct the reader to Spilimbergo et al. [43] for the exact solution of the Riemann problem for the presented model but without transport, that is, concerning only the variables A, Au, K, A_0, p_e. On

the other hand we refer also to [38, 42] for the exact solution of the Riemann problem for the same model with transport but with a momentum correction coefficient $\alpha = 1$.

Figure 1 shows the structure of the exact solution of the Riemann problem (18) for the homogeneous 1D blood flow equations (11). There are two wave families associated with the two real eigenvalues $\lambda_1 = \alpha u - c_\alpha$, $\lambda_6 = \alpha u + c_\alpha$. The two waves are associated with genuinely nonlinear fields and can be either shocks (elastic jumps) or rarefactions (Smoller [63]). The waves associated with the eigenvalues $\lambda_2 = \lambda_3 = \lambda_4 = 0$ and $\lambda_5 = u$ are related to linearly degenerate fields and are contact discontinuities.

3 | Splitting at the Level of PDEs

We split $\mathbf{M}(\mathbf{Q})$ in (12) into the sum of an advection and a pressure matrix as follows (see Toro et al. [57])

$$\mathbf{M}(\mathbf{Q}) = \mathcal{A}(\mathbf{Q}) + \mathcal{P}(\mathbf{Q}), \tag{21}$$

and we propose to split system (11) via (21) into the two subsystems of PDEs

$$\begin{cases} \partial_t \mathbf{Q} + \mathcal{A}(\mathbf{Q})\partial_x \mathbf{Q} = \mathbf{0}, & (22) \\ \partial_t \mathbf{Q} + \mathcal{P}(\mathbf{Q})\partial_x \mathbf{Q} = \mathbf{0}, & (23) \end{cases}$$

where

$$\mathbf{Q} = \begin{bmatrix} A \\ Au \\ K \\ A_0 \\ p_e \\ A\phi \end{bmatrix}, \quad \mathcal{A}(\mathbf{Q}) = \begin{bmatrix} 0 & 0 & 0 & 0 & 0 & 0 \\ -\alpha u^2 & 2\alpha u & 0 & 0 & 0 & 0 \\ 0 & 0 & 0 & 0 & 0 & 0 \\ 0 & 0 & 0 & 0 & 0 & 0 \\ 0 & 0 & 0 & 0 & 0 & 0 \\ -u\phi & \phi & 0 & 0 & 0 & u \end{bmatrix},$$

$$\mathcal{P}(\mathbf{Q}) = \begin{bmatrix} 0 & 1 & 0 & 0 & 0 & 0 \\ c^2 & 0 & \frac{A}{\rho}\psi_K & \frac{A}{\rho}\psi_{A_0} & \frac{A}{\rho} & 0 \\ 0 & 0 & 0 & 0 & 0 & 0 \\ 0 & 0 & 0 & 0 & 0 & 0 \\ 0 & 0 & 0 & 0 & 0 & 0 \\ 0 & 0 & 0 & 0 & 0 & 0 \end{bmatrix}. \tag{24}$$

c is the *wave speed* (13), ψ_K, ψ_{A_0} are defined in (9). System (22) is called *advection system*, system (23) is called *pressure system*. The aim is to build a numerical scheme for the complete system (11), from the solution of the Riemann problem for the pressure system (23). This solution will fully determine the different parts of the final numerical scheme.

It is important to note that this particular splitting assigns the momentum correction coefficient α to the advection system, thereby significantly simplifying the eigenstructure and wave relations of the pressure system used for the final numerical scheme.

In the next section we will present the pressure system and introduce the associated Riemann problem. The actual numerical splitting scheme is treated in Sections 6 and 7.

4 | The Pressure System

In this section, we describe theoretically the pressure system built from the splitting in Section 3. We study the eigenstructure, the characteristic fields, the Riemann invariants and the Riemann problem for it. As previously stated, the pressure system does not include the momentum correction coefficient α, and thus every result presented hereafter is independent of the value of this latter and, consequently, of the specific blood flow velocity profile considered.

4.1 | Eigenstructure and Characteristic Fields

The pressure system is presented in (23), (24), while to close the system, the tube law (4) is added. The eigenvalues of the matrix $\mathcal{P}(\mathbf{Q})$ in (24) are all real for parameters in (6), (7), and given by

$$\lambda_{\mathcal{P}_1} = -c, \quad \lambda_{\mathcal{P}_2} = \lambda_{\mathcal{P}_3} = \lambda_{\mathcal{P}_4} = \lambda_{\mathcal{P}_5} = 0, \quad \lambda_{\mathcal{P}_6} = c, \tag{25}$$

and a possible choice of right eigenvectors corresponding to eigenvalues (25) is

$$\mathbf{R}_{\mathcal{P}_1} = \begin{bmatrix} 1 \\ -c \\ 0 \\ 0 \\ 0 \\ 0 \end{bmatrix}, \quad \mathbf{R}_{\mathcal{P}_2} = \begin{bmatrix} 0 \\ 0 \\ 1 \\ 0 \\ -\psi_k \\ 0 \end{bmatrix}, \quad \mathbf{R}_{\mathcal{P}_3} = \begin{bmatrix} 0 \\ 0 \\ 0 \\ 1 \\ -\psi_{A_0} \\ 0 \end{bmatrix},$$

$$\mathbf{R}_{\mathcal{P}_4} = \begin{bmatrix} 1 \\ 0 \\ 0 \\ 0 \\ -\frac{\rho}{A}c^2 \\ 0 \end{bmatrix}, \quad \mathbf{R}_{\mathcal{P}_5} = \begin{bmatrix} 0 \\ 0 \\ 0 \\ 0 \\ 0 \\ 1 \end{bmatrix}, \quad \mathbf{R}_{\mathcal{P}_6} = \begin{bmatrix} 1 \\ c \\ 0 \\ 0 \\ 0 \\ 0 \end{bmatrix}, \tag{26}$$

where c is the wave speed (13).

Proposition 3 (Hyperbolicity). *System (23) is hyperbolic under the following hypotheses*:

1. *the set of admissible solutions is restricted to* $\mathbf{Q} \in \Omega_p = [\mathbb{R}^+ \times \mathbb{R} \times \Omega_\pi \times \mathbb{R}_0^+] \subset \mathbb{R}^6$ *with* $\Omega_\pi \subseteq [\mathbb{R}^+ \times \mathbb{R}^+ \times \mathbb{R}]$;
2. *the pressure function (4) is a monotonically increasing function of the cross-sectional area A, that is,* $\frac{\partial p}{\partial A} > 0$.

Proof. This can be clearly seen from the definition of wave speed given in (13). Under the conditions considered in this proposition $c \in \mathbb{R}^+ \, \forall \mathbf{Q} \in \Omega_p$, which results in $\lambda_{\mathcal{P}_1} \in \mathbb{R}^-$, $\lambda_{\mathcal{P}_6} \in \mathbb{R}^+$, $\forall \mathbf{Q} \in \Omega_p$. In particular this is true for the parameters given in (6), (7). □

Proposition 4 (Nature of the $\lambda_{\mathcal{P}_1}$- and $\lambda_{\mathcal{P}_6}$-characteristic fields). *Under the hypotheses of Proposition 3,*

- *in case of arteries (parameters are given in (6), (7)) the* $\lambda_{\mathcal{P}_1}$- *and* $\lambda_{\mathcal{P}_6}$-*characteristic fields are genuinely nonlinear with*

$$\nabla\lambda_{\boldsymbol{p}_1}(\mathbf{Q})\cdot\mathbf{R}_{\boldsymbol{p}_1}(\mathbf{Q})<0,\quad \forall\mathbf{Q}\in\Omega_p,$$
$$\nabla\lambda_{\boldsymbol{p}_6}(\mathbf{Q})\cdot\mathbf{R}_{\boldsymbol{p}_6}(\mathbf{Q})>0,\quad \forall\mathbf{Q}\in\Omega_p,$$

- *in case of veins (parameters are given in (6), (7)) the genuine nonlinearity for the $\lambda_{\boldsymbol{p}_1}$- and $\lambda_{\boldsymbol{p}_6}$-characteristic fields is lost. In fact*

$$\nabla\lambda_{\boldsymbol{p}_1}(\mathbf{Q})\cdot\mathbf{R}_{\boldsymbol{p}_1}(\mathbf{Q})\quad\begin{cases}>0 & \text{for}\quad A<A_{cL},\\ =0 & \text{for}\quad A=A_{cL},\\ <0 & \text{for}\quad A>A_{cL},\end{cases}$$

$$\nabla\lambda_{\boldsymbol{p}_6}(\mathbf{Q})\cdot\mathbf{R}_{\boldsymbol{p}_6}(\mathbf{Q})\quad\begin{cases}<0 & \text{for}\quad A<A_{cR},\\ =0 & \text{for}\quad A=A_{cR},\\ >0 & \text{for}\quad A>A_{cR},\end{cases}$$

where A_{cL}, A_{cR}, for parameters in (7), are

$$A_{cL}\approx 0.7190\ A_{0L},\qquad A_{cR}\approx 0.7190\ A_{0R}. \tag{27}$$

Proof. Hint. It can be easily verified that

$$\nabla\lambda_{\boldsymbol{p}_1}(\mathbf{Q})\cdot\mathbf{R}_{\boldsymbol{p}_1}(\mathbf{Q})=-\frac{\partial c}{\partial A}(A,K_L,A_{0L}), \tag{28}$$

and

$$\nabla\lambda_{\boldsymbol{p}_6}(\mathbf{Q})\cdot\mathbf{R}_{\boldsymbol{p}_6}(\mathbf{Q})=\frac{\partial c}{\partial A}(A,K_R,A_{0R}), \tag{29}$$

where $\mathbf{R}_{\boldsymbol{p}_1}$ and $\mathbf{R}_{\boldsymbol{p}_6}$ are the right eigenvectors (26) and c is the wave speed (13). The use of the left and right parameters in (28) and (29) is explained in Proposition 7, being the discontinuities associated with eigenvalues $\lambda_{\boldsymbol{p}_2}=\lambda_{\boldsymbol{p}_3}=\lambda_{\boldsymbol{p}_4}=\lambda_{\boldsymbol{p}_5}=0$ the only ones related to the aforementioned parameters. For the genuine nonlinearity we must prove that $\frac{\partial c}{\partial A}\neq 0$, with

$$\frac{\partial c}{\partial A}(A,K_j,A_{0j})=\frac{\frac{K_j}{\rho}\left(\left(\frac{A}{A_{0j}}\right)^m m^2-\left(\frac{A}{A_{0j}}\right)^n n^2\right)}{2A\sqrt{\frac{K_j}{\rho}\left(\left(\frac{A}{A_{0j}}\right)^m m-\left(\frac{A}{A_{0j}}\right)^n n\right)}},$$
$$\text{with}\quad j=L,R.$$

The remaining part of the proof is similar to the corresponding one presented in Spilimbergo et al. [58]. □

Proposition 5 (Nature of the $\lambda_{\boldsymbol{p}_2}$, $\lambda_{\boldsymbol{p}_3}$, $\lambda_{\boldsymbol{p}_4}$, $\lambda_{\boldsymbol{p}_5}$-characteristic fields). *Under the hypotheses of Proposition 3, the $\lambda_{\boldsymbol{p}_2}$, $\lambda_{\boldsymbol{p}_3}$, $\lambda_{\boldsymbol{p}_4}$, $\lambda_{\boldsymbol{p}_5}$-characteristic fields are linearly degenerate.*

Proof. It can be easily verified that

$$\nabla\lambda_{\boldsymbol{p}_k}(\mathbf{Q})\cdot\mathbf{R}_{\boldsymbol{p}_k}(\mathbf{Q})=0,\qquad k=2,3,4,5,\quad\forall\mathbf{Q}\in\Omega_p.$$ □

4.2 | Riemann Invariants and Jump Conditions

Proposition 6 (Generalized Riemann invariants for the $\lambda_{\boldsymbol{p}_1}$- and $\lambda_{\boldsymbol{p}_6}$-characteristic fields). *The Riemann invariants are given by*

$$q+\int c(A,K,A_0)dA=const,\quad K=const,\quad A_0=const,$$
$$p_e=const,\quad A\phi=const,$$

for the $\lambda_{\boldsymbol{p}_1}$-characteristic field,

$$q-\int c(A,K,A_0)dA=const,\quad K=const,\quad A_0=const,$$
$$p_e=const,\quad A\phi=const,$$

for the $\lambda_{\boldsymbol{p}_6}$-characteristic field.

Proof. We proceed to solve the problem by applying the generalized Riemann invariants method (for example see Toro [41] and Toro and Siviglia [38]), that is, for a given hyperbolic system of n unknowns $[w_1,w_2,\ldots,w_n]^T$, for any $\lambda_{\boldsymbol{p}_k}$-characteristic field with right eigenvector $\mathrm{R}_{\boldsymbol{p}_k}=[r_{1,k},r_{2,k},\ldots,r_{n,k}]^T$ the generalized Riemann invariants are solutions of the following $n-1$ ordinary differential equations in phase-plane

$$\frac{dw_1}{r_{1,k}}=\frac{dw_2}{r_{2,k}}=\cdots=\frac{dw_n}{r_{n,k}}.$$

For the $\lambda_{\boldsymbol{p}_1}$-characteristic field we have

$$\frac{dA}{1}=\frac{dq}{-c}=\frac{dK}{0}=\frac{dA_0}{0}=\frac{dp_e}{0}=\frac{d(A\phi)}{0},$$

that is, from the first and the second term

$$(-c)dA=dq,$$

from which integrating we obtain the first equation of the statement. From the other terms we obtain

$$K=const,\qquad A_0=const,\qquad p_e=const,\qquad A\phi=const.$$

An analogue proof for the $\lambda_{\boldsymbol{p}_6}$-characteristic field. □

Proposition 7 (Jump conditions across the stationary contact discontinuities associated with eigenvalues $\lambda_{\boldsymbol{p}_2}=\lambda_{\boldsymbol{p}_3}=\lambda_{\boldsymbol{p}_4}=\lambda_{\boldsymbol{p}_5}=0$). *Across the four superimposed contact discontinuities the following relations hold*

$$q=Au=const,\qquad \psi+p_e=const. \tag{30}$$

Proof. We proceed to solve the problem by employing the generalized Riemann invariants method with the approach presented in Spilimbergo et al. [42]. We consider matrix $\boldsymbol{\mathcal{P}}(\mathbf{Q})$ in (24) that is,

$$\boldsymbol{\mathcal{P}}(\mathbf{Q})=\begin{bmatrix}0&1&0&0&0&0\\ c^2&0&\frac{A}{\rho}\psi_K&\frac{A}{\rho}\psi_{A_0}&\frac{A}{\rho}&0\\ 0&0&0&0&0&0\\ 0&0&0&0&0&0\\ 0&0&0&0&0&0\\ 0&0&0&0&0&0\end{bmatrix}.$$

For an arbitrary right eigenvector $\mathbf{R}=[r_1,r_2,r_3,r_4,r_5,r_6]^T$ we have

$$\boldsymbol{\mathcal{P}}\mathbf{R}=\lambda\mathbf{R},$$

which gives the algebraic system

$$\begin{cases} r_2 = \lambda r_1, \\ c^2 r_1 + \frac{A}{\rho}\psi_K r_3 + \frac{A}{\rho}\psi_{A_0} r_4 + \frac{A}{\rho} r_5 = \lambda r_2, \\ 0 = \lambda r_3, \\ 0 = \lambda r_4, \\ 0 = \lambda r_5, \\ 0 = \lambda r_6. \end{cases} \tag{31}$$

Putting $\lambda = 0$ in (31) system (31) becomes

$$\begin{cases} r_2 = 0, \\ c^2 r_1 + \frac{A}{\rho}\psi_K r_3 + \frac{A}{\rho}\psi_{A_0} r_4 + \frac{A}{\rho} r_5 = 0, \\ 0 = 0, \\ 0 = 0, \\ 0 = 0, \\ 0 = 0. \end{cases} \tag{32}$$

We notice that from the first of (32) $r_2 = 0$. Employing the second equation of (32) we can compute the value of one among r_1, r_3, r_4 and r_5 in terms of the others. Subsequently, we have four identities $0 = 0$, from which no information can be deduced. In this computation, by means of the second equation of system (32), we will determine the value of r_5 with respect to r_1, r_3 and r_4, while the values of r_1, r_3, r_4 and r_6 will be assigned arbitrarily. By setting for example $r_1 = \beta$, $r_3 = \gamma$, $r_4 = \epsilon$, $r_6 = \delta$, for $\beta, \gamma, \epsilon, \delta \in \mathbb{R}$, arbitrary constants, we obtain

$$\mathbf{R}_0 = \begin{bmatrix} \beta \\ 0 \\ \gamma \\ \epsilon \\ \left[-c^2\beta - \frac{A}{\rho}\psi_K\gamma - \frac{A}{\rho}\psi_{A_0}\epsilon\right]\frac{\rho}{A} \\ \delta \end{bmatrix}.$$

This is a general form of a vector belonging to the subspace associated with $\lambda_{\mathcal{P}k} = 0$ for every choice of $\beta, \gamma, \epsilon, \delta, \in \mathbb{R}$. We then apply the generalized Riemann invariants method (see Proposition 6) to this vector obtaining

$$\frac{dA}{\beta} = \frac{dq}{0} = \frac{dK}{\gamma} = \frac{dA_0}{\epsilon} = \\ = \frac{dp_e}{\left[-c^2\beta - \frac{A}{\rho}\psi_K\gamma - \frac{A}{\rho}\psi_{A_0}\epsilon\right]\frac{\rho}{A}} = \frac{d(A\phi)}{\delta}. \tag{33}$$

From the second term of (33)

$$q = const.$$

From the equality between the first and the fifth terms of (33)

$$\frac{dA}{\beta} = \frac{dp_e}{\left[-c^2\beta - \frac{A}{\rho}\psi_K\gamma - \frac{A}{\rho}\psi_{A_0}\epsilon\right]\frac{\rho}{A}},$$

that becomes

$$-c^2\frac{\rho}{A}dA - \psi_K\frac{\gamma}{\beta}dA - \psi_{A_0}\frac{\epsilon}{\beta}dA = dp_e. \tag{34}$$

Considering the first and the third terms of (33) coupled together and then the first and the fourth terms of (33)

$$\gamma dA = \beta dK, \quad \epsilon dA = \beta dA_0,$$

being c defined in (13) we have

$$-c^2\frac{\rho}{A}dA = -\psi_A dA,$$

so (34) becomes

$$-\psi_A dA - \psi_K dK - \psi_{A_0} dA_0 - dp_e = 0. \tag{35}$$

Considering that

$$d\psi = \psi_A dA + \psi_K dK + \psi_{A_0} dA_0,$$

(35) becomes

$$-d\psi - dp_e = 0,$$

from that, integrating, we obtain the second of (30). From the first and the sixth terms of (33)

$$\frac{dA}{\beta} = \frac{d(A\phi)}{\delta}, \tag{36}$$

that leads to

$$\frac{dA}{A} = \left(\frac{\beta}{\delta - \beta\phi}\right)d\phi. \tag{37}$$

Unfortunately β and δ are arbitrary, so from (36) and (37) we can only assume that

$$A\phi \neq const, \qquad A \neq const, \qquad \phi \neq const. \tag{38}$$

□

4.3 | Riemann Problem for the Pressure System

The Riemann problem for system (23) is

$$\begin{cases} \partial_t \mathbf{Q} + \boldsymbol{\mathcal{P}}(\mathbf{Q})\partial_x \mathbf{Q} = \mathbf{0}, & x \in \mathbb{R}, \quad t \in \mathbb{R}_0^+, \\ \mathbf{Q}(x,0) = \begin{cases} \mathbf{Q}_L, & \text{if} \quad x < x_d, \\ \mathbf{Q}_R & \text{if} \quad x > x_d, \end{cases} \end{cases} \tag{39}$$

where $x_d \in \mathbb{R}$ is the spatial location of the discontinuity at $t = 0$. For the purposes of this article, we always consider $x, x_d \in \mathbb{R}_0^+$. The initial data are $\mathbf{Q}_L$ and $\mathbf{Q}_R$ in (19). The unknowns are $\mathbf{Q}^*_{\mathcal{P}L}$ and $\mathbf{Q}^*_{\mathcal{P}R}$ defined as

$$\mathbf{Q}^*_{\mathcal{P}L} = \begin{bmatrix} A_L^* \\ q_L^* = A_L^* u_L^* \\ K_L \\ A_{0L} \\ p_{eL} \\ A_L^*\phi_L^* \end{bmatrix}, \qquad \mathbf{Q}^*_{\mathcal{P}R} = \begin{bmatrix} A_R^* \\ q_R^* = A_R^* u_R^* \\ K_R \\ A_{0R} \\ p_{eR} \\ A_R^*\phi_R^* \end{bmatrix}, \tag{40}$$

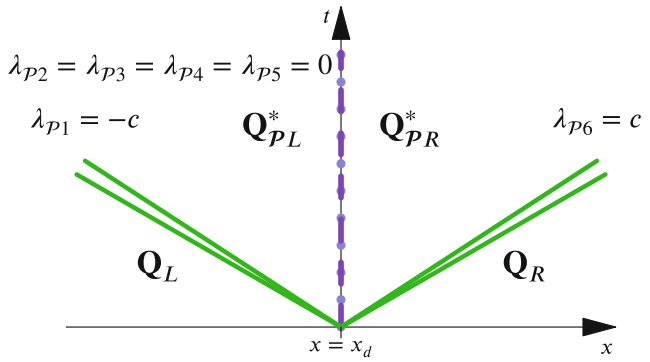

FIGURE 2 | The configuration of the exact solution of the Riemann problem for the pressure system (39). The green solid lines, in case of arteries, represent waves associated with genuinely nonlinear fields, while in case of veins this property is lost. The purple dashed line represents the contact discontinuity for the passive scalar and is associated with a linearly degenerate field, the indigo dotted line represents the three superimposed contact discontinuities for the parameters and is associated with linearly degenerate fields. [Colour figure can be viewed at wileyonlinelibrary.com]

thanks to Propositions 6 and 7 explaining that the λ_{p_2}, λ_{p_3}, λ_{p_4}-contact discontinuities are the only discontinuities for parameters K, A_0 and p_e that are only space-dependent. Clearly the values of A_j^*, q_j^*, ϕ_j^*, $j = L,\ R$ in (40) are in general different from the ones in (20).

Figure 2 depicts the structure of the exact solution of the Riemann problem (39) for the pressure system (23): the waves related to the λ_{p_2}, λ_{p_3}, λ_{p_4}, λ_{p_5}-characteristic fields are associated with linearly degenerate fields and are contact discontinuities, while the waves related to the λ_{p_1}- and λ_{p_6}-characteristic fields, in case of arteries, are associated with genuine nonlinear fields (Proposition 4) and can be either shocks (elastic jumps) or rarefactions (Smoller [63]); in case of veins, the loss of genuine nonlinearity can lead to a formation of compound waves (Liu [64]).

Remark 3. It is worth noting that for the pressure system, the wave pattern associated with the λ_{p_1}- and λ_{p_6}-characteristic fields will always be *subcritical*, since

$$\lambda_{p_1}(\mathbf{Q}) < 0 \quad \text{and} \quad \lambda_{p_6}(\mathbf{Q}) > 0, \quad \text{that is } c > 0, \quad \forall \mathbf{Q} \in \Omega_p.$$

Remark 4. The purpose of this article is not to provide a comprehensive account of the exact solution of the Riemann problem for the pressure system (39). Our assumption is that the waves associated with the λ_{p_1}- and λ_{p_6}-characteristic fields are always rarefaction waves, while still recognizing the existence of the contact discontinuities associated with the λ_{p_2}, λ_{p_3}, λ_{p_4}, λ_{p_5}-characteristic fields. This decision is based on the proposed numerical schemes and the complexity of the mathematical analysis of the solution in case of veins, due to the loss of genuine nonlinearity of the λ_{p_1}- and λ_{p_6}-characteristic fields (Proposition 4). The complete exact solution of the Riemann problem for the pressure system, for both arteries and veins, will be presented in detail in a separate publication. The current work solely focuses on observing the behavior of the splitting schemes in scenarios where the genuine nonlinearity is lost for the λ_{p_1}- and λ_{p_6}-characteristic fields of the pressure system.

5 | Approximate Riemann Solvers for the Pressure System

Having introduced the wave relations in case of rarefactions and contact discontinuities (Propositions 6, 7), we can introduce two approximate Riemann solvers for the pressure system (23), a first building block for the new splitting schemes for the complete system of 1D blood flow equations (11), that will be presented in Section 6.

For the purposes of this article, we restrict ourselves to the presentation of the solution in the *Star Region*, that is the region in the (x, t) plane included between the outer waves, that is, the green lines in Figure 2, in other words the unknowns $\mathbf{Q}^*_{pL}$ and $\mathbf{Q}^*_{pR}$.

5.1 | A Two-Rarefaction Approximate Riemann Solver for the Pressure System

The two-rarefaction approximate Riemann solver operates under the assumption that the waves associated with the λ_{p_1} and λ_{p_6}-characteristic fields are rarefaction waves. On the other hand the contact discontinuities are taken into account. The solution in the Star Region in this case is denoted as

$$\mathbf{Q}^*_{TR,L} = \begin{bmatrix} A^*_{TR,L} \\ q^*_{TR} \\ K_L \\ A_{0L} \\ p_{eL} \\ A^*_{TR,L}\phi^*_{TR,L} \end{bmatrix}, \qquad \mathbf{Q}^*_{TR,R} = \begin{bmatrix} A^*_{TR,R} \\ q^*_{TR} \\ K_R \\ A_{0R} \\ p_{eR} \\ A^*_{TR,R}\phi^*_{TR,R} \end{bmatrix}. \tag{41}$$

The states (41) are obtained as the solution of the following system [38, 42, 43, 62]

$$\begin{cases} f_1(\mathrm{x}_1, \mathrm{x}_2) = \mathrm{x}_2 - q_L + f_L(\mathrm{x}_1) = 0, \\ f_2(\mathrm{x}_3, \mathrm{x}_4) = \mathrm{x}_4 - q_R - f_R(\mathrm{x}_3) = 0, \\ f_3(\mathrm{x}_2, \mathrm{x}_4) = \mathrm{x}_2 - \mathrm{x}_4 = 0, \\ f_4(\mathrm{x}_1, \mathrm{x}_3) = K_L\left[\left(\frac{\mathrm{x}_1}{A_{0L}}\right)^m - \left(\frac{\mathrm{x}_1}{A_{0L}}\right)^n\right] - \\ \qquad -K_R\left[\left(\frac{\mathrm{x}_3}{A_{0R}}\right)^m - \left(\frac{\mathrm{x}_3}{A_{0R}}\right)^n\right] + (p_{eL} - p_{eR}) = 0, \end{cases} \tag{42}$$

where

$$f_L(\mathrm{x}_1) = \int_{A_L}^{\mathrm{x}_1} c(\sigma, K_L, A_{0L})d\sigma \quad \text{(left rarefaction)}, \tag{43}$$

$$f_R(\mathrm{x}_3) = \int_{A_R}^{\mathrm{x}_3} c(\sigma, K_R, A_{0R})d\sigma \quad \text{(right rarefaction)}, \tag{44}$$

while c is the wave speed (13) and

$$\boldsymbol{X} = \begin{bmatrix} \mathrm{x}_1 \\ \mathrm{x}_2 \\ \mathrm{x}_3 \\ \mathrm{x}_4 \end{bmatrix} = \begin{bmatrix} A^*_{TR,L} \\ q^*_{TR,L} \\ A^*_{TR,R} \\ q^*_{TR,R} \end{bmatrix}.$$

System (42) is solved with a globally convergent Newton–Raphson method with initial points A_L, q_L, A_R, q_R

(see Appendix C). Moreover, integrals in (43) and (44) in case of veins are calculated with a three-points Gauss quadrature rule, while in case of arteries (with $m = 0.5$ and $n = 0$ in (7)) the solution is explicit. The values of $\phi^*_{TR,L}$ and $\phi^*_{TR,R}$ are calculated from Proposition 6, that is,

$$\phi^*_{TR,L} = \frac{A_L}{A^*_{TR,L}}\phi_L, \qquad \phi^*_{TR,R} = \frac{A_R}{A^*_{TR,R}}\phi_R.$$

Remark 5. System (42) is obtained putting together the considered wave relations. In particular the first and the second equations describe the rarefaction waves relations: for a left rarefaction, the left generalized Riemann invariant calculated in Proposition 6

$$q + \int c(\sigma, K, A_0)d\sigma = const,$$

can be written as

$$q^*_{TR,L} - q_L + \int_{A_L}^{A^*_{TR,L}} c(\sigma, K_L, A_{0L})d\sigma = 0;$$

for a right rarefaction, the right generalized Riemann invariant calculated in Proposition 6

$$q - \int c(\sigma, K, A_0)d\sigma = const,$$

can be written as

$$q^*_{TR,R} - q_R - \int_{A_R}^{A^*_{TR,R}} c(\sigma, K_R, A_{0R})d\sigma = 0;$$

(see for example Toro and Siviglia [38]). The third and the fourth equations regard the jump conditions across the stationary contact discontinuities described in Proposition 7, in particular from $q = const$ we obtain $q^*_{TR,L} = q^*_{TR,R}$, and from $\psi + p_e = const$ the fourth equation, considering ψ defined in (5).

5.2 | A Linearized Two-Rarefaction Approximate Riemann Solver for the Pressure System

We proceed as in the case of the two-rarefaction Riemann solver and additionally linearize the relations (43), (44). The solution in the Star Region in this case is

$$\mathbf{Q}^*_{LTR,L} = \begin{bmatrix} A^*_{LTR,L} \\ q^*_{LTR} \\ K_L \\ A_{0L} \\ p_{eL} \\ A^*_{LTR,L}\phi^*_{LTR,L} \end{bmatrix}, \quad \mathbf{Q}^*_{LTR,R} = \begin{bmatrix} A^*_{LTR,R} \\ q^*_{LTR} \\ K_R \\ A_{0R} \\ p_{eR} \\ A^*_{LTR,R}\phi^*_{LTR,R} \end{bmatrix}. \quad (45)$$

To obtain (45) we must solve again (42) where we now approximate (43), (44) with

$$f_L(\mathrm{x}_1) = \int_{A_L}^{\mathrm{x}_1} c(\sigma, K_L, A_{0L})d\sigma \approx c_L(\mathrm{x}_1 - A_L) \quad \text{(left rarefaction)},$$

$$f_R(\mathrm{x}_3) = \int_{A_R}^{\mathrm{x}_3} c(\sigma, K_R, A_{0R})d\sigma \approx c_R(\mathrm{x}_3 - A_R) \quad \text{(right rarefaction)},$$

while $c_L = c(A_L, K_L, A_{0L})$ and $c_R = c(A_R, K_R, A_{0R})$ are the wave speeds (13) and

$$\boldsymbol{X} = \begin{bmatrix} \mathrm{x}_1 \\ \mathrm{x}_2 \\ \mathrm{x}_3 \\ \mathrm{x}_4 \end{bmatrix} = \begin{bmatrix} A^*_{LTR,L} \\ q^*_{LTR,L} \\ A^*_{LTR,R} \\ q^*_{LTR,R} \end{bmatrix}.$$

System (42) now reduces to

$$\begin{cases} f_5(\mathrm{x}_1, \mathrm{x}_3) = -q_L + c_L(\mathrm{x}_1 - A_L) + q_R + c_R(\mathrm{x}_3 - A_R) = 0, \\ f_4(\mathrm{x}_1, \mathrm{x}_3) = K_L\left[\left(\frac{\mathrm{x}_1}{A_{0L}}\right)^m - \left(\frac{\mathrm{x}_1}{A_{0L}}\right)^n\right] - \\ \qquad -K_R\left[\left(\frac{\mathrm{x}_3}{A_{0R}}\right)^m - \left(\frac{\mathrm{x}_3}{A_{0R}}\right)^n\right] + (p_{eL} - p_{eR}) = 0. \end{cases} \quad (46)$$

From the first equation of (46) we obtain

$$\mathrm{x}_1 = \frac{q_L - q_R - c_R\mathrm{x}_3 + c_R A_R + c_L A_L}{c_L}, \quad (47)$$

so the second equation becomes

$$f_4(\mathrm{x}_3) = K_L\left[\left(\frac{q_L - q_R - c_R\mathrm{x}_3 + c_R A_R + c_L A_L}{c_L A_{0L}}\right)^m - \right.$$
$$\left. -\left(\frac{q_L - q_R - c_R\mathrm{x}_3 + c_R A_R + c_L A_L}{c_L A_{0L}}\right)^n\right] -$$
$$- K_R\left[\left(\frac{\mathrm{x}_3}{A_{0R}}\right)^m - \left(\frac{\mathrm{x}_3}{A_{0R}}\right)^n\right] + (p_{eL} - p_{eR}) = 0. \quad (48)$$

Equation (48) is solved with a globally convergent Newton-Raphson method of initial point A_R.

Having found $\mathrm{x}_3 = A^*_{LTR,R}$ from (48), we calculate $\mathrm{x}_1 = A^*_{LTR,L}$ from (47) and after that, we calculate $\mathrm{x}_2 = \mathrm{x}_4 = q^*_{LTR,L} = q^*_{LTR,R}$ from the first or the second of (42) in their linearized version, that is,

$$q^*_{LTR} = q_L - c_L(A^*_{LTR,L} - A_L), \text{ or } q^*_{LTR} = q_R + c_R(A^*_{LTR,R} - A_R). \quad (49)$$

It is worth noting that, while in Section 5.1 for both arteries and veins a nonlinear system must be solved (with a globally convergent Newton–Raphson method), in this case it is necessary to solve only equation (48) for both arteries and veins. Putting $n = 0$ for arteries, the numerical computation in this case results to be even more efficient.

The values of $\phi^*_{LTR,L}$ and $\phi^*_{LTR,R}$ are calculated from Proposition 6, that is,

$$\phi^*_{LTR,L} = \frac{A_L}{A^*_{LTR,L}}\phi_L, \qquad \phi^*_{LTR,R} = \frac{A_R}{A^*_{LTR,R}}\phi_R.$$

6 | Advection-Pressure Numerical Splitting Schemes for the Complete System of 1D Blood Flow Equations With Transport

In this section we present the two new splitting schemes for the complete system of 1D blood flow equations with transport (11), built including the two approximate Riemann solvers for the pressure system treated in Section 5. We work within the path-conservative framework presented in Parés [30]. At the beginning we provide a brief introduction to path-conservative schemes. Subsequently we present our new splitting schemes in which we avoid the use of any path, thus simplifying the computational complexity.

6.1 | A Brief Overview of the Path-Conservative Approach

Considering a general $N \times N$ quasi-linear hyperbolic system

$$\partial_t \mathbf{Q} + \mathbf{M}(\mathbf{Q})\partial_x \mathbf{Q} = \mathbf{0}, \tag{50}$$

with the vectors of variables denoted as

$$\mathbf{Q} = [q_1, q_2, ..., q_N]^T \in \Omega_q.$$

Here, Ω_q is the so-called domain of definition of PDEs (50) and is supposed to be a convex set.

Definition 1 (Path). $\boldsymbol{\Psi}(\mathbf{Q}_L, \mathbf{Q}_R, s)$ with $0 \le s \le 1$, is a Lipschitz continuous function that connects the left state $\mathbf{Q}_L$ to the right state $\mathbf{Q}_R$ in phase space, satisfying

$$\boldsymbol{\Psi}(\mathbf{Q}_L, \mathbf{Q}_R, 0) = \mathbf{Q}_L, \qquad \boldsymbol{\Psi}(\mathbf{Q}_L, \mathbf{Q}_R, 1) = \mathbf{Q}_R.$$

Parés [30] proposed a simple straight-line segment path

$$\boldsymbol{\Psi}(\mathbf{Q}_L, \mathbf{Q}_R, s) = \mathbf{Q}_L + s(\mathbf{Q}_R - \mathbf{Q}_L), \quad \text{with } 0 \le s \le 1,$$

to connect the two states.

Definition 2 (Path-conservative scheme [30]). Given a family of paths $\boldsymbol{\Psi}$, a numerical scheme is said to be $\boldsymbol{\Psi}$-conservative (path-conservative) if it can be written under the form

$$\mathbf{Q}_i^{n+1} = \mathbf{Q}_i^n - \frac{\Delta t}{\Delta x}(\mathbf{D}^+_{i-\frac{1}{2}} + \mathbf{D}^-_{i+\frac{1}{2}}),$$

with

$$\mathbf{D}^{\pm}_{i+\frac{1}{2}} = \mathbf{D}^{\pm}(\mathbf{Q}_L, \mathbf{Q}_R),$$

where $\mathbf{Q}_L$ and $\mathbf{Q}_R$ are the left and right state with respect to $x_{i+\frac{1}{2}}$; $\mathbf{D}^-$ and $\mathbf{D}^+$ are two continuous functions satisfying

$$\mathbf{D}^{\pm}(\mathbf{Q}, \mathbf{Q}) = 0, \quad \forall \mathbf{Q} \in \Omega_q,$$

and

$$\mathbf{D}^-(\mathbf{Q}_L, \mathbf{Q}_R) + \mathbf{D}^+(\mathbf{Q}_L, \mathbf{Q}_R) = \mathbf{D}^-_{i+\frac{1}{2}} + \mathbf{D}^+_{i+\frac{1}{2}} =$$
$$= \int_0^1 \mathbf{M}(\boldsymbol{\Psi}(\mathbf{Q}_L, \mathbf{Q}_R, s)) \frac{\partial \boldsymbol{\Psi}}{\partial s}(\mathbf{Q}_L, \mathbf{Q}_R, s) ds,$$

for every $\mathbf{Q}_L, \mathbf{Q}_R \in \Omega_q$.

See Parés [30] to gain more information concerning the characteristics of a *path-conservative* scheme.

6.2 | The New Advection-Pressure Splitting Schemes

The first order, path-conservative method (Parés [30]) employed is thus

$$\mathbf{Q}_i^{n+1} = \mathbf{Q}_i^n - \frac{\Delta t}{\Delta x}(\mathbf{D}^+_{i-\frac{1}{2}} + \mathbf{D}^-_{i+\frac{1}{2}}), \tag{51}$$

where

$$\mathbf{Q}_i^n \approx \frac{1}{\Delta x}\int_{x_{i-\frac{1}{2}}}^{x_{i+\frac{1}{2}}} \mathbf{Q}(x, t^n) dx,$$

with $\Delta x = x_{i+\frac{1}{2}} - x_{i-\frac{1}{2}}$, $\Delta t = t^{n+1} - t^n$. The aim is to compute the fluctuations $\mathbf{D}^{\pm}_{i+\frac{1}{2}}$ without the necessity of introducing a path. First of all, we want to use the advection-pressure splitting technique already applied to the PDEs in Section 3, also for the numerical scheme, so we split the fluctuations in this way

$$\mathbf{D}^{\pm}_{i+\frac{1}{2}} = \mathbf{D}^{\pm}_{\mathcal{A},i+\frac{1}{2}} + \mathbf{D}^{\pm}_{\mathcal{P},i+\frac{1}{2}},$$

where $\mathbf{D}^{\pm}_{\mathcal{A},i+\frac{1}{2}}$ are the fluctuations related to the advection system and $\mathbf{D}^{\pm}_{\mathcal{P},i+\frac{1}{2}}$ are the fluctuations related to the pressure system.

From Parés [30] and Dumbser and Toro [46], we know that in case of conservative systems, given a consistent conservative first order numerical scheme with numerical flux function $\mathbf{F}_{i+\frac{1}{2}}$, it can be written under the form (51) by defining

$$\mathbf{D}^+_{i-\frac{1}{2}} = \mathbf{F}(\mathbf{Q}_i) - \mathbf{F}_{i-\frac{1}{2}}, \qquad \mathbf{D}^-_{i+\frac{1}{2}} = \mathbf{F}_{i+\frac{1}{2}} - \mathbf{F}(\mathbf{Q}_i), \tag{52}$$

where $\mathbf{F}$ is the physical conservative flux of the system.

We want to apply (52) to both the advection and pressure fluctuations. In the following subsections we explain the procedure.

6.2.1 | The Fluctuations for the Pressure System

The pressure system (23) is not conservative. However looking in more detail it can be observed that this latter is *locally* conservative. Before explaining extensively this concept, we present the following result.

Proposition 8. *The pressure system (23), (24) can be written in conservative form if the parameters K, A_0 and p_e are constant values in space and time. With these hypotheses we can define $\mathbf{F}_{\mathcal{P}}(\mathbf{Q})$ the physical conservative flux of the pressure system*

$$\mathbf{F}_{\mathcal{P}}(\mathbf{Q}) = \begin{bmatrix} Au \\ \int c(A)^2 \, dA \\ 0 \\ 0 \\ 0 \\ 0 \end{bmatrix} =$$

$$= \begin{bmatrix} Au \\ \frac{KA}{\rho}\left(\frac{m}{m+1}\left(\frac{A}{A_0}\right)^m - \frac{n}{n+1}\left(\frac{A}{A_0}\right)^n\right) \\ 0 \\ 0 \\ 0 \\ 0 \end{bmatrix}. \tag{53}$$

Proof. The motivation for (53) is clear: in case of parameters K, A_0 and p_e constant values in space and time, the 1D blood flow model (11) can be written in conservative form, and consequently the pressure system resulting from the splitting is conservative in turn (see Spilimbergo et al. [58]). In detail, the pressure system (23), (24) is

$$\begin{cases} \partial_t A + \partial_x(Au) = 0, \\ \partial_t(Au) + \frac{A}{\rho}\partial_x p = 0, \\ \partial_t K = 0, \\ \partial_t A_0 = 0, \\ \partial_t p_e = 0, \\ \partial_t(A\phi) = 0. \end{cases} \tag{54}$$

In case of parameters K, A_0 and p_e constant values in space and time, the pressure term of the second equation in (54) becomes

$$\frac{A}{\rho}\partial_x p = \frac{A}{\rho}\frac{\partial p}{\partial A}\partial_x A = c(A)^2\partial_x A = \partial_x \int c(A)^2 dA,$$

being c the wave speed in (13). □

As "consistent conservative first order numerical scheme" we use a Godunov-type scheme. Unfortunately the Godunov state at the interface $x_{i+\frac{1}{2}}$, for each cell i, does not exist in general for the pressure system derived from a non-conservative system of 1D blood flow equations. In fact we have two different solutions (exact or approximate) in the Star Region

$$\mathbf{Q}^*_{PRESS\ L,i+\frac{1}{2}} = \begin{bmatrix} A^*_{PRESS\ L,i+\frac{1}{2}} \\ q^*_{PRESS\ L,i+\frac{1}{2}} \\ K_{L,i+\frac{1}{2}} \\ A_{0L,i+\frac{1}{2}} \\ p_{eL,i+\frac{1}{2}} \\ A^*_{PRESS\ L,i+\frac{1}{2}}\phi^*_{PRESS\ L,i+\frac{1}{2}} \end{bmatrix},$$

$$\mathbf{Q}^*_{PRESS\ R,i+\frac{1}{2}} = \begin{bmatrix} A^*_{PRESS\ R,i+\frac{1}{2}} \\ q^*_{PRESS\ R,i+\frac{1}{2}} \\ K_{R,i+\frac{1}{2}} \\ A_{0R,i+\frac{1}{2}} \\ p_{eR,i+\frac{1}{2}} \\ A^*_{PRESS\ R,i+\frac{1}{2}}\phi^*_{PRESS\ R,i+\frac{1}{2}} \end{bmatrix}, \tag{55}$$

of the Riemann problem for the pressure system

$$\begin{cases} \partial_t \mathbf{Q} + \boldsymbol{\mathcal{P}}(\mathbf{Q})\partial_x \mathbf{Q} = \mathbf{0}, \quad x \in \mathbb{R}, \quad t > t^n, \\ \mathbf{Q}(x, t^n) = \begin{cases} \mathbf{Q}_L = \mathbf{Q}^n_i & \text{if} \quad x < x_{i+\frac{1}{2}}, \\ \mathbf{Q}_R = \mathbf{Q}^n_{i+1} & \text{if} \quad x > x_{i+\frac{1}{2}}, \end{cases} \end{cases} \tag{56}$$

for each cell i, with $\boldsymbol{\mathcal{P}}(\mathbf{Q})$ defined in (24).

However the fluctuations for the pressure system from (52) finally can be written as

$$\begin{aligned} \mathbf{D}^+_{\boldsymbol{\mathcal{P}},i-\frac{1}{2}} &= \mathbf{F}_{\boldsymbol{\mathcal{P}}}(\mathbf{Q}_i) - \mathbf{F}_{\boldsymbol{\mathcal{P}}}(\mathbf{Q}^*_{PRESS\ R,i-\frac{1}{2}}), \\ \mathbf{D}^-_{\boldsymbol{\mathcal{P}},i+\frac{1}{2}} &= \mathbf{F}_{\boldsymbol{\mathcal{P}}}(\mathbf{Q}^*_{PRESS\ L,i+\frac{1}{2}}) - \mathbf{F}_{\boldsymbol{\mathcal{P}}}(\mathbf{Q}_i), \end{aligned} \tag{57}$$

considering that for each cell i, $\mathbf{Q}_i$, $\mathbf{Q}^*_{PRESS\ L,i+\frac{1}{2}}$ and $\mathbf{Q}^*_{PRESS\ R,i-\frac{1}{2}}$ share the same values of the parameters K, A_0 and p_e, thus the pressure system (23) is locally conservative between these states, and $\mathbf{Q}^*_{PRESS\ L,i+\frac{1}{2}}$ and $\mathbf{Q}^*_{PRESS\ R,i-\frac{1}{2}}$ are taken as approximation of the sought Godunov states.

6.2.2 | The Fluctuations for the Advection System

It is worth noting that the advection system (22) is actually conservative, that is, it can be written as

$$\partial_t \mathbf{Q} + \partial_x \mathbf{F}_{\boldsymbol{\mathcal{A}}}(\mathbf{Q}) = \mathbf{0},$$

with the physical flux

$$\mathbf{F}_{\boldsymbol{\mathcal{A}}}(\mathbf{Q}) = \begin{bmatrix} 0 \\ \alpha A u^2 \\ 0 \\ 0 \\ 0 \\ Au\phi \end{bmatrix}.$$

(52) is adapted into

$$\begin{aligned} \mathbf{D}^+_{\boldsymbol{\mathcal{A}},i-\frac{1}{2}} &= \mathbf{F}_{\boldsymbol{\mathcal{A}}}(\mathbf{Q}_i) - \boldsymbol{\mathcal{A}}_{i-\frac{1}{2}}, \\ \mathbf{D}^-_{\boldsymbol{\mathcal{A}},i+\frac{1}{2}} &= \boldsymbol{\mathcal{A}}_{i+\frac{1}{2}} - \mathbf{F}_{\boldsymbol{\mathcal{A}}}(\mathbf{Q}_i). \end{aligned} \tag{58}$$

The numerical flux $\boldsymbol{\mathcal{A}}_{i+\frac{1}{2}}$ is taken as a modification of the TV-advection flux defined in [57, 58] for the conservative 1D blood flow model and is defined as

$$\boldsymbol{\mathcal{A}}_{i+\frac{1}{2}} = \begin{bmatrix} 0 \\ \alpha q^*_{PRESS,i+\frac{1}{2}} u_{i+\frac{1}{2}} \\ 0 \\ 0 \\ 0 \\ q^*_{PRESS,i+\frac{1}{2}}\phi_{i+\frac{1}{2}} \end{bmatrix}, \tag{59}$$

where, recalling Proposition 7

$$q^*_{PRESS,i+\frac{1}{2}} = q^*_{PRESS\,L,i+\frac{1}{2}} = q^*_{PRESS\,R,i+\frac{1}{2}}, \tag{60}$$

is the second component of (55). It is worth noting that although the advection system is conservative, and thus the Godunov state calculated at $x_{i+\frac{1}{2}}$, for each cell i, does exist, in our case we are using the solution of the Riemann problem for the pressure system (55), this latter lacking this particular state; thus (60) is defined *by continuity* (Proposition 7). Instead $u_{i+\frac{1}{2}}$ and $\phi_{i+\frac{1}{2}}$ are defined by approximation. We propose to use

$$u_{i+\frac{1}{2}} = \begin{cases} u_L & \text{if} \begin{cases} q^*_{PRESS,i+\frac{1}{2}} > 0, \\ K_{L,i+\frac{1}{2}} = K_{R,i+\frac{1}{2}}, \\ A_{0L,i+\frac{1}{2}} = A_{0R,i+\frac{1}{2}}, \\ p_{eL,i+\frac{1}{2}} = p_{eR,i+\frac{1}{2}}, \end{cases} \\ u_R & \text{if} \begin{cases} q^*_{PRESS,i+\frac{1}{2}} \le 0, \\ K_{L,i+\frac{1}{2}} = K_{R,i+\frac{1}{2}}, \\ A_{0L,i+\frac{1}{2}} = A_{0R,i+\frac{1}{2}}, \\ p_{eL,i+\frac{1}{2}} = p_{eR,i+\frac{1}{2}}, \end{cases} \\ \frac{u^*_{PRESS\,L,i+\frac{1}{2}} + u^*_{PRESS\,R,i+\frac{1}{2}}}{2} & \text{if} \begin{cases} K_{L,i+\frac{1}{2}} \neq K_{R,i+\frac{1}{2}}, \\ A_{0L,i+\frac{1}{2}} \neq A_{0R,i+\frac{1}{2}}, \\ p_{eL,i+\frac{1}{2}} \neq p_{eR,i+\frac{1}{2}}, \end{cases} \end{cases} \tag{61}$$

$$\phi_{i+\frac{1}{2}} = \begin{cases} \phi_L & \text{if} \quad q^*_{PRESS,i+\frac{1}{2}} > 0, \\ \phi_R & \text{if} \quad q^*_{PRESS,i+\frac{1}{2}} \le 0. \end{cases} \tag{62}$$

6.2.3 | The Final Splitting Schemes for the Complete System of 1D Blood Flow Equations

Finally scheme (51) becomes

$$\mathbf{Q}_i^{n+1} = \mathbf{Q}_i^n - \frac{\Delta t}{\Delta x}(\mathbf{D}^+_{\mathcal{A},i-\frac{1}{2}} + \mathbf{D}^-_{\mathcal{A},i+\frac{1}{2}}) - \frac{\Delta t}{\Delta x}(\mathbf{D}^+_{\mathcal{P},i-\frac{1}{2}} + \mathbf{D}^-_{\mathcal{P},i+\frac{1}{2}}),$$

that with (57) and (58) is

$$\begin{aligned} \mathbf{Q}_i^{n+1} =& \mathbf{Q}_i^n - \frac{\Delta t}{\Delta x}(\mathbf{F}_{\mathcal{A}}(\mathbf{Q}_i^n) - \mathcal{A}_{i-\frac{1}{2}} + \mathcal{A}_{i+\frac{1}{2}} - \mathbf{F}_{\mathcal{A}}(\mathbf{Q}_i^n)) - \\ & - \frac{\Delta t}{\Delta x}(\mathbf{F}_{\mathcal{P}}(\mathbf{Q}_i^n) - \mathbf{F}_{\mathcal{P}}(\mathbf{Q}^*_{PRESS\,R,i-\frac{1}{2}}) + \\ & + \mathbf{F}_{\mathcal{P}}(\mathbf{Q}^*_{PRESS\,L,i+\frac{1}{2}}) - \mathbf{F}_{\mathcal{P}}(\mathbf{Q}_i^n)). \end{aligned} \tag{63}$$

Simplifying (63) the final scheme is

$$\begin{aligned} \mathbf{Q}_i^{n+1} =& \mathbf{Q}_i^n - \frac{\Delta t}{\Delta x}(\mathcal{A}_{i+\frac{1}{2}} - \mathcal{A}_{i-\frac{1}{2}}) - \\ & - \frac{\Delta t}{\Delta x}(\mathbf{F}_{\mathcal{P}}(\mathbf{Q}^*_{PRESS\,L,i+\frac{1}{2}}) - \mathbf{F}_{\mathcal{P}}(\mathbf{Q}^*_{PRESS\,R,i-\frac{1}{2}})). \end{aligned} \tag{64}$$

Considering (64) we present two possibilities for $\mathbf{Q}^*_{PRESS\,J,i+\frac{1}{2}}$, $J = L, R$; that consequently lead to two different final numerical schemes:

TV*+TR in which $\mathbf{Q}^*_{PRESS\,L,i+\frac{1}{2}} = \mathbf{Q}^*_{TR,L,i+\frac{1}{2}}$ and $\mathbf{Q}^*_{PRESS\,R,i+\frac{1}{2}} = \mathbf{Q}^*_{TR,R,i+\frac{1}{2}}$, the approximate two rarefaction solution of the Riemann problem for the pressure system (56) in the Star Region presented in Section 5.1, for each cell i,

TV*+Lin.TR in which $\mathbf{Q}^*_{PRESS\,L,i+\frac{1}{2}} = \mathbf{Q}^*_{LTR,L,i+\frac{1}{2}}$ and $\mathbf{Q}^*_{PRESS\,R,i+\frac{1}{2}} = \mathbf{Q}_{LTR,R,i+\frac{1}{2}}$, the approximate linearized two rarefaction solution of the Riemann problem for the pressure system (56) in the Star Region presented in Section 5.2, for each cell i.

Remark 6. A key property of a numerical scheme is its ability to accurately resolve solution features related to intermediate, possibly slow moving, waves. A specific case for the PDEs system under study in this article, is that of an isolated discontinuity in the passive scalar ϕ. Below we show that the numerical schemes proposed in this section preserve exactly this type of discontinuities if the solution is stationary ($u(x,t) = 0$, $\forall x \in \mathbb{R}$, $\forall t \in \mathbb{R}^+_0$).

Proposition 9. *The two new presented splitting methods,* **TV*+TR** *and* **TV*+Lin.TR**, *solve exactly isolated stationary discontinuities for the passive scalar ϕ.*

Proof. Consider a Riemann problem with the following initial conditions

$$\mathbf{Q}(x,0) = \begin{cases} \tilde{\mathbf{Q}}_L & \text{if} \quad x < x_d, \\ \tilde{\mathbf{Q}}_R & \text{if} \quad x > x_d, \end{cases} \tag{65}$$

with

$$\tilde{\mathbf{Q}}_L = \begin{bmatrix} A_L \\ 0 \\ K_L \\ A_{0L} \\ p_{eL} \\ A_L\phi_L \end{bmatrix}, \qquad \tilde{\mathbf{Q}}_R = \begin{bmatrix} A_R \\ 0 \\ K_R \\ A_{0R} \\ p_{eR} \\ A_R\phi_R \end{bmatrix}, \tag{66}$$

and with $p(\tilde{\mathbf{Q}}_L) = p(\tilde{\mathbf{Q}}_R)$, being p the pressure (4). These initial conditions correspond to a stationary exact solution of the Riemann problem for the complete system (10). This can be easily proved. For the details of the exact solution of the Riemann problem for the 1D blood flow equation with an advection equation for the passive scalar transport and a general constant momentum correction coefficient see Spilimbergo [62], and also Spilimbergo et al. [43] for the same model without the passive scalar. The exact solution of the Riemann problem for the 1D blood flow equations with transport, for a momentum correction coefficient $\alpha = 1$, is also described in [38, 42].

Actually the initial data (65), (66) lead to a (two-rarefaction approximate) stationary solution also of the Riemann problem for the pressure system (39), in fact substituting (66) as the unknowns in (42), this latter system is solved.

Assume the discretization of the domain $[x_L, x_R]$ is such that the index of the cell just to the left of x_d is ζ and that the one of the cell immediately to the right of the x_d is $\zeta + 1$. In this case, the initial conditions for the numerical scheme (64) are

$$\mathbf{Q}_i^0 = \begin{cases} \tilde{\mathbf{Q}}_L & \text{if} \quad i < \zeta, \\ \tilde{\mathbf{Q}}_R & \text{if} \quad i > \zeta, \end{cases} \qquad \text{for each cell } i. \tag{67}$$

Then, by construction, the Newton-Raphson method described in Appendix C, employed to solve numerically system (42), preserves the stationary solution of the Riemann problem for the pressure system, since in this case (66) used as initial guess for the method, solves the nonlinear system (42) exactly. Therefore, the numerical solution provided by the two-rarefaction approximate Riemann problem solver will necessarily be (67) $\forall\, t > 0$, with the consequence that $\mathbf{Q}^*_{\text{PRESS } L,i+\frac{1}{2}} = \mathbf{Q}_i^n$ and $\mathbf{Q}^*_{\text{PRESS } R,i+\frac{1}{2}} = \mathbf{Q}_{i+1}^n$, $\forall$ cell i where they exist; subsequently $\forall$ cell i $\mathbf{Q}^*_{\text{PRESS } L,i+\frac{1}{2}} = \mathbf{Q}^*_{\text{PRESS } R,i-\frac{1}{2}}$. It follows that, from (64), method **TV*+TR** becomes

$$\mathbf{Q}_i^{n+1} = \mathbf{Q}_i^n - \frac{\Delta t}{\Delta x}(\boldsymbol{\mathcal{A}}_{i+\frac{1}{2}} - \boldsymbol{\mathcal{A}}_{i-\frac{1}{2}}).$$

In particular, since $q^*_{\text{PRESS } L,i+\frac{1}{2}} = q^*_{\text{PRESS } R,i-\frac{1}{2}} = 0 \;\; \forall\, i$, it follows that

$$\boldsymbol{\mathcal{A}}_{i+\frac{1}{2}} = \begin{bmatrix} 0 \\ 0 \\ 0 \\ 0 \\ 0 \\ 0 \end{bmatrix} \qquad \forall i,$$

consequently $\mathbf{Q}_i^{n+1} = \mathbf{Q}_i^n$, $\forall\, i$ and $\forall$ successive time steps n. In conclusion method **TV*+TR** solves exactly the stationary contact discontinuity for the passive scalar of the complete 1D blood flow model (10).

A similar discussion can be made for the case of method **TV*+Lin.TR**, and for the linearized solver presented in Section 5.2.

It is worth noting that the aforementioned property depends on the specific solver used for the approximate solution of the Riemann problem for the pressure system and not on the splitting itself. □

7 | Numerical Results

Within this section, we present test problems and evaluate the effectiveness of the numerical splitting methods of type TV: **TV*+TR**, **TV*+Lin.TR** introduced in Section 6. We propose seven test problems; these tests have been chosen to represent the different admissible solutions of the non-conservative 1D blood flow equations (11), (12), in the case of arteries (Tests 1, 2, 3) and veins (Tests 4, 5, 6, 7), namely smooth solutions (rarefactions), elastic jumps (shocks), and contact discontinuities. The contact discontinuity, out of the three waves, typically proves to be the most challenging. This is particularly true for linearized or incomplete solvers, as they encounter excessive numerical diffusion resulting in the smearing of the contact discontinuity. The two new methods presented will prove to be able to capture also these waves.

Tests are constructed to provide an explanation of the necessity to substitute the TV-advection flux already presented in [57, 58] for modeling the complete conservative 1D blood flow model, with the new proposed numerical advection flux (59), to handle non-conservative systems. The aforementioned TV-advection flux for conservative blood flow equations was

$$\boldsymbol{A}_{TV,i+\frac{1}{2}} = \begin{bmatrix} 0 \\ \alpha q^*_{PRESS,i+\frac{1}{2}} u_{TV,i+\frac{1}{2}} \\ 0 \\ 0 \\ 0 \\ q^*_{PRESS,i+\frac{1}{2}} \phi_{i+\frac{1}{2}} \end{bmatrix}, \tag{68}$$

where

$$u_{TV,i+\frac{1}{2}} = \begin{cases} u_L & \text{if} \quad q^*_{PRESS,i+\frac{1}{2}} > 0, \\ u_R & \text{if} \quad q^*_{PRESS,i+\frac{1}{2}} \leq 0, \end{cases}$$

while $\phi_{i+\frac{1}{2}}$ was as in (62) [57, 58]. The use of (68) for the non-conservative 1D blood flow model leads to a lack of accuracy in the results of certain tests, as it will be shown in the next sections.

In addition, in case of veins, the tests are designed to explore different placements of A_{cL} and A_{cR} in (27) with respect to the range of the test results. These values are of crucial importance in determining the wave pattern of the pressure system resulting from the splitting at the level of PDEs (Section 3), in fact, for some particular positions of these terms, compound waves can arise. It is worth noting that this specific matter will not be addressed from the theoretical point of view in this article, instead, the focus is on demonstrating the effectiveness of the presented schemes, even in cases where the genuine nonlinearity of the $\lambda_{\mathcal{P}_1}$- and $\lambda_{\mathcal{P}_6}$-characteristic fields of the pressure system is lost.

The numerical results of methods **TV*+TR** and **TV*+Lin.TR** are compared with the exact solution of the Riemann problem for the full system of non-conservative 1D blood flow equations (11), (12), and selected methods in literature. The initial data, expressed in terms of the physical variables A, u, and ϕ, and the parameters K, A_0 and p_e can be found in Table 1. The other model parameters are provided in Table 2. The description of the numerical results is covered in Section 7.1, while an efficiency test is performed in Section 7.2.

7.1 | Results

The numerical results for both methods **TV*+TR** and **TV*+Lin.TR** (also called TV*-methods) are plotted against the exact solution of the Riemann problem for the full system of non-conservative 1D blood flow equations (11), (12), [38, 42, 43, 62], and the results of the following numerical methods

TABLE 1 | Left and right initial conditions for Tests from 1 to 7. The units of measures used for this article are: m, s, kg, Pa.

	Test	$A_L[m^2]$	$u_L[m/s]$	$K_L[Pa]$	$A_{0L}[m^2]$	$p_{eL}[Pa]$	ϕ_L
Left data	1	$1.0228A_{0L}$	0.0	K_{ref}	$2.0A_{0,ref}$	9999.15	1.0
	2	$1.6A_{0L}$	1.0	K_{ref}	$0.5A_{0,ref}$	3999.66	1.0
	3	$1.1A_{0L}$	1.0	K_{ref}	$0.5A_{0,ref}$	3999.66	0.5
	4	$1.8 \cdot 10^{-5}$	0.5	K_{ref}	$A_{0,ref}$	60.0	0.5
	5	A_{0L}	0.1	$60.0K_{ref}$	$A_{0,ref}$	100.0	0.5
	6	$1.3 \cdot 10^{-5}$	0.0	K_{ref}	$1.5A_{0,ref}$	40.0	0.5
	7	$1.5 \cdot 10^{-5}$	−0.3	$8.0K_{ref}$	$A_{0,ref}$	0.0	0.5
	Test	$A_R[m^2]$	$u_R[m/s]$	$K_R[Pa]$	$A_{0R}[m^2]$	$p_{eR}[Pa]$	ϕ_R
Right data	1	$0.9977A_{0R}$	0.0	$10.0K_{ref}$	$A_{0,ref}$	11340.56820743433	0.5
	2	$1.05A_{0R}$	0.0	$10.0K_{ref}$	$A_{0,ref}$	0.0	0.5
	3	$0.7A_{0R}$	−0.5	$10.0K_{ref}$	$0.2A_{0,ref}$	0.0	1.0
	4	$1.8 \cdot 10^{-5}$	−0.2	$0.7K_{ref}$	$1.2A_{0,ref}$	10.0	1.0
	5	A_{0R}	0.2	K_{ref}	$1.1A_{0,ref}$	60.0	1.0
	6	$1.9 \cdot 10^{-5}$	0.0	$10.0K_{ref}$	$A_{0,ref}$	0.0	1.0
	7	$2.0 \cdot 10^{-5}$	0.6	K_{ref}	$1.5A_{0,ref}$	10.0	1.0

TABLE 2 | Parameters used for Tests 1 to 7: blood density ρ; reference vessel wall stiffness K_{ref}; reference cross-sectional area $A_{0,ref}$; domain length ℓ; location of the initial discontinuity x_d and output time t_{End}. Regarding the resulting wave pattern, *R=rarefaction, S=shock, C_u=contact discontinuity associated with $\lambda = u$, C_0=contact discontinuity associated with $\lambda = 0$.*

Test	Vessel	Wave pattern	$\rho[kg/m^3]$	$K_{ref}[Pa]$	$A_{0,ref}[m^2]$	ℓ [m]	$x_d[m]$	$t_{End}[s]$
1	Artery	Stationary	1000.0	58725.0	$3.1353 \cdot 10^{-4}$	0.2	0.5ℓ	0.007
2	Artery	SC_0C_uS	1000.0	58725.0	$3.1353 \cdot 10^{-4}$	0.2	0.3ℓ	0.007
3	Artery	RC_0C_uS	1050.0	50000.0	$3.1353 \cdot 10^{-4}$	0.2	0.3ℓ	0.007
4	Vein	SC_0C_uS	1050.0	300.0	$2.8274 \cdot 10^{-5}$	0.5	0.5ℓ	0.2
5	Vein	RC_0C_uR	1000.0	33.0	$2.8274 \cdot 10^{-5}$	1.1	0.75ℓ	0.11
6	Vein	RC_0C_uS	1050.0	30.0	$2.8274 \cdot 10^{-5}$	0.5	0.4ℓ	0.25
7	Vein	SC_uC_0R	1050.0	300.0	$2.8274 \cdot 10^{-5}$	0.8	0.6ℓ	0.12

DOT+WB well-balanced version of DOT solver applied to the full system of non-conservative 1D blood flow equations (11), (12). This combines the DOT solver presented in Dumbser and Toro [46] with the path described in Müller and Toro [48], modified for a generic momentum correction coefficient (see [43, 62] for a detailed presentation)

TV+PMG+TR a numerical scheme for the full system of non-conservative 1D blood flow equations (11), (12). It combines the TV splitting at the level of PDEs presented in this article, the Parés-Muñoz-Godunov scheme (Parés and Muñoz [65]) applied to the pressure system, in conjunction with the approximate two-rarefaction Riemann solver for the pressure system described in Section 5.1, and the original TV-advection flux (68).

This scheme is a generalization of the TV+PMG+Ex.RS scheme described in Toro et al. [57] for non-conservative systems: in fact this latter was presented for a single discontinuous parameter without transport added and included an exact Riemann solver for the pressure system, considered only for the case of arteries. We extend the method to three discontinuous parameters and a passive scalar transport added, using the original TV-advection flux reported in (68) and substituting the exact Riemann solver with the approximate two-rarefaction one. This latter choice is necessary as we extend the discussion to veins, being the exact solution of the Riemann problem for the pressure system in case of veins nontrivial, due to the loss of genuine nonlinearity.

For both schemes the integrals defining the fluctuations are computed with a 3-points Gauss quadrature rule (see [43, 62]). All results are presented for two different values of the momentum correction coefficient α in (3), that is, $\alpha = 1$ associated with a uniform velocity profile, which corresponds to an inviscid fluid, and $\alpha = 4/3$, that is related to a parabolic velocity profile; and are calculated with a mesh of $I = 50$ computational cells (Figures 3–9) and a Courant–Friedrichs–Lewy number $C_{cfl} = 0.9$ defined as follows

Definition 3.

$$C_{cfl} = \frac{\Delta t}{\Delta x} S^n_{max}, \tag{69}$$

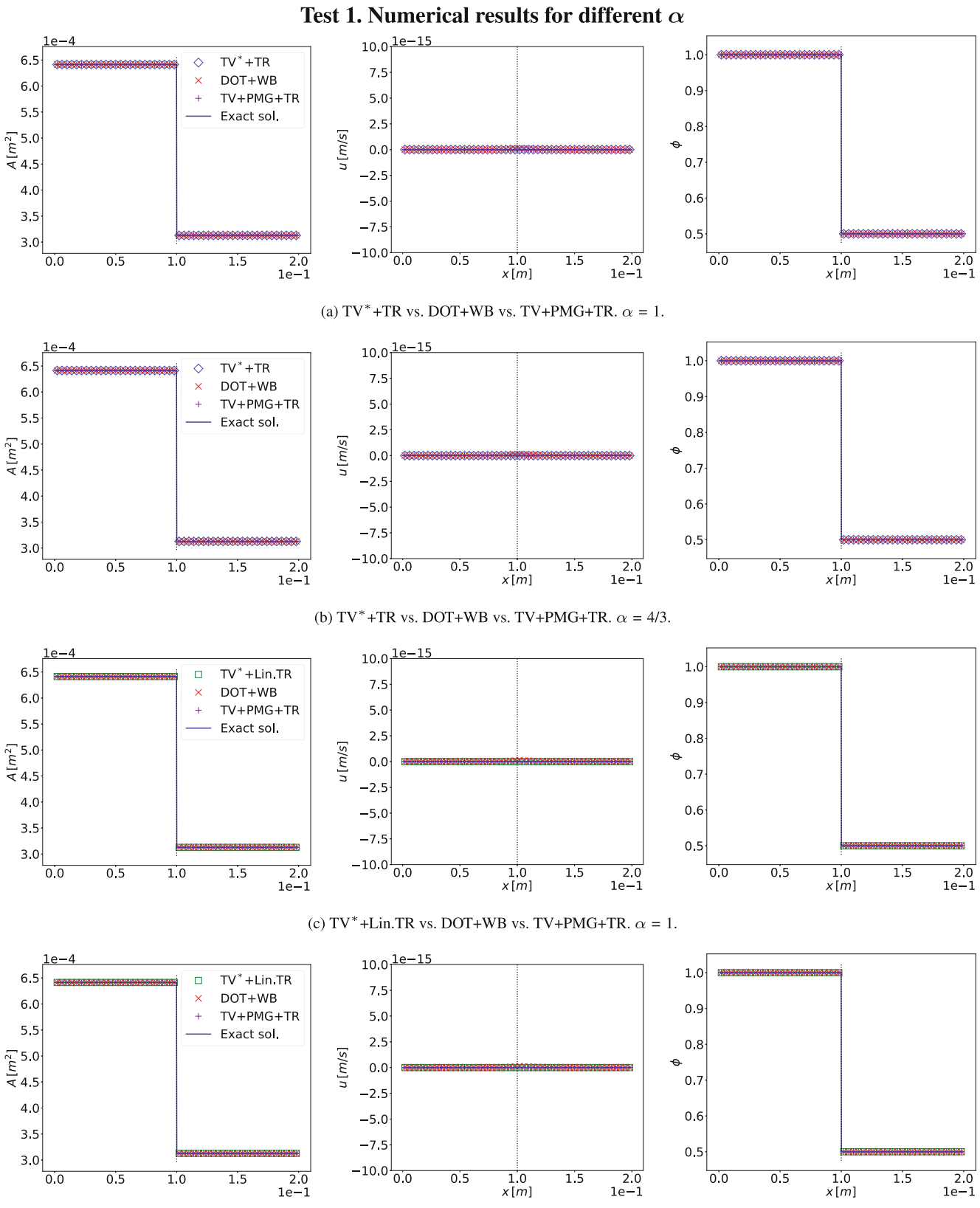

(a) TV*+TR vs. DOT+WB vs. TV+PMG+TR. $\alpha = 1$.

(b) TV*+TR vs. DOT+WB vs. TV+PMG+TR. $\alpha = 4/3$.

(c) TV*+Lin.TR vs. DOT+WB vs. TV+PMG+TR. $\alpha = 1$.

(d) TV*+Lin.TR vs. DOT+WB vs. TV+PMG+TR. $\alpha = 4/3$.

FIGURE 3 | Test 1. Artery. Stationary. Numerical results of methods **TV*+TR**, **TV*+Lin.TR** versus the DOT+WB solver, the TV+PMG+TR solver with $C_{cfl} = 0.9$, $I = 50$ cells, and the exact solution of the Riemann problem for the complete 1D non-conservative blood flow equations with momentum correction coefficient $\alpha = 1$ and $\alpha = 4/3$. Initial conditions and parameters are given in Tables 1 and 2. The dotted black vertical line displayed in the plots represents the initial discontinuity x_d. [Colour figure can be viewed at wileyonlinelibrary.com]

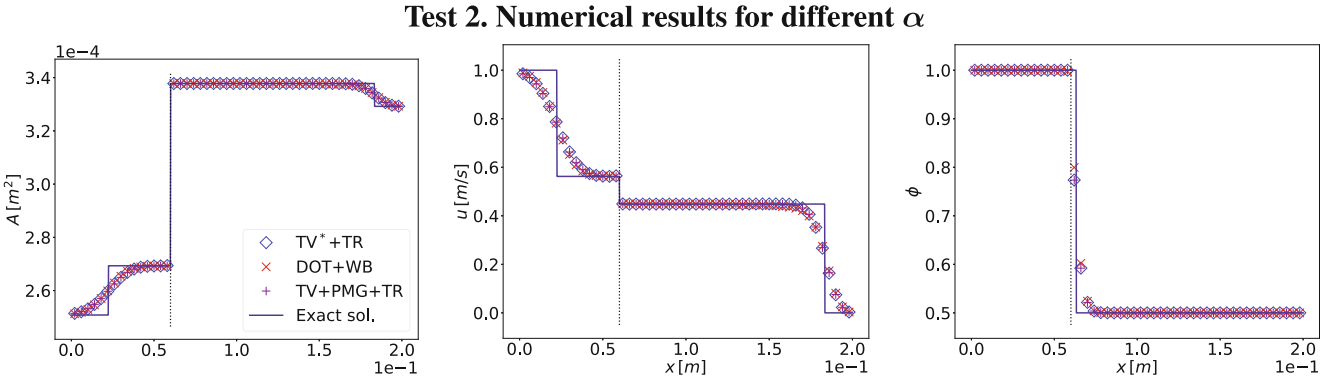

(a) TV*+TR vs. DOT+WB vs. TV+PMG+TR. $\alpha = 1$.

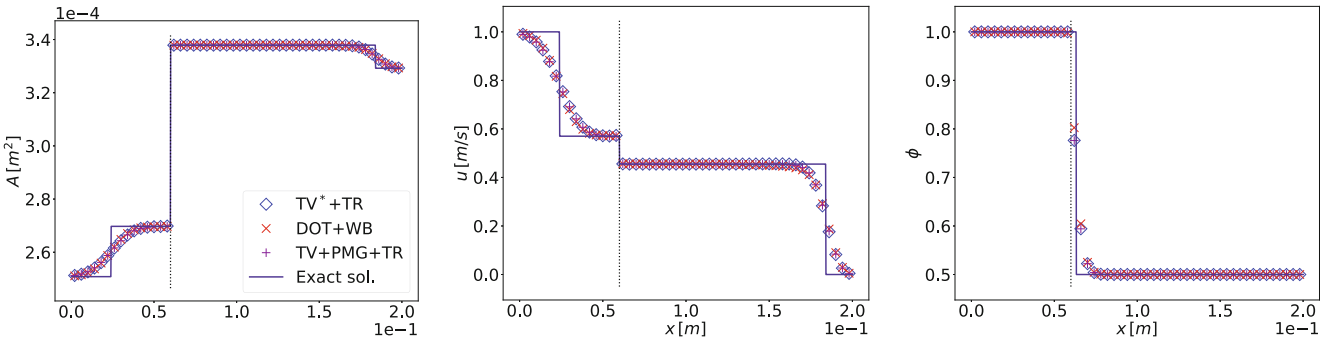

(b) TV*+TR vs. DOT+WB vs. TV+PMG+TR. $\alpha = 4/3$.

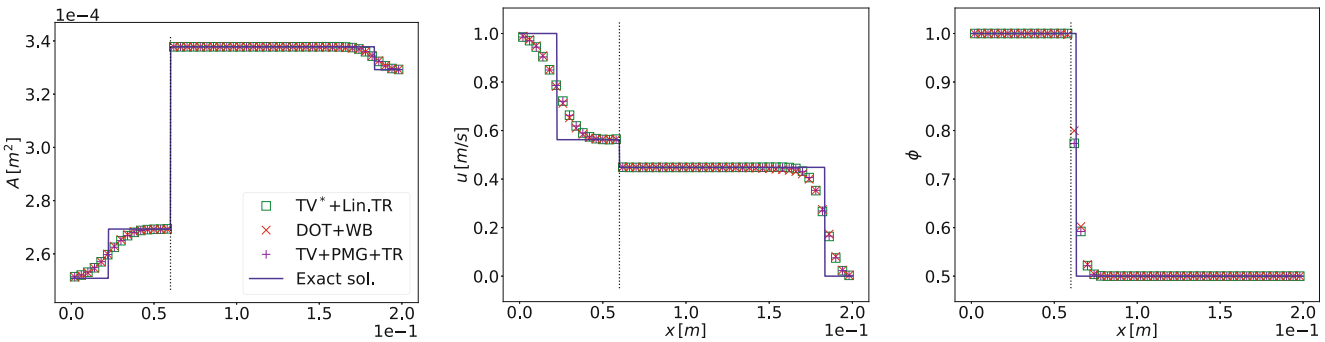

(c) TV*+Lin.TR vs. DOT+WB vs. TV+PMG+TR. $\alpha = 1$.

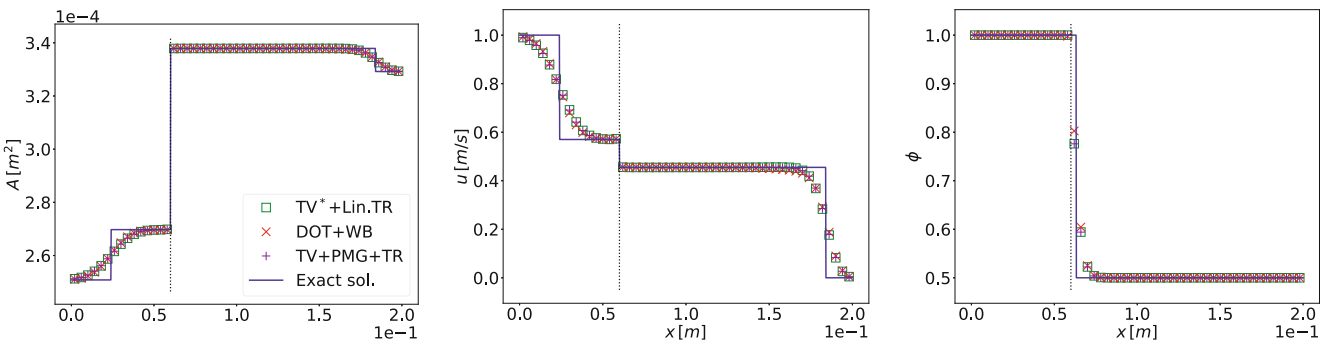

(d) TV*+Lin.TR vs. DOT+WB vs. TV+PMG+TR. $\alpha = 4/3$.

FIGURE 4 | Test 2. Artery. SC_0C_uS. Numerical results of methods **TV*+TR**, **TV*+Lin.TR** versus the DOT+WB solver, the TV+PMG+TR solver with $C_{cfl} = 0.9$, $I = 50$ cells, and the exact solution of the Riemann problem for the complete 1D non-conservative blood flow equations with momentum correction coefficient $\alpha = 1$ and $\alpha = 4/3$. Initial conditions and parameters are given in Tables 1 and 2. The dotted black vertical line displayed in the plots represents the initial discontinuity x_d. [Colour figure can be viewed at wileyonlinelibrary.com]

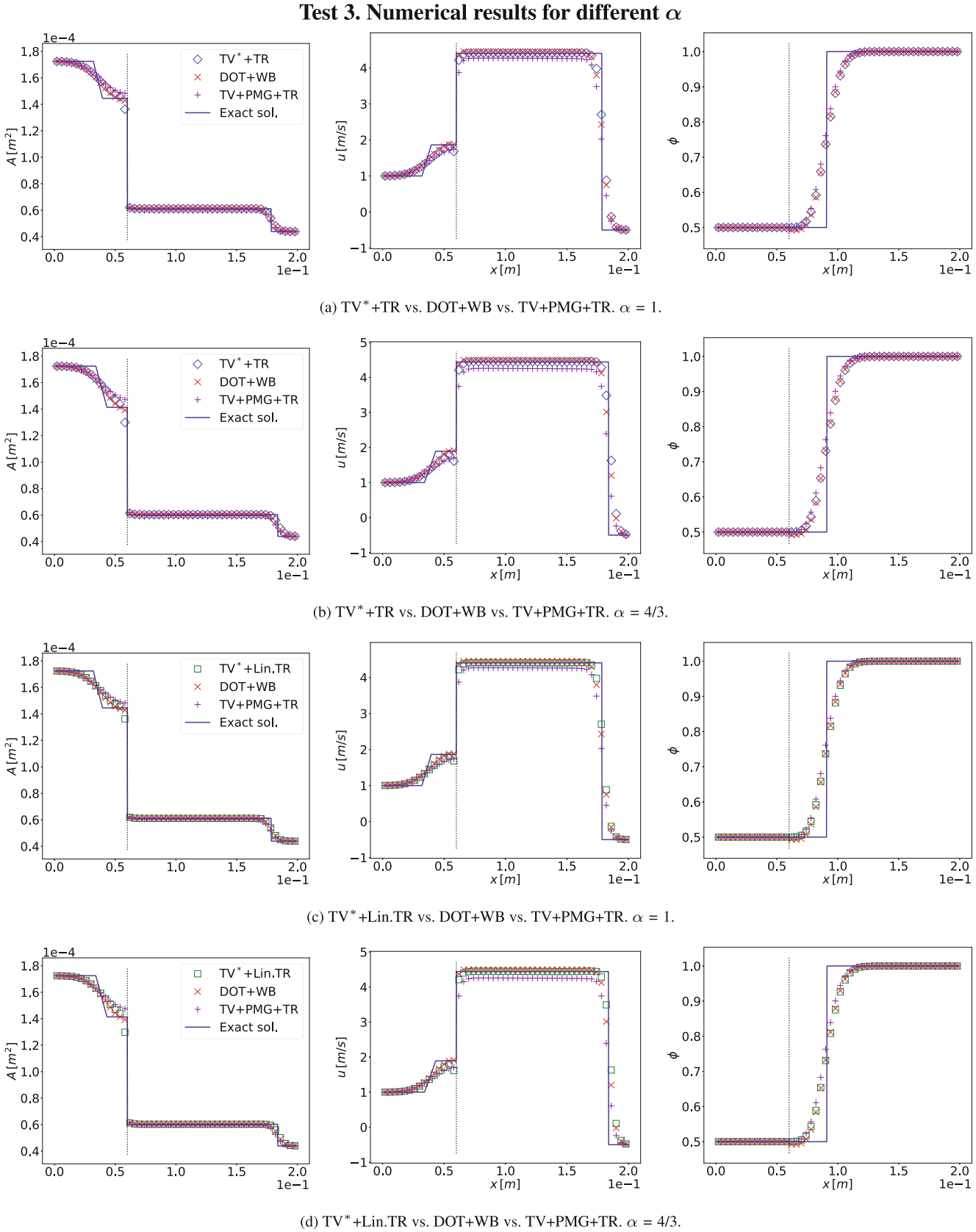

(a) TV*+TR vs. DOT+WB vs. TV+PMG+TR. $\alpha = 1$.

(b) TV*+TR vs. DOT+WB vs. TV+PMG+TR. $\alpha = 4/3$.

(c) TV*+Lin.TR vs. DOT+WB vs. TV+PMG+TR. $\alpha = 1$.

(d) TV*+Lin.TR vs. DOT+WB vs. TV+PMG+TR. $\alpha = 4/3$.

FIGURE 5 | Test 3. Artery. RC_0C_uS. Numerical results of methods **TV*+TR**, **TV*+Lin.TR** versus the DOT+WB solver, the TV+PMG+TR solver with $C_{cfl} = 0.9$, $I = 50$ cells, and the exact solution of the Riemann problem for the complete 1D non-conservative blood flow equations with momentum correction coefficient $\alpha = 1$ and $\alpha = 4/3$. Initial conditions and parameters are given in Tables 1 and 2. The dotted black vertical line displayed in the plots represents the initial discontinuity x_d. [Colour figure can be viewed at wileyonlinelibrary.com]

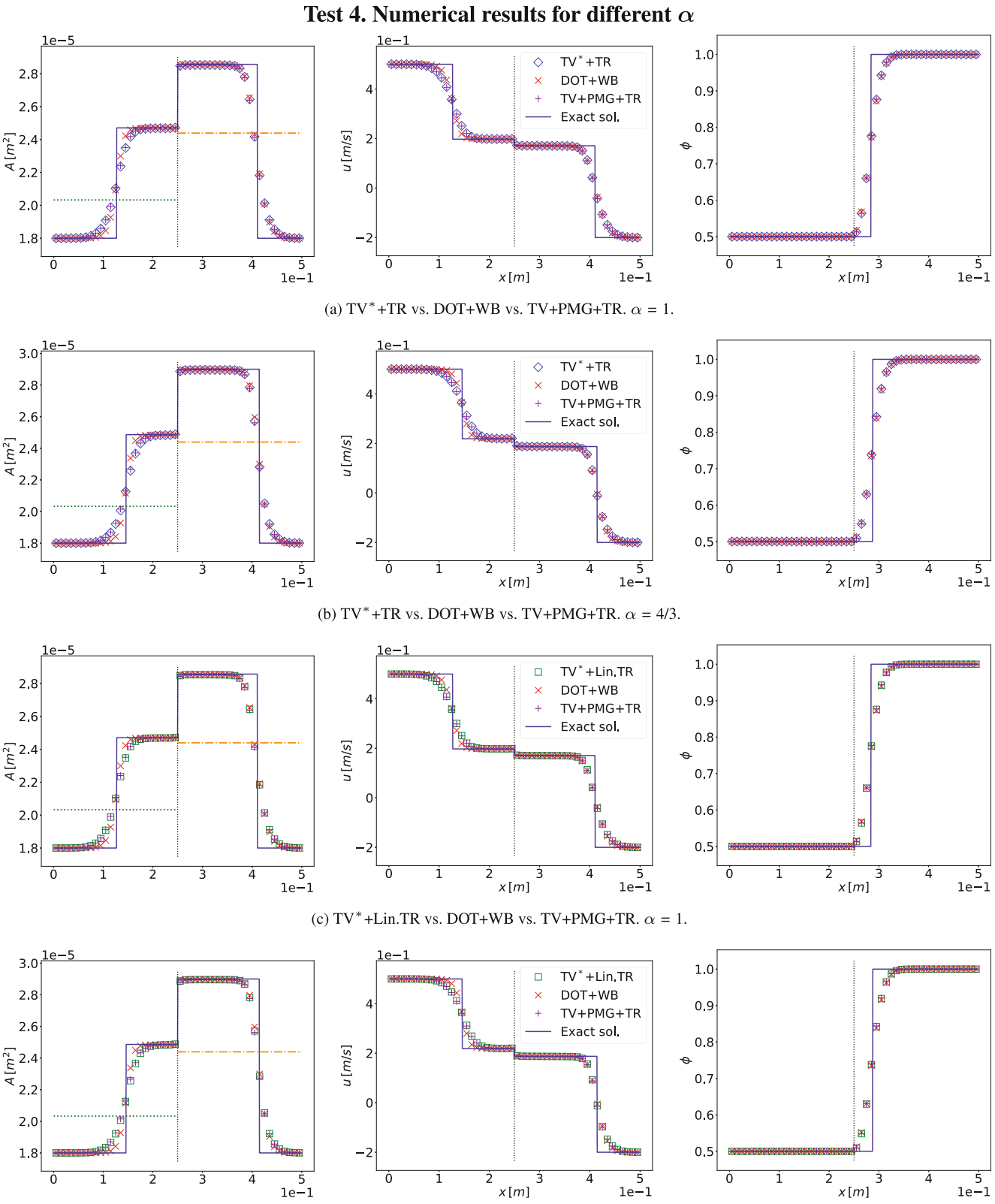

(a) TV*+TR vs. DOT+WB vs. TV+PMG+TR. $\alpha = 1$.

(b) TV*+TR vs. DOT+WB vs. TV+PMG+TR. $\alpha = 4/3$.

(c) TV*+Lin.TR vs. DOT+WB vs. TV+PMG+TR. $\alpha = 1$.

(d) TV*+Lin.TR vs. DOT+WB vs. TV+PMG+TR. $\alpha = 4/3$.

FIGURE 6 | Test 4. Vein. SC_0C_uS. Numerical results of methods **TV*+TR**, **TV*+Lin.TR** versus the DOT+WB solver, the TV+PMG+TR solver with $C_{cfl} = 0.9$, $I = 50$ cells, and the exact solution of the Riemann problem for the complete 1D non-conservative blood flow equations with momentum correction coefficient $\alpha = 1$ and $\alpha = 4/3$. Initial conditions and parameters are given in Tables 1 and 2. The dotted black vertical line displayed in the plots represents the initial discontinuity x_d. The horizontal lines depicted in the plots of the first column are: the dotted green one is the value of A_{cL} in (27), the dashed orange one is the value of A_{cR} in (27). [Colour figure can be viewed at wileyonlinelibrary.com]

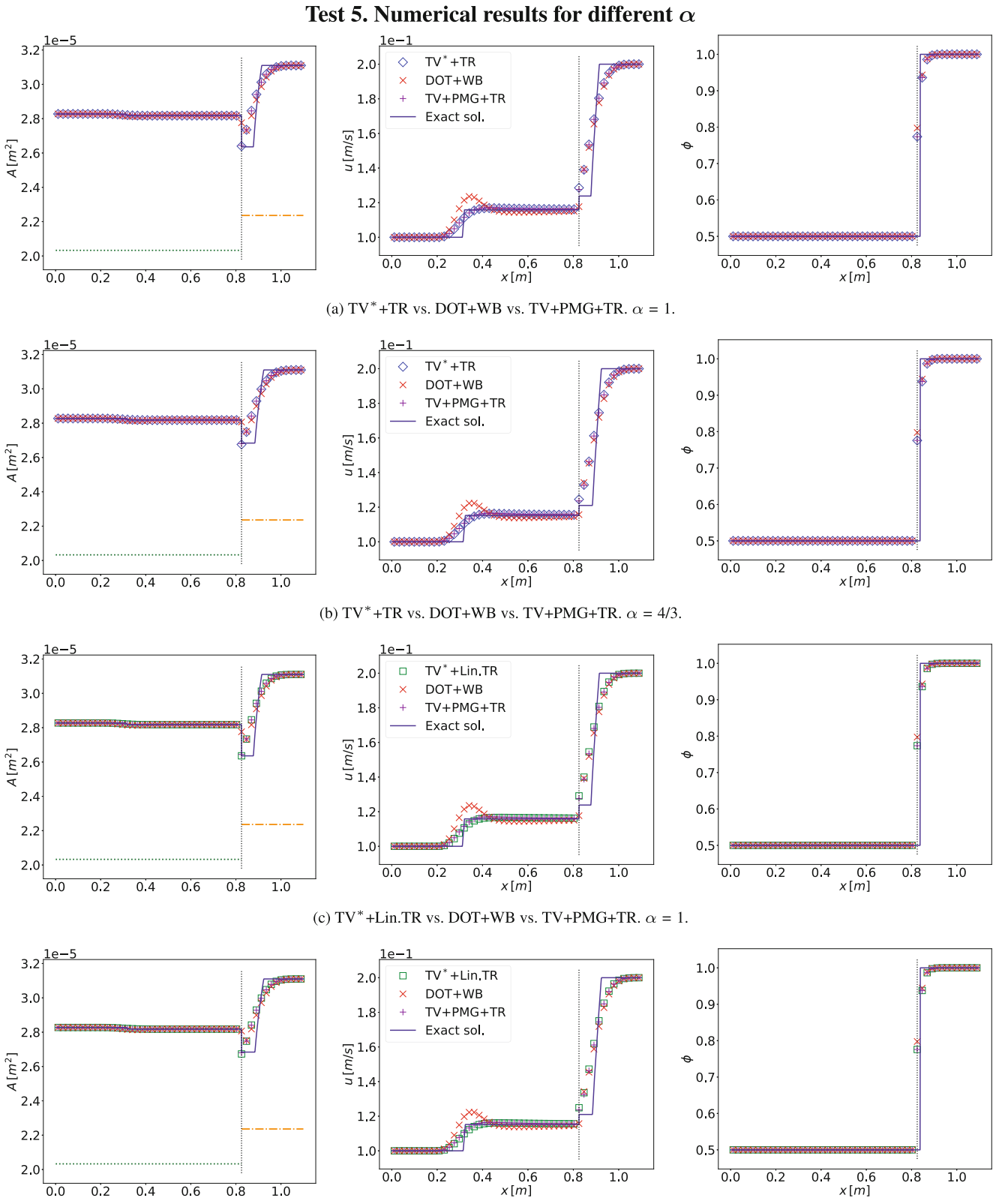

(a) TV*+TR vs. DOT+WB vs. TV+PMG+TR. $\alpha = 1$.

(b) TV*+TR vs. DOT+WB vs. TV+PMG+TR. $\alpha = 4/3$.

(c) TV*+Lin.TR vs. DOT+WB vs. TV+PMG+TR. $\alpha = 1$.

(d) TV*+Lin.TR vs. DOT+WB vs. TV+PMG+TR. $\alpha = 4/3$.

FIGURE 7 | Test 5. Vein. RC_0C_uR. Numerical results of methods **TV*+TR**, **TV*+Lin.TR** versus the DOT+WB solver, the TV+PMG+TR solver with $C_{cfl} = 0.9$, $I = 50$ cells, and the exact solution of the Riemann problem for the complete 1D non-conservative blood flow equations with momentum correction coefficient $\alpha = 1$ and $\alpha = 4/3$. Initial conditions and parameters are given in Tables 1 and 2. The dotted black vertical line displayed in the plots represents the initial discontinuity x_d. The horizontal lines depicted in the plots of the first column are: the dotted green one is the value of A_{eL} in (27), the dashed orange one is the value of A_{eR} in (27). [Colour figure can be viewed at wileyonlinelibrary.com]

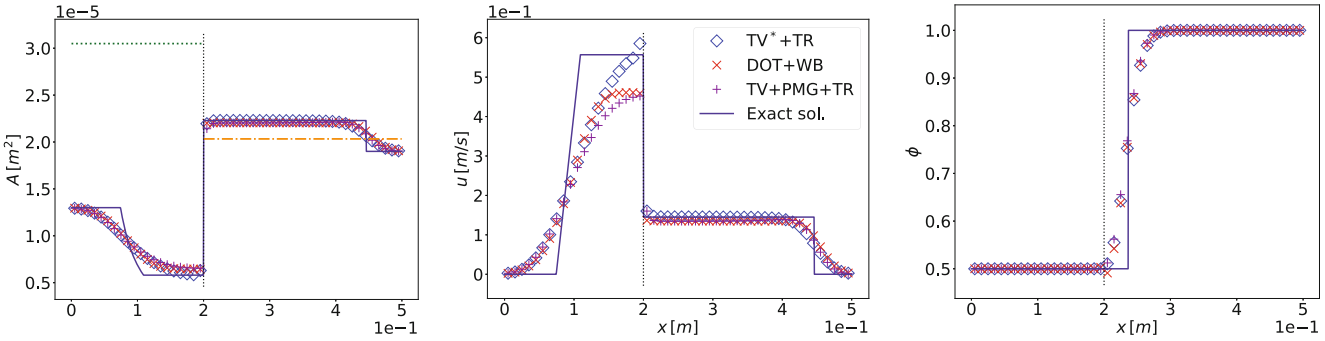

(a) TV*+TR vs. DOT+WB vs. TV+PMG+TR. $\alpha = 1$.

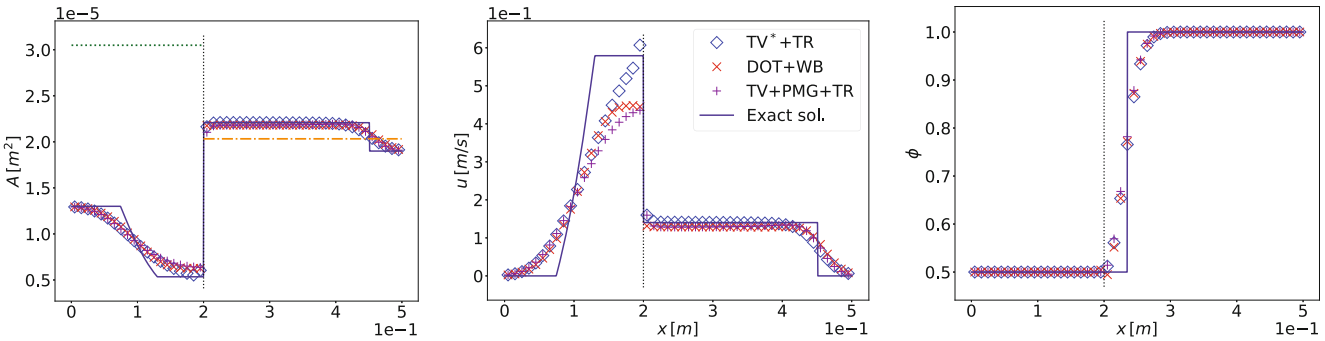

(b) TV*+TR vs. DOT+WB vs. TV+PMG+TR. $\alpha = 4/3$.

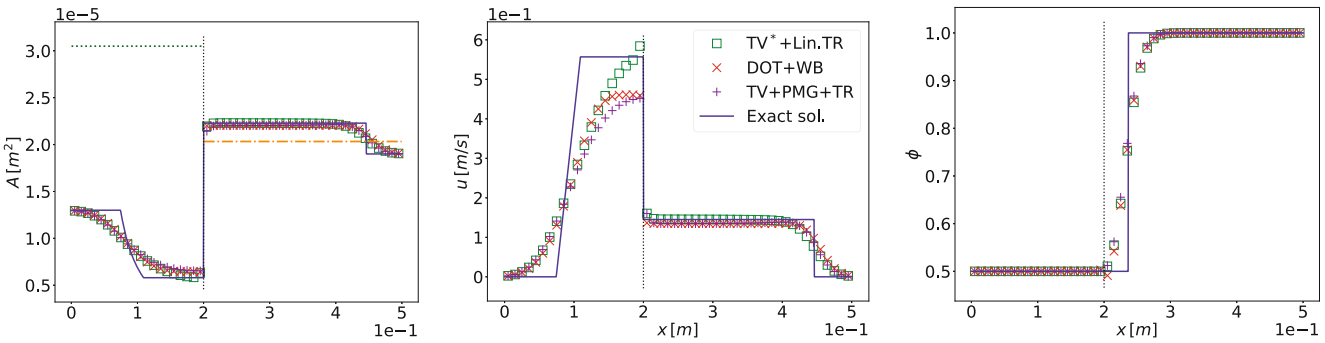

(c) TV*+Lin.TR vs. DOT+WB vs. TV+PMG+TR. $\alpha = 1$.

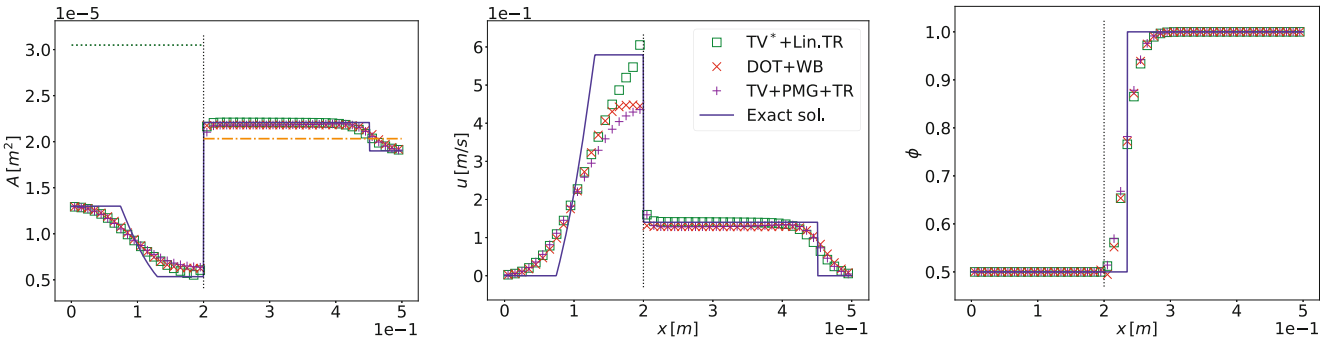

(d) TV*+Lin.TR vs. DOT+WB vs. TV+PMG+TR. $\alpha = 4/3$.

FIGURE 8 | Test 6. Vein. RC_0C_uS. Numerical results of methods **TV*** and **TV*+Lin.TR** versus the DOT+WB solver, the TV+PMG+TR solver with $C_{cfl} = 0.9$, $I = 50$ cells, and the exact solution of the Riemann problem for the complete 1D non-conservative blood flow equations with momentum correction coefficient $\alpha = 1$ and $\alpha = 4/3$. Initial conditions and parameters are given in Tables 1 and 2. The dotted black vertical line displayed in the plots represents the initial discontinuity x_d. The horizontal lines depicted in the plots of the first column are: the dotted green one is the value of A_{cL} in (27), the dashed orange one is the value of A_{cR} in (27). [Colour figure can be viewed at wileyonlinelibrary.com]

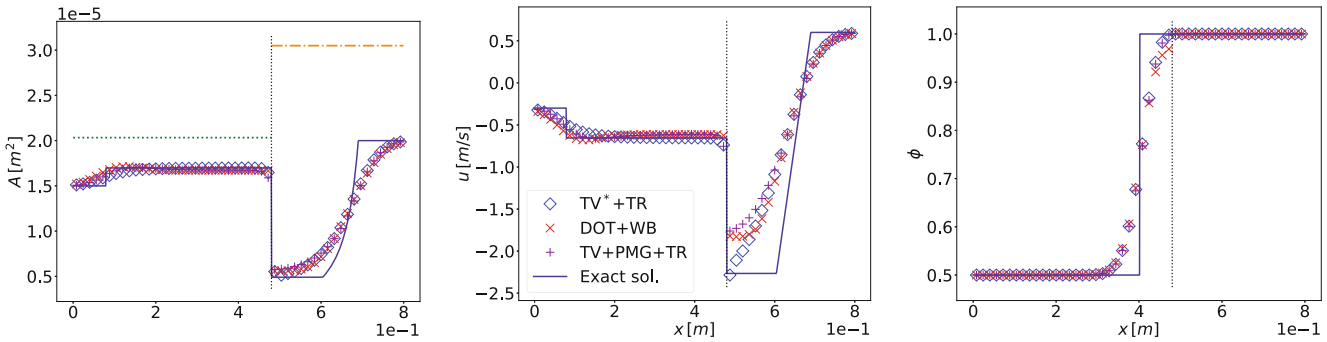

(a) TV*+TR vs. DOT+WB vs. TV+PMG+TR. $\alpha = 1$.

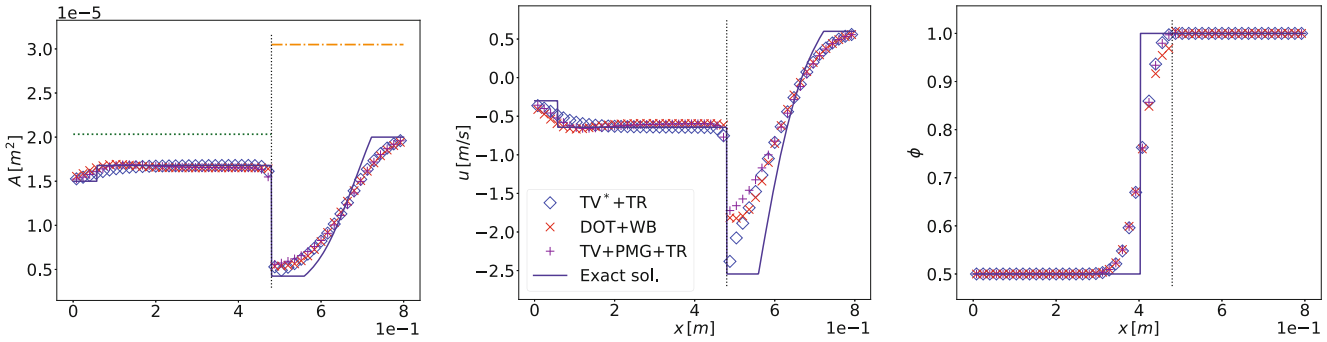

(b) TV*+TR vs. DOT+WB vs. TV+PMG+TR. $\alpha = 4/3$.

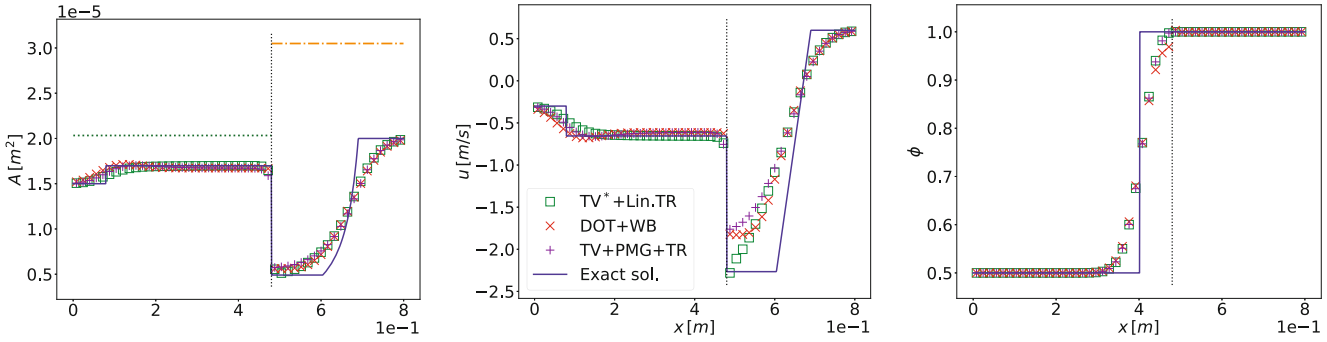

(c) TV*+Lin.TR vs. DOT+WB vs. TV+PMG+TR. $\alpha = 1$.

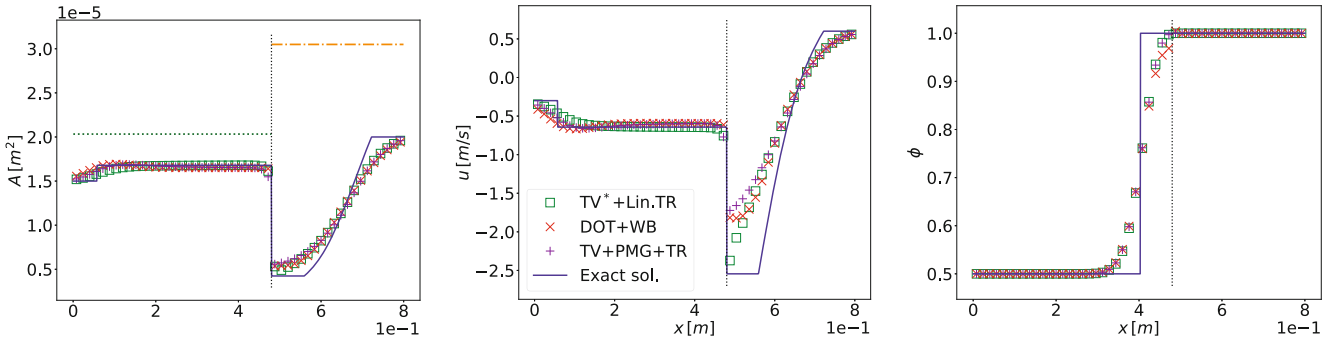

(d) TV*+Lin.TR vs. DOT+WB vs. TV+PMG+TR. $\alpha = 4/3$.

FIGURE 9 | Test 7. Vein. SC_uC_0R. Numerical results of methods **TV*+TR**, **TV*+Lin.TR** versus the DOT+WB solver, the TV+PMG+TR solver with $C_{cfl} = 0.9$, $I = 50$ cells, and the exact solution of the Riemann problem for the complete 1D non-conservative blood flow equations with momentum correction coefficient $\alpha = 1$ and $\alpha = 4/3$. Initial conditions and parameters are given in Tables 1 and 2. The dotted black vertical line displayed in the plots represents the initial discontinuity x_d. The horizontal lines depicted in the plots of the first column are: the dotted green one is the value of A_{cL} in (27), the dashed orange one is the value of A_{cR} in (27). [Colour figure can be viewed at wileyonlinelibrary.com]

where

$$S^n_{max} = max_i \left\{ max_k \left| \lambda^n_{k,i} \right| \right\}, \quad k = 1, ...N, \quad i = 1, ..., I;$$

with $\lambda^n_{k,i}$ the *k-th* eigenvalue of the *complete system* (14) evaluated in cell i at time t^n, and N is the number of eigenvalues of the considered system.

7.1.1 | Test 1 (Artery)

The solution of Test 1 consists of a stationary solution (Figure 3). The results of the two new splitting methods proposed in this article perfectly describe the type of problem and in particular the contact discontinuity for the passive scalar is flawlessly portrayed.

7.1.2 | Test 2 (Artery)

The solution of Test 2 contains a left shock, a middle stationary contact discontinuity associated with the eigenvalues $\lambda_2 = \lambda_3 = \lambda_4 = 0$, a contact discontinuity associated with the eigenvalue $\lambda_5 = u$ and a right shock: SC_0C_uS (Figure 4). This test does not present any particular trouble, and all the three methods give similar outcomes. We can appreciate monotone shocks, that is, there are no spurious oscillations in the vicinity of shocks and also the contact discontinuity for the passive scalar presents a minimal smearing while its propagation speed is correct.

7.1.3 | Test 3 (Artery)

The solution of Test 3 shows a left rarefaction, a middle stationary contact discontinuity associated with the eigenvalues $\lambda_2 = \lambda_3 = \lambda_4 = 0$, a contact discontinuity associated with the eigenvalue $\lambda_5 = u$ and a right shock: RC_0C_uS (Figure 5). The TV*-methods and the DOT+PM one result to be more accurate than the TV+PMG+TR scheme on reaching the exact value of the solution in the Star Region regarding variables A and u. On the contrary the computation of the concentration of the passive scalar ϕ is unchanged in the TV*-methods and the TV+PMG+TR one, presents a little diffusion but is analogous to that of DOT+WB method.

7.1.4 | Test 4 (Vein)

The Test 4 scenario features a left shock, a middle stationary contact discontinuity associated with the eigenvalues $\lambda_2 = \lambda_3 = \lambda_4 = 0$, a contact discontinuity associated with the eigenvalue $\lambda_5 = u$ and a right shock: SC_0C_uS (Figure 6). The test was formulated and designed in order to evaluate the effectiveness of the TV*-methods when A_{cL} and A_{cR} in (27) are located *inside* the range depicted by the test results. Reported results suggest that the TV*-methods are not affected by the loss of genuine nonlinearity that occurs for the pressure system, with minimal diffusion in the approximation of the contact discontinuity for the passive scalar.

7.1.5 | Test 5 (Vein)

The solution of Test 5 consists of a left rarefaction, a middle stationary contact discontinuity associated with the eigenvalues $\lambda_2 = \lambda_3 = \lambda_4 = 0$, a contact discontinuity associated with the eigenvalue $\lambda_5 = u$ and a right rarefaction: RC_0C_uR (Figure 7). In this case A_{cL} and A_{cR} in (27) are located *below* the range of the test results. Reported results suggest that the TV*-methods act in an appropriate manner also for this particular position of the critical area values. Finally the contact discontinuity for the passive scalar is depicted with minimal diffusion.

7.1.6 | Test 6 (Vein)

The solution of Test 6 contains a left rarefaction, a middle stationary contact discontinuity associated with the eigenvalues $\lambda_2 = \lambda_3 = \lambda_4 = 0$, a contact discontinuity associated with the eigenvalue $\lambda_5 = u$ and a right shock: RC_0C_uS (Figure 8). The TV*-methods prove to be more accurate than the TV+PMG+TR scheme and also the DOT+WB method fails on reaching the exact value of the solution in the Star Region regarding variables A and u. On the contrary, the computation of the concentration of the passive scalar ϕ is unchanged both in the TV*-methods and in the TV+PMG+TR one. In this test A_{cL} is located *above* the test results and A_{cR} is located *inside* the results range of the right wave.

7.1.7 | Test 7 (Vein)

The solution of Test 7 shows a left shock, a contact discontinuity associated with the eigenvalue $\lambda_5 = u$, a middle stationary contact discontinuity associated with the eigenvalues $\lambda_2 = \lambda_3 = \lambda_4 = 0$ and a right rarefaction: SC_uC_0R (Figure 9). Similarly to Test 6, the TV*-methods prove to be more accurate than the TV+PMG+TR and DOT+WB schemes. As usual the computation of the concentration of the passive scalar ϕ is comparable and presents a little diffusion. In this test A_{cL} and A_{cR} in (27) are located *above* the test results.

Remark 7. It is worth noting that although the flow rate q is constant across the initial discontinuity of the parameters as described in Propositions 13 and 15, in some cases (in this article in Tests 3, 6, 7) the numerical solutions obtained with numerical schemes **TV*+TR, TV*+Lin.TR** can present a jump in this variable in correspondence of the initial discontinuity x_d. This issue is due to the particular approximation of the advection flux, that is, the pressure system approximation in scheme (64), does not present any jump. This topic has not been further deepened in this article and will be the subject of future studies.

We conclude this section with some remarks regarding the stability of the numerical schemes presented in this article. For the model linear advection equation, the TV splitting approach reduces to the Godunov upwind scheme, as discussed by Toro and Vázquez-Cendón [54]; such method has been proved to be linearly stable, with C_{cfl} number stability limit equal to unity (see for example Toro [41] p. 419). For the nonlinear system studied in this article, we have conducted an empirical study through several demanding test problems and have verified that the C_{cfl} stability limit is actually unity. In particular, for all Tests 1–7 described in Tables 1, 2, we confirmed that the C_{cfl} stability limit is 1. It is relevant to point out that, when enforcing the C_{cfl} stability condition for nonlinear systems, one should strictly utilise bounds for the local true wave speeds, as discussed in Toro

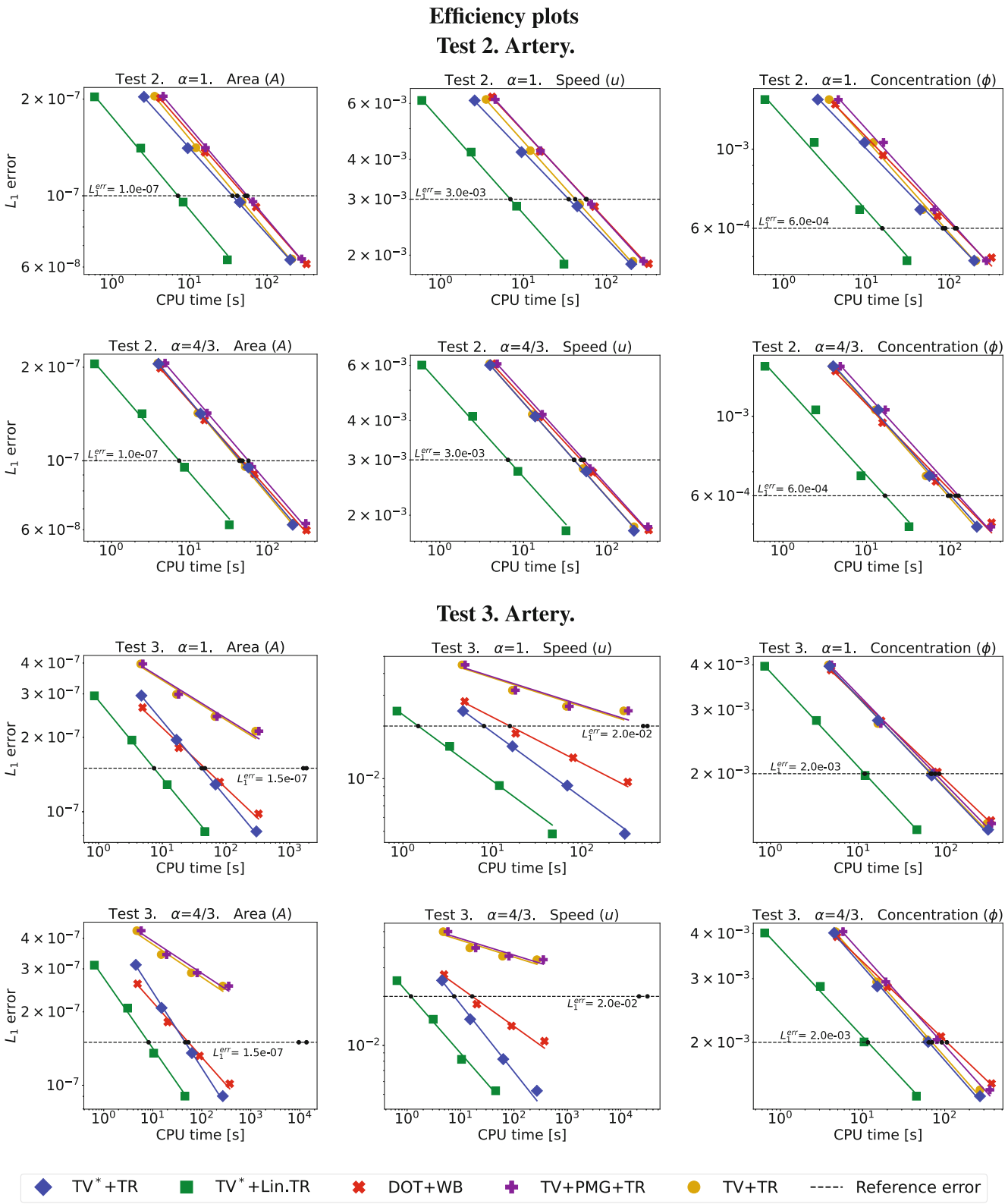

FIGURE 10 | Efficiency plots for Tests 2, 3 in Tables 1 and 2, calculated for meshes $I = [50, 100, 200, 400]$ and for momentum correction coefficient $\alpha = 1$ and $\alpha = 4/3$. The lines represent the least square approximation of the data. [Colour figure can be viewed at wileyonlinelibrary.com]

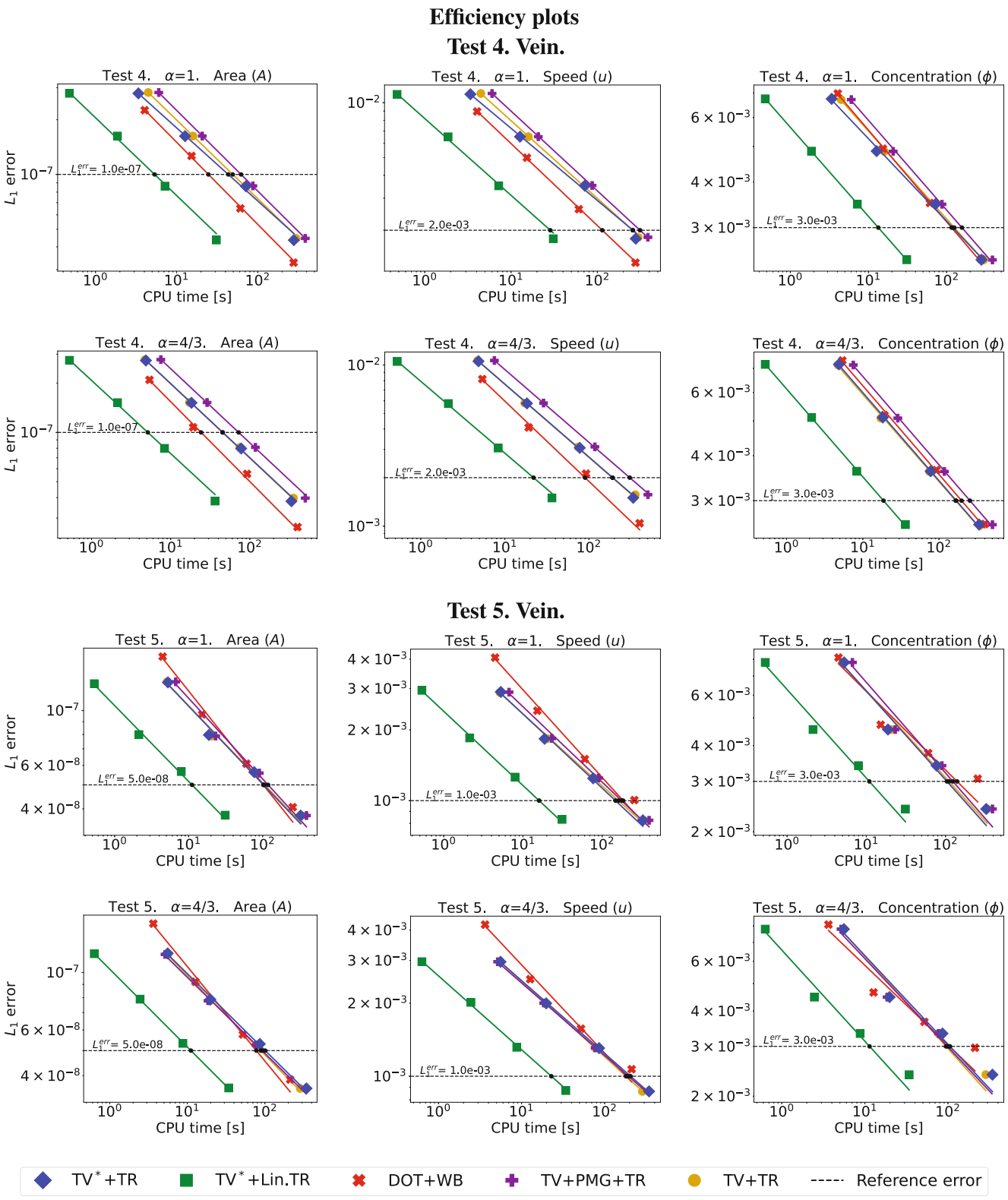

FIGURE 11 | Efficiency plots for Tests 4, 5 in Tables 1 and 2, calculated for meshes $I = [50, 100, 200, 400]$ and for momentum correction coefficient $\alpha = 1$ and $\alpha = 4/3$. The lines represent the least square approximation of the data. [Colour figure can be viewed at wileyonlinelibrary.com]

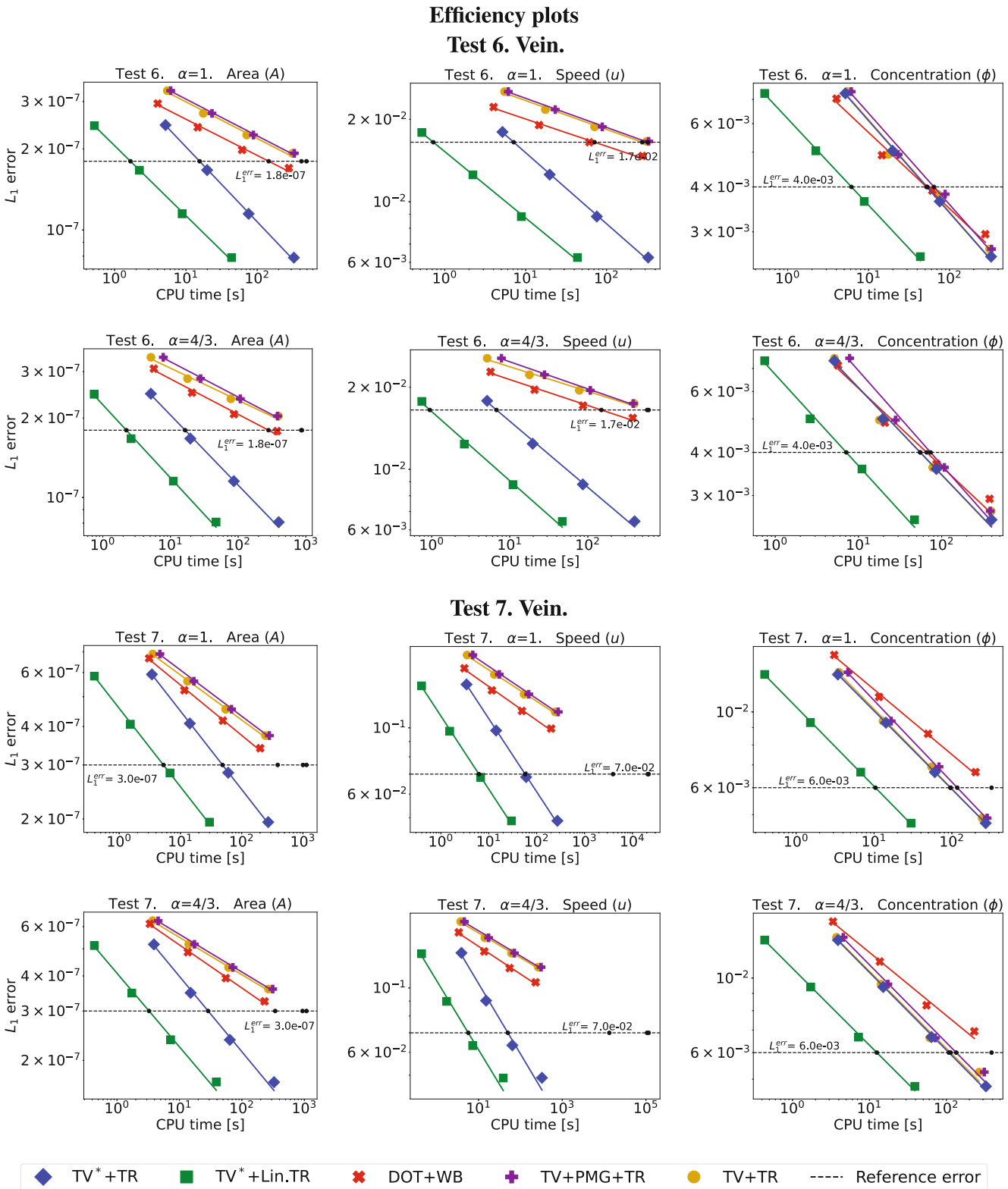

FIGURE 12 | Efficiency plots for Tests 6, 7 in Tables 1 and 2, calculated for meshes $I = [50, 100, 200, 400]$ and for momentum correction coefficient $\alpha = 1$ and $\alpha = 4/3$. The lines represent the least square approximation of the data. [Colour figure can be viewed at wileyonlinelibrary.com]

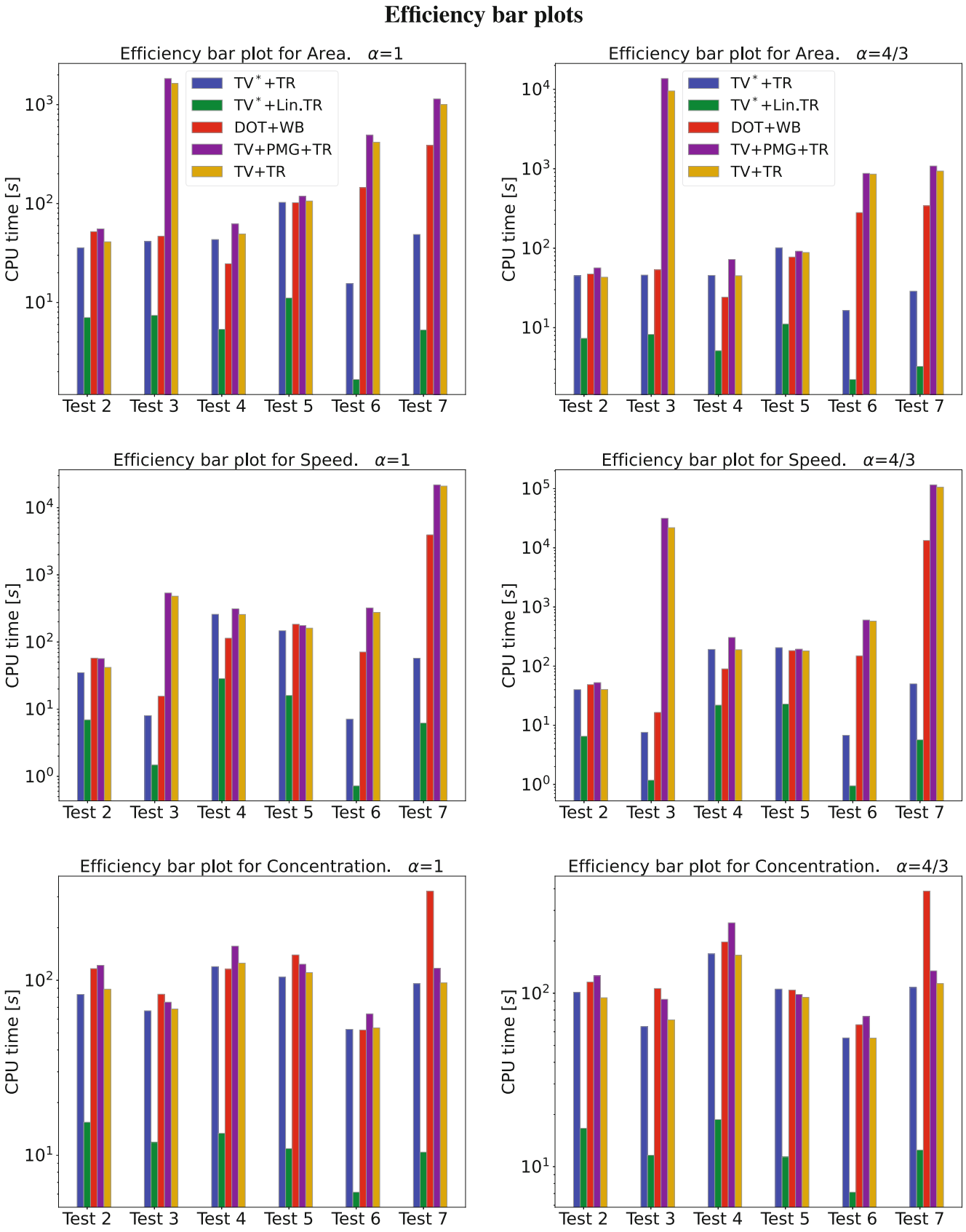

FIGURE 13 | Efficiency bar plots for Tests 2, 3, 4, 5, 6, 7 in Tables 1 and 2 representing the actual time each method takes to reach errors given in Figures 10–12 for each variable, displayed in a logarithmic scale. [Colour figure can be viewed at wileyonlinelibrary.com]

et al. [66]. However, in our experiments we used the simple wave speed estimates (69), which do not constitute bounds for the true wave speeds; nonetheless, the schemes were still seen to be stable. Moreover, we also conducted numerical experiments for C_{cfl} coefficients greater than 1 and confirmed that in such cases the schemes are seen to be unstable.

7.2 | Efficiency: Error Against CPU Time

Efficiency is determined by the CPU time required by a method to achieve a specified error E. In order to evaluate the efficiency of the TV*-methods **TV*+TR** and **TV*+Lin.TR** discussed in this research, we compare their results to those obtained with well-known numerical methods in literature. We consider the DOT+WB solver already treated, the TV+PMG+TR solver discussed in Section 7.1, and the TV+TR solver constructed applying the original TV-advection flux in (68) to the numerical method **TV*+TR**. This choice is made to prove that the increase of accuracy of the TV*-methods **TV*+TR**,**TV*+Lin.TR**, is actually due to the modification applied to the original TV-advection flux in (68) that leads to the TV*-advection flux in (59). Here we calculate the CPU cost and the L_1 error for each method cited above, for variables $w_1 = A$, $w_2 = u$ and $w_3 = \phi$, with meshes $I = [50, 100, 200, 400]$ and a $C_{cfl} = 0.9$. The L_1 error is defined

$$L_1^{err}(t_{End}, \Delta x_j) = \Delta x_j \sum_{i=1}^{I_j} |w_{k,i}^{t_{End}} - w_{k,i}^{e,t_{End}}|, \quad k = 1, 2, 3;$$

being t_{End} the output time, $w_{k,i}^{t_{End}}$ the numerical value of the k-th variable w at time t_{End} in the cell i, $w_{k,i}^{e,t_{End}}$ the exact solution value of the same variable at the same time in the same cell, and $\Delta x_j = \ell / I_j$, with ℓ the vessel length and I_j the actual mesh. Results are depicted in Figures 10–13.

In case of arteries, Test 1 shows a stationary solution and the efficiency test was not performed. Regarding the other tests, the two new methods and in particular the **TV*+Lin.TR** solver, prove to be the most accurate and efficient numerical methods among these considered, for both the values of the momentum correction coefficient analysed (Figures 10 and 13). This scheme is usually an order of magnitude faster with respect to the others. Test 3, in particular, shows a remarkable improvement of the efficiency, in reaching the given error, of the two TV*-methods in describing variables A and u for both values of the momentum correction coefficient, with respect to the other considered methods. In describing the concentration ϕ the accuracy is comparable but the CPU time proves to be an order of magnitude lower in the **TV*+Lin.TR** method.

Regarding veins, Test 4 shows a comparable accuracy between the given methods, the more efficient one is again the **TV*+Lin.TR** scheme, for both the values of the momentum correction coefficient (Figures 10 and 13). This scheme proves to be an order of magnitude faster than the others. Test 5 depicts again the higher efficiency of the new **TV*+Lin.TR** scheme in describing the three unknowns A, u and ϕ, with respect to all the methods considered, while the **TV*+TR** scheme reaches an efficiency comparable with the other reference schemes, for both values of α (Figures 11 and 13). A similar scenario of Test 3 instead, is faced in Tests 6 and 7 where the level of both accuracy and efficiency is significantly improved by the two new TV*-methods with respect to the others, for variables A and u. The **TV*+TR** and the **TV*+Lin.TR** schemes are respectively at least one and two orders of magnitude faster than the others in reaching the given error, up to four orders of magnitude faster in the case of the **TV*+Lin.TR** scheme describing variable u for $\alpha = \frac{4}{3}$. Regarding the concentration ϕ, the efficiency of the two TV*-methods is still the best one, and the accuracy attained is comparable with the one of the other methods (Figures 12 and 13).

Furthermore it is worth noting that for particular Riemann problems (here Tests, 3, 6, 7) the jump in the vicinity of the initial discontinuity of the parameters does not affect the overall accuracy of the two new methods. In addition it is of utmost significance to recognize the CPU time saving that characterizes the TV+TR and the TV*-methods using (64) with respect to the TV+PMG+TR one, circumventing the computations of path and matrices (Figure 13). Finally it can be observed that in general the particular position of A_{cL} and A_{cR} in (27), with respect to the problem outcomes, does not affect the accuracy of the results of the new TV*-splitting methods presented in this article, however it should be kept in mind that the **TV*+Lin.TR** method, although being really efficient, is build from a linearized solver that is not a robust method, in fact it may lead the **TV*+Lin.TR** scheme to crush due to the heavy approximation applied to the wave relations (Section 5.2). However, when possible, it proves to be a very efficient alternative to the robust **TV*+TR** solver.

8 | Conclusions

In this article, we have started presenting an advection-pressure splitting method at PDEs level for the non-conservative hyperbolic system of 1D blood flow equations as depicted in [38], this latter describes both arteries and veins and includes discontinuous parameters, an advection equation for a passive scalar transport and in addition we consider a general constant momentum correction coefficient. We separate the given system in advection and pressure systems, having these latter a simpler eigenstructure with respect to the initial one.

Consequently we have presented two approximated Riemann problem solvers for the obtained pressure system.

After, two final simple, finite volume-type, first order, advection-pressure splitting numerical schemes, for the aforementioned complete non-conservative 1D blood flow model with transport, have been built. They are constructed from the previously mentioned approximate Riemann solvers, these latter benefiting from the simpler eigenstructure of the pressure system with respect to the complete one. This eigenstructure is also not affected by the computation of the different momentum correction coefficients, so it is independent of the different velocity profiles. The new splitting numerical schemes have also been derived from a conservative form of the path-conservative schemes for the non-conservative pressure system, obviating the use of any path necessary for the path-conservative methods. This latter feature, in particular, can be applied to other type of non-conservative hyperbolic systems of PDEs. Regarding the

advection numerical flux, a modification with respect to the one described in Toro et al. [57], and Spilimbergo et al. [58] constructed to discretize conservative systems of 1D blood flow equations, is presented to adequately address a greater number of discontinuous parameters. These numerical schemes have been compared with some selected ones in literature and the exact solution of the Riemann problem for the complete system, in various test problems for arteries and veins, in subcritical regime, proving that the final splitting schemes continue to operate effectively despite the lack of genuine nonlinearity in two characteristic fields of the pressure system. Finally an efficiency analysis has been carried out. The two proposed methods have proved to be in general considerably more efficient than the considered reference methods and can be contemplated as competitive methods to implement in computing software in computational haemodynamics.

The upcoming study will utilise the methods presented in this work to address 1D blood flow model networks. Furthermore, a thorough examination of the entire solution of the Riemann problem for the pressure system will be carried out, with emphasis on inspecting the consequences of the absence of genuine nonlinearity.

Author Contributions

The author takes full responsibility for this article.

Acknowledgments

Alessandra Spilimbergo is a member of "Gruppo Nazionale per il Calcolo Scientifico dell'Istituto Nazionale di Alta Matematica" (INdAM-GNCS, Italy). She acknowledges the University of Trento for supporting the research through her Ph.D. fellowship. She also acknowledges the PRIN 2022 project (Next Generation EU) "High order structure-preserving semi-implicit schemes for hyperbolic equations", CUP B53D23009330006, for supporting her current position during the preparation of the manuscript.

Lucas O. Müller acknowledges funding from the European Union under NextGenerationEU, Mission 4, Component 2 – PRIN 2022 (D.D. 104/22), project title: Immersed methods for multiscale and multiphysics problems, CUP: E53D23005920006.

Open access publishing facilitated by Università degli Studi di Trento, as part of the Wiley - CRUI-CARE agreement.

Conflicts of Interest

The authors declare no conflicts of interest.

Data Availability Statement

Data sharing not applicable to this article as no datasets were generated or analysed during the current study.

References

1. C. Figueroa, C. Taylor, and A. Marsden, *Blood Flow*, 2nd ed. (Wiley, 2017), 1–31, https://doi.org/10.1002/9781119176817.ecm2068.

2. A. Quarteroni, L. Dede, F. Regazzoni, and C. Vergara, "A Mathematical Model of the Human Heart Suitable to Address Clinical Problems," *Japan Journal of Industrial and Applied Mathematics* 40, no. 3 (2023): 1547–1567, https://doi.org/10.1007/s13160-023-00579-6.

3. C. Taylor, M. Draney, J. Ku, et al., "Predictive Medicine: Computational Techniques in Therapeutic Decision-Making," *Computer Aided Surgery* 4, no. 5 (1999): 231–247, https://doi.org/10.3109/10929089909148176.

4. Y. Bazilevs, V. Calo, Y. Zhang, and T. Hughes, "Isogeometric Fluid-Structure Interaction Analysis With Applications to Arterial Blood Flow," *Computational Mechanics* 38 (2006): 310–322, https://doi.org/10.1007/s00466-006-0084-3.

5. P. Crosetto, P. Reymond, S. Deparis, D. Kontaxakis, N. Stergiopulos, and A. Quarteroni, "Fluid-Structure Interaction Simulation of Aortic Blood Flow," *Computers and Fluids* 43, no. 1 (2011): 46–57, https://doi.org/10.1016/j.compfluid.2010.11.032.

6. T. Hughes and J. Lubliner, "On the One-Dimensional Theory of Blood Flow in the Larger Vessels," *Mathematical Biosciences* 18 (1973): 161–170, https://doi.org/10.1016/0025-5564(73)90027-8.

7. N. Xiao, J. Alastruey, and A. Figueroa, "A Systematic Comparison Between 1-D and 3-D Hemodynamics in Compliant Arterial Models," *International Journal for Numerical Methods in Biomedical Engineering* 30, no. 2 (2014): 204–231, https://doi.org/10.1002/cnm.2598.

8. L. Grinberg, E. Cheever, T. Anor, J. Madsen, and G. Karniadakis, "Modeling Blood Flow Circulation in Intracranial Arterial Networks: A Comparative 3D/1D Simulation Study," *Annals of Biomedical Engineering* 39 (2011): 297–309, https://doi.org/10.1007/s10439-010-0132-1.

9. S. Sherwin, L. Formaggia, J. Peiró, and V. Franke, "Computational Modelling of 1D Blood Flow With Variable Mechanical Properties and Its Application to the Simulation of Wave Propagation in the Human Arterial System," *International Journal for Numerical Methods in Fluids* 43, no. 6–7 (2003): 673–700, https://doi.org/10.1002/fld.543.

10. D. Bessems, M. Rutten, and F. van de Vosse, "A Wave Propagation Model of Blood Flow in Large Vessels Using an Approximate Velocity Profile Function," *Journal of Fluid Mechanics* 580 (2007): 145–168, https://doi.org/10.1017/S0022112007005344.

11. P. Blanco, S. Watanabe, and R. Feijóo, "Identification of Vascular Territory Resistances in One-Dimensional Hemodynamics Simulations," *Journal of Biomechanics* 45, no. 12 (2012): 2066–2073, https://doi.org/10.1016/j.jbiomech.2012.06.002.

12. L. Formaggia, D. Lamponi, and A. Quarteroni, "One-Dimensional Models for Blood Flow in Arteries," *Journal of Engineering Mathematics* 47 (2003): 251–276, https://doi.org/10.1023/B:ENGI.0000007980.01347.29.

13. K. Low, R. van Loon, I. Sazonov, R. Bevan, and P. Nithiarasu, "An Improved Baseline Model for a Human Arterial Network to Study the Impact of Aneurysms on Pressure-Flow Waveforms," *International Journal for Numerical Methods in Biomedical Engineering* 28, no. 12 (2012): 1224–1246, https://doi.org/10.1002/cnm.2533.

14. J. Mynard and P. Nithiarasu, "A 1D Arterial Blood Flow Model Incorporating Ventricular Pressure, Aortic Valve and Regional Coronary Flow Using the Locally Conservative Galerkin (LCG) Method," *Communications in Numerical Methods in Engineering* 24, no. 5 (2008): 367–417, https://doi.org/10.1002/cnm.1117.

15. S. Sherwin, V. Franke, J. Peiró, and K. Parker, "One-Dimensional Modelling of a Vascular Network in Space-Time Variables," *Journal of Engineering Mathematics* 47 (2003): 217–250, https://doi.org/10.1023/B:ENGI.0000007979.32871.e2.

16. L. Müller and E. Toro, "Enhanced Global Mathematical Model for Studying Cerebral Venous Blood Flow," *Journal of Biomechanics* 47, no. 13 (2014): 3361–3372, https://doi.org/10.1016/j.jbiomech.2014.08.005.

17. L. Müller and E. Toro, "A Global Multi-Scale Model for the Human Circulation With Emphasis on the Venous System," *International Journal for Numerical Methods in Biomedical Engineering* 30, no. 7 (2014): 681–725, https://doi.org/10.1002/cnm.2622.

18. J. Mynard and J. Smolich, "One-Dimensional Haemodynamic Modeling and Wave Dynamics in the Entire Adult Circulation," *Annals of*

Biomedical Engineering 43 (2015): 1443–1460, https://doi.org/10.1007/s10439-015-1313-8.

19. J. Alastruey, K. Parker, J. Peiró, and S. Sherwin, "Lumped Parameter Outflow Models for 1-D Blood Flow Simulations: Effect on Pulse Waves and Parameter Estimation," *Communications in Computational Physics* 4, no. 2 (2008): 317–336.

20. P. Blanco, S. Watanabe, M. Passos, P. Lemos, and R. Feijóo, "An Anatomically Detailed Arterial Network Model for One-Dimensional Computational Hemodynamics," *IEEE Transactions on Biomedical Engineering* 62, no. 2 (2015): 736–753, https://doi.org/10.1109/TBME.2014.2364522.

21. B. Ghitti, E. Toro, and L. Müller, "Nonlinear Lumped-Parameter Models for Blood Flow Simulations in Networks of Vessels," *ESAIM. M2AN* 56, no. 5 (2022): 1579–1627, https://doi.org/10.1051/m2an/2022052.

22. F. Liang, S. Takagi, R. Himeno, and H. Liu, "Biomechanical Characterization of Ventricular-Arterial Coupling During Aging: A Multi-Scale Model Study," *Journal of Biomechanics* 42, no. 6 (2009): 692–704, https://doi.org/10.1016/j.jbiomech.2009.01.010.

23. P. Blanco and R. Feijóo, "A Dimensionally-Heterogeneous Closed-Loop Model for the Cardiovascular System and Its Applications," *Medical Engineering & Physics* 35, no. 5 (2013): 652–667, https://doi.org/10.1016/j.medengphy.2012.07.011.

24. L. Formaggia, A. Quarteroni, and C. Vergara, "On the Physical Consistency Between Three-Dimensional and One-Dimensional Models in Haemodynamics," *Journal of Computational Physics* 244 (2013): 97–112, https://doi.org/10.1016/j.jcp.2012.08.001.

25. L. Formaggia, J. Gerbeau, F. Nobile, and A. Quarteroni, "On the Coupling of 3D and 1D Navier–Stokes Equations for Flow Problems in Compliant Vessels," *Computer Methods in Applied Mechanics and Engineering* 191, no. 6–7 (2001): 561–582, https://doi.org/10.1016/S0045-7825(01)00302-4.

26. A. Quarteroni, A. Manzoni, and C. Vergara, "The Cardiovascular System: Mathematical Modelling, Numerical Algorithms and Clinical Applications," *Acta Numerica* 26 (2017): 365–590, https://doi.org/10.1017/S0962492917000046.

27. S. Čanić and E. Kim, "Mathematical Analysis of the Quasilinear Effects in a Hyperbolic Model Blood Flow Through Compliant Axi-Symmetric Vessels," *Mathematical Methods in the Applied Sciences* 26, no. 14 (2003): 1161–1186, https://doi.org/10.1002/mma.407.

28. A. Bermudez and M. Vázquez, "Upwind Methods for Hyperbolic Conservation Laws With Source Terms," *Computers & Fluids* 23, no. 8 (1994): 1049–1071, https://doi.org/10.1016/0045-7930(94)90004-3.

29. J. Greenberg, A. LeRoux, R. Baraille, and A. Noussair, "Analysis and Approximation of Conservation Laws With Source Terms," *SIAM Journal on Numerical Analysis* 34, no. 5 (1997): 1980–2007, https://doi.org/10.1137/S0036142995286751.

30. C. Parés, "Numerical Methods for Nonconservative Hyperbolic Systems: A Theoretical Framework," *SIAM Journal on Numerical Analysis* 44 (2006): 300–321, https://doi.org/10.1137/050628052.

31. O. Delestre and P. Lagree, "A Well-Balanced Finite Volume Scheme for Blood Flow Simulation," *International Journal for Numerical Methods in Fluids* 72 (2012): 177–205, https://doi.org/10.1002/fld.3736.

32. A. Ghigo, O. Delestre, J. Fullana, and P. Lagrée, "Low-Shapiro Hydrostatic Reconstruction Technique for Blood Flow Simulation in Large Arteries With Varying Geometrical and Mechanical Properties," *Journal of Computational Physics* 331 (2017): 108–136, https://doi.org/10.1016/j.jcp.2016.11.032.

33. G. Li, O. Delestre, and L. Yuan, "Well-Balanced Discontinuous Galerkin Method and Finite Volume WENO Scheme Based on Hydrostatic Reconstruction for Blood Flow Model in Arteries," *International Journal for Numerical Methods in Fluids* 86, no. 7 (2018): 491–508, https://doi.org/10.1002/fld.4463.

34. J. Murillo and P. García-Navarro, "A Roe Type Energy Balanced Solver for 1D Arterial Blood Flow and Transport," *Computers and Fluids* 117 (2015): 149–167, https://doi.org/10.1016/j.compfluid.2015.05.003.

35. Z. Wang, G. Li, and O. Delestre, "Well-Balanced Finite Difference Weighted Essentially Non-Oscillatory Schemes for the Blood Flow Model," *International Journal for Numerical Methods in Fluids* 82, no. 9 (2016): 607–622, https://doi.org/10.1002/fld.4232.

36. L. Formaggia, A. Quarteroni, and A. Veneziani, *Cardiovascular Mathematics. Modeling and Simulation of the Circulatory System* (Springer, 2009), https://doi.org/10.1007/978-88-470-1152-6.

37. A. Bernard, W. Hunt, W. Timlake, and E. Varley, "A Theory of Fluid Flow in Compliant Tubes," *Biophysical Journal* 6, no. 6 (1966): 717–724, https://doi.org/10.1016/S0006-3495(66)86690-0.

38. E. Toro and A. Siviglia, "Flow in Collapsible Tubes With Discontinuous Mechanical Properties: Mathematical Model and Exact Solutions," *Communications in Computational Physics* 13, no. 2 (2013): 361–385, https://doi.org/10.4208/cicp.210611.240212a.

39. E. Godlewski and P. Raviart, *Numerical Approximation of Hyperbolic Systems of Conservation Laws* (Springer, 2021), https://doi.org/10.1007/978-1-0716-1344-3.

40. R. Leveque, *Numerical Methods for Conservation Laws* (Birkhäuser Verlag, 1999), https://doi.org/10.1007/978-3-0348-5116-9.

41. E. Toro, *Riemann Solvers and Numerical Methods for Fluid Dynamics: A Practical Introduction*, 3rd ed. (Springer-Verlag, 2009), https://doi.org/10.1007/b79761.

42. A. Spilimbergo, E. Toro, and L. Müller, "One-Dimensional Blood Flow With Discontinuous Properties and Transport: Mathematical Analysis and Numerical Schemes," *Communications in Computational Physics* 29, no. 3 (2021): 649–697, https://doi.org/10.4208/cicp.OA-2020-0132.

43. A. Spilimbergo, E. Toro, and L. Müller, "Exact Solution of the Riemann Problem for the One-Dimensional Blood Flow Equations With General Constant Momentum Correction Coefficient," *Communications in Computational Physics* 36, no. 3 (2024): 711–780, https://doi.org/10.4208/cicp.oa-2023-0250.

44. G. Dal Maso, P. LeFloch, and F. Murat, "Definition and Weak Stability of Nonconservative Products," *Journal de Mathématiques Pures et Appliquées* 74 (1995): 483–548.

45. M. Dumbser and E. Toro, "On Universal Osher-Type Schemes for General Nonlinear Hyperbolic Conservation Laws," *Communications in Computational Physics* 10, no. 3 (2011): 635–671, https://doi.org/10.4208/cicp.170610.021210a.

46. M. Dumbser and E. Toro, "A Simple Extension of the Osher Riemann Solver to Non-Conservative Hyperbolic Systems," *Journal of Scientific Computing* 48 (2011): 70–88, https://doi.org/10.1007/s10915-010-9400-3.

47. S. Osher and F. Solomon, "Upwind Difference Schemes for Hyperbolic Systems of Conservation Laws," *Mathematics of Computation* 38, no. 158 (1982): 339–374, https://doi.org/10.2307/2007275.

48. L. Müller and E. Toro, "Well-Balanced High-Order Solver for Blood Flow in Networks of Vessels With Variable Properties," *International Journal for Numerical Methods in Biomedical Engineering* 29 (2013): 1388–1411, https://doi.org/10.1002/cnm.2580.

49. M. J. Castro, A. Milanés, and C. Parés, "Well-Balanced Numerical Schemes Based on a Generalized Hydrostatic Reconstruction Technique," *Mathematical Models and Methods in Applied Sciences* 17, no. 12 (2007): 2055–2113, https://doi.org/10.1142/S021820250700256X.

50. L. Müller, C. Parés, and E. Toro, "Well-Balanced High-Order Numerical Schemes for One-Dimensional Blood Flow in Vessels With Varying Mechanical Properties," *Journal of Computational Physics* 242 (2013): 53–85, https://doi.org/10.1016/j.jcp.2013.01.050.

51. E. Pimentel-García, L. Müller, E. Toro, and C. Parés, "High-Order Fully Well-Balanced Numerical Methods for One-Dimensional Blood

Flow With Discontinuous Properties," *Journal of Computational Physics* 475 (2023): 111869, https://doi.org/10.1016/j.jcp.2022.111869.

52. M. Liou and C. Steffen, "A New Flux Splitting Scheme," *Journal of Computational Physics* 107, no. 1 (1993): 23–39, https://doi.org/10.1006/jcph.1993.1122.

53. J. Steger and R. Warming, "Flux Vector Splitting of the Inviscid Gasdynamic Equations With Application to Finite-Difference Methods," *Journal of Computational Physics* 40, no. 2 (1981): 263–293, https://doi.org/10.1016/0021-9991(81)90210-2.

54. E. Toro and M. Vázquez-Cendón, "Flux Splitting Schemes for the Euler Equations," *Computers & Fluids* 70 (2012): 1–12, https://doi.org/10.1016/j.compfluid.2012.08.023.

55. B. van Leer, "Flux Vector Splitting for the Euler Equations," ICASE (1982).

56. G. Zha and E. Bilgen, "Numerical Solutions of Euler Equations by Using a New Flux Vector Splitting Scheme," *International Journal for Numerical Methods in Fluids* 17, no. 2 (1993): 115–144, https://doi.org/10.1002/fld.1650170203.

57. E. Toro, A. Siviglia, A. Spilimbergo, and L. Müller, "Advection-Pressure Splitting Schemes for the Equations of Blood Flow. Conservative and Non-Conservative Forms," *East Asian Journal on Applied Mathematics* 14, no. 2 (2024): 223–259, https://doi.org/10.4208/eajam.2023-045.090523.

58. A. Spilimbergo, E. Toro, A. Siviglia, and L. Müller, "Flux Vector Splitting Schemes Applied to a Conservative 1D Blood Flow Model With Transport for Arteries and Veins," *Computers and Fluids* 271 (2024): 106165, https://doi.org/10.1016/j.compfluid.2023.106165.

59. A. Siviglia, D. Vanzo, and E. Toro, "A Splitting Scheme for the Coupled Saint-Venant-Exner Model," *Advances in Water Resources* 159 (2022): 104062, https://doi.org/10.1016/j.advwatres.2021.104062.

60. N. Smith, A. Pullan, and P. Hunter, "An Anatomically Based Model of Transient Coronary Blood Flow in the Heart," *SIAM Journal on Applied Mathematics* 62, no. 3 (2002): 990–1018, https://doi.org/10.1137/S0036139999355199.

61. C. Colombo, A. Siviglia, E. Toro, D. Bia, Y. Zócalo, and L. O. Muller, "Tube Law Parametrization Using In Vitro Data for One-Dimensional Blood Flow in Arteries and Veins," *International Journal for Numerical Methods in Biomedical Engineering* 40, no. 4 (2024): e3803, https://doi.org/10.1002/cnm.3803.

62. A. Spilimbergo, *Theoretical and Numerical Aspects of Advection-Pressure Splitting for 1D Blood Flow Models*, PhD Thesis (University of Trento, 2024), https://doi.org/10.15168/11572_407653.

63. J. Smoller, *Shock Waves and Reaction-Diffusion Equations*, 2nd ed. (Springer New York, 1994), https://doi.org/10.1007/978-1-4612-0873-0.

64. T. Liu, "The Riemann Problem for General 2×2 Conservation Laws," *Transactions of the American Mathematical Society* 199 (1974): 89–112, https://doi.org/10.2307/1996875.

65. C. Parés and M. Muñoz-Ruiz, "On Some Difficulties of the Numerical Approximation of Nonconservative Hyperbolic Systems," *Boletín de la Sociedad Española de Matemática Aplicada* 47 (2009): 19–48.

66. E. Toro, L. Müller, and A. Siviglia, "Bounds for Wave Speeds in the Riemann Problem: Direct Theoretical Estimates," *Computers and Fluids* 209 (2020): 104640, https://doi.org/10.1016/j.compfluid.2020.104640.

Appendix A

Nature of the λ_1- and λ_6- Characteristic Fields of the Complete System of 1D Blood Flow Equations

In this appendix, we prove the nature of the λ_1- and λ_6- characteristic fields of system (11).

Proposition 10 (Nature of the λ_1-characteristic field). *Under the hypotheses of Proposition 1, the λ_1-characteristic field of system (11) is genuinely nonlinear with*

$$\nabla\lambda_1(\mathbf{Q})\cdot\mathbf{R}_1(\mathbf{Q})<0,\quad \forall\mathbf{Q}\in\overline{\Omega}_d,$$

provided $m>0$, $-2\le n\le 0$.

Proof. From (14)

$$\begin{aligned}\nabla\lambda_1(\mathbf{Q}) &= \\ &= \left[\frac{\partial\lambda_1(\mathbf{Q})}{\partial A},\frac{\partial\lambda_1(\mathbf{Q})}{\partial q},\frac{\partial\lambda_1(\mathbf{Q})}{\partial K},\frac{\partial\lambda_1(\mathbf{Q})}{\partial A_0},\frac{\partial\lambda_1(\mathbf{Q})}{\partial p_e},\frac{\partial\lambda_1(\mathbf{Q})}{\partial(A\phi)}\right]= \\ &= \left[-\alpha\frac{u}{A}-\frac{\partial c_\alpha}{\partial A},\frac{\alpha}{A}-\frac{\partial c_\alpha}{\partial q},\frac{\partial\lambda_1(\mathbf{Q})}{\partial K},\frac{\partial\lambda_1(\mathbf{Q})}{\partial A_0},0,0\right].\end{aligned}$$

Then, being $\mathbf{R}_1(\mathbf{Q})$ in (16) and recalling that $q=Au$, after manipulations one obtains

$$\nabla\lambda_1(\mathbf{Q})\cdot\mathbf{R}_1(\mathbf{Q})=-\frac{2\alpha(Ac_\alpha+q-\alpha q)^2+A^3\frac{\partial c}{\partial A}2c}{2A^3c_\alpha}.$$

The denominator is always positive. To check the genuine nonlinearity the numerator must be different from zero. In particular we will prove that

$$2\alpha(Ac_\alpha+q-\alpha q)^2+A^3\frac{\partial c}{\partial A}2c>0. \tag{A1}$$

(A1) can be written as

$$-\frac{\partial c}{\partial A}-\frac{c}{A}g_1(\mathbf{Q},\alpha)<0, \tag{A2}$$

with

$$g_1(\mathbf{Q},\alpha)=\frac{\alpha}{c^2}[c_\alpha+(1-\alpha)u]^2;$$

that can be proved to be

$$g_1(\mathbf{Q},\alpha)\ge 1,\qquad g_1(\mathbf{Q},1)=1,\quad \forall\mathbf{Q}\in\overline{\Omega}_d.$$

For $\alpha=1$ (A2) is satisfied if parameters m and n are in the range we consider, that is, $m>0$, $-2\le n\le 0$. It follows that for this same range of the parameters, for $\alpha\in[1,2]$ (A2) holds too, consequently we have proved the statement. □

Proposition 11 (Nature of the λ_6-characteristic field). *Under the hypotheses of Proposition 1 and Proposition 10 the λ_6-characteristic field of system (11) is genuinely nonlinear with*

$$\nabla\lambda_6(\mathbf{Q})\cdot\mathbf{R}_6(\mathbf{Q})>0,\quad \forall\mathbf{Q}\in\overline{\Omega}_d.$$

Proof. From (14)

$$\begin{aligned}\nabla\lambda_6(\mathbf{Q}) &= \\ &= \left[\frac{\partial\lambda_6(\mathbf{Q})}{\partial A},\frac{\partial\lambda_6(\mathbf{Q})}{\partial q},\frac{\partial\lambda_6(\mathbf{Q})}{\partial K},\frac{\partial\lambda_6(\mathbf{Q})}{\partial A_0},\frac{\partial\lambda_6(\mathbf{Q})}{\partial p_e},\frac{\partial\lambda_6(\mathbf{Q})}{\partial(A\phi)}\right]= \\ &= \left[-\alpha\frac{u}{A}+\frac{\partial c_\alpha}{\partial A},\frac{\alpha}{A}+\frac{\partial c_\alpha}{\partial q},\frac{\partial\lambda_6(\mathbf{Q})}{\partial K},\frac{\partial\lambda_6(\mathbf{Q})}{\partial A_0},0,0\right].\end{aligned}$$

Then, being $\mathbf{R}_6(\mathbf{Q})$ in (16) and recalling that $q=Au$, after some manipulations one obtains

$$\nabla\lambda_6(\mathbf{Q})\cdot\mathbf{R}_6(\mathbf{Q})=\frac{2\alpha(Ac_\alpha-q+\alpha q)^2+A^3\frac{\partial c}{\partial A}2c}{2A^3c_\alpha}.$$

The denominator is always positive. To check the genuine nonlinearity the numerator must be different from zero. In particular we will prove that

$$2\alpha(Ac_\alpha-q+\alpha q)^2+A^3\frac{\partial c}{\partial A}2c>0. \tag{A3}$$

(A3) can be written as

$$\frac{\partial c}{\partial A} + \frac{c}{A} g_2(\mathbf{Q}, \alpha) > 0, \tag{A4}$$

with

$$g_2(\mathbf{Q}, \alpha) = \frac{\alpha}{c^2}[(\alpha - 1)u + c_\alpha]^2;$$

that can be proved to be

$$g_2(\mathbf{Q}, \alpha) \geq 1, \qquad g_2(\mathbf{Q}, 1) = 1, \quad \forall \mathbf{Q} \in \overline{\Omega}_d.$$

For $\alpha = 1$ (A4) is satisfied if parameters m and n are in the range we consider, that is, $m > 0$, $-2 \leq n \leq 0$. It follows that for this same range of the parameters, for $\alpha \in [1, 2]$, (A4) holds too, consequently we have the statement. □

Appendix B

Generalized Riemann Invariants and Jump Conditions for the Complete System of 1D Blood Flow Equations

In this appendix, we treat the generalized Riemann invariants and the jump conditions for system (11). This topic has already been presented in Spilimbergo et al. [43] in an extensive manner for the complete system (11) without the advection equation for the passive scalar. Regarding the addition of this last equation, we refer the reader also to Spilimbergo [62].

Proposition 12 (Generalized Riemann invariants for the λ_1- and λ_6-characteristic fields). *A not complete list of Riemann invariants is*

$$K = const, \quad A_0 = const, \quad p_e = const, \quad \phi = const,$$

for the λ_1-characteristic field;

$$K = const, \quad A_0 = const, \quad p_e = const, \quad \phi = const,$$

for the λ_6-characteristic field.

Regarding the relations between variables A and u no closed form is present for $\alpha > 1$. For further details and a possible solution see Spilimbergo et al. [43].

Proof. The problem can be solved applying the generalized Riemann invariants method (for example see Toro [41] and Toro and Siviglia [38]), that is, for a given hyperbolic system of n unknowns $[w_1, w_2, \ldots, w_n]^T$, for any λ_k-characteristic field with right eigenvector $\mathbf{R}_k = [r_{1,k}, r_{2,k}, \ldots, r_{n,k}]^T$ the generalized Riemann invariants are solutions of the following $n - 1$ ordinary differential equations in phase-plane

$$\frac{dw_1}{r_{1,k}} = \frac{dw_2}{r_{2,k}} = \cdots = \frac{dw_n}{r_{n,k}}.$$

For the λ_1-characteristic field we have

$$\frac{dA}{1} = \frac{d(Au)}{\alpha u - c_\alpha} = \frac{dK}{0} = \frac{dA_0}{0} = \frac{dp_e}{0} = \frac{d(A\phi)}{\phi}.$$

From the equality between the first and the second terms results

$$(\alpha u - u - c_\alpha) dA - A du = 0,$$

this ODE can not be solved in a closed form and has been solved numerically in Spilimbergo et al. [43]. From the equality between the first and the sixth terms

$$d(A\phi) = \phi dA \rightarrow \phi = const.$$

From the equality between the third, fourth and fifth terms

$$K = const, \quad A_0 = const, \quad p_e = const.$$

For the λ_6-characteristic field

$$\frac{dA}{1} = \frac{d(Au)}{\alpha u + c_\alpha} = \frac{dK}{0} = \frac{dA_0}{0} = \frac{dp_e}{0} = \frac{d(A\phi)}{\phi},$$

that is, from the equality between the first and the second terms

$$(\alpha u - u + c_\alpha) dA - A du = 0,$$

this ODE again can not be solved in a closed form and has been solved numerically in Spilimbergo et al. [43]. From the equality between the first and the sixth terms

$$d(A\phi) = \phi dA \rightarrow \phi = const.$$

From the equality between the third, fourth and fifth terms

$$K = const, \quad A_0 = const, \quad p_e = const. \tag{B1}$$

□

Proposition 13 (Jump conditions across the stationary contact discontinuities associated with eigenvalues $\lambda_2 = \lambda_3 = \lambda_4 = 0$ (Case 1 and Case 2 of Figure 1)). *Across the stationary contact discontinuities associated with eigenvalues $\lambda_2 = \lambda_3 = \lambda_4 = 0$ the following relations hold*

$$Au = const, \quad \frac{1}{2}\alpha\rho u^2 + \psi + p_e = const, \quad \phi = const. \tag{B2}$$

Proof. This problem can be solved by applying the generalized Riemann invariants method already described in the proof of Proposition 12, following the approach presented in Spilimbergo et al. [42]. For an arbitrary right eigenvector $\mathbf{R} = [r_1, r_2, r_3, r_4, r_5, r_6]^T$ we clearly have

$$\mathbf{MR} = \lambda \mathbf{R},$$

being $\mathbf{M}$ defined in (12), which gives the algebraic system

$$\begin{cases} r_2 = \lambda r_1, \\ (c^2 - \alpha u^2) r_1 + 2\alpha u r_2 + \frac{A}{\rho}\psi_K r_3 + \frac{A}{\rho}\psi_{A_0} r_4 + \frac{A}{\rho} r_5 = \lambda r_2, \\ 0 = \lambda r_3, \\ 0 = \lambda r_4, \\ 0 = \lambda r_5, \\ -u\phi r_1 + \phi r_2 + u r_6 = \lambda r_6. \end{cases} \tag{B3}$$

Substituting $\lambda = 0$ in (B3), we first notice that $r_2 = 0$. After this latter substitution system (B3) becomes

$$\begin{cases} r_2 = 0, \\ (c^2 - \alpha u^2) r_1 + \frac{A}{\rho}\psi_K r_3 + \frac{A}{\rho}\psi_{A_0} r_4 + \frac{A}{\rho} r_5 = 0, \\ 0 = 0, \\ 0 = 0, \\ 0 = 0, \\ -u\phi r_1 + u r_6 = 0. \end{cases} \tag{B4}$$

Employing the second equation of (B4) we can compute the value of one among r_1, r_3, r_4 and r_5 in terms of the others. Subsequently, we have three identities $0 = 0$, from which no information can be deduced. Then by means of the last equation of (B4), we can compute the value of one among r_1 and r_6 in terms of the other one. In this computation, using the second equation of system (B4), we will determine the value of r_5 with respect to r_1, r_3 and r_4, while by means of the last equation of system (B4), we will determine the value of r_6 with respect to r_1. The values of r_1,

r_3 and r_4 will be assigned arbitrarily. By setting $r_1 = \beta$, $r_3 = \gamma$, $r_4 = \epsilon$, for $\beta, \gamma, \epsilon \in \mathbb{R}$ arbitrary constants, we obtain

$$\mathbf{R}_0 = \begin{bmatrix} \beta \\ 0 \\ \gamma \\ \epsilon \\ \left[(\alpha u^2 - c^2)\beta - \frac{A}{\rho}\psi_K \gamma - \frac{A}{\rho}\psi_{A_0}\epsilon\right]\frac{\rho}{A} \\ \phi\beta \end{bmatrix}, \tag{B5}$$

that is a general vector belonging to the subspace associated with $\lambda = 0$. At this point we can apply the generalized Riemann invariants method to vector (B5) that is,

$$\frac{dA}{\beta} = \frac{d(Au)}{0} = \frac{dK}{\gamma} = \frac{dA_0}{\epsilon} = \\ = \frac{dp_e}{\left[(\alpha u^2 - c^2)\beta - \frac{A}{\rho}\psi_K \gamma - \frac{A}{\rho}\psi_{A_0}\epsilon\right]\frac{\rho}{A}} = \frac{d(A\phi)}{\phi\beta}, \tag{B6}$$

from the second term of (B6) we obtain

$$d(Au) = 0 \rightarrow Au = const,$$

from the equality between the first and the fifth terms of (B6) we have

$$\frac{dA}{\beta} = \frac{dp_e}{\left[(\alpha u^2 - c^2)\beta - \frac{A}{\rho}\psi_K \gamma - \frac{A}{\rho}\psi_{A_0}\epsilon\right]\frac{\rho}{A}},$$

that becomes

$$(\alpha u^2 - c^2)\frac{\rho}{A}dA - \psi_K \frac{\gamma}{\beta}dA - \psi_{A_0}\frac{\epsilon}{\beta}dA = dp_e. \tag{B7}$$

Considering the first and the third terms of (B6) coupled together and then the first and the fourth terms of (B6)

$$\gamma dA = \beta dK, \quad \epsilon dA = \beta dA_0,$$

being c defined in (13) and $d(Au) = 0$, it follows that

$$(\alpha u^2 - c^2)\frac{\rho}{A}dA = -\alpha\rho u du - \psi_A dA,$$

consequentially (B7) becomes

$$-\alpha\rho u du - \psi_A dA - \psi_K dK - \psi_{A_0}dA_0 - dp_e = 0. \tag{B8}$$

Considering that

$$d\psi = \psi_A dA + \psi_K dK + \psi_{A_0}dA_0,$$

(B8) becomes

$$-\alpha\rho u du - d\psi - dp_e = 0,$$

from that, integrating, we obtain the second of (B2). From the equality between the first and the last terms of (B6) we obtain

$$\frac{dA}{\beta} = \frac{d(A\phi)}{\phi\beta} \rightarrow d\phi = 0,$$

or in other words

$$\phi = const.$$

□

Proposition 14 (Generalized Riemann invariants for the contact discontinuity associated with eigenvalue $\lambda_5 = u \neq 0$ (Case 1 and Case 2 of Figure 1)). *Across the stationary contact discontinuity associated with eigenvalue $\lambda_5 = u \neq 0$ the following relations hold*

$$A = const, \quad Au = const, \quad K = const, \quad A_0 = const, \\ p_e = const.$$

Proof. Applying the aforementioned generalized Riemann invariants method [38, 41], we obtain

$$\frac{dA}{0} = \frac{d(Au)}{0} = \frac{dK}{0} = \frac{dA_0}{0} = \frac{dp_e}{0} = \frac{d(A\phi)}{1},$$

from which the statement is straightforward. □

Proposition 15 (Jump conditions across the stationary contact discontinuities associated with eigenvalues $\lambda_2 = \lambda_3 = \lambda_4 = \lambda_5 = 0$ (Case 3 of Figure 1)). *Across the stationary contact discontinuities associated with eigenvalues $\lambda_2 = \lambda_3 = \lambda_4 = \lambda_5 = 0$ the following relations hold*

$$Au = 0, \qquad \psi + p_e = const. \tag{B9}$$

Proof. This problem can again be solved by employing the aforementioned generalized Riemann invariants method with the approach presented in Spilimbergo et al. [42], already described in the Proof of Proposition 13, now applied to matrix $\mathbf{M}$ in (12) but considering $u = 0$ (the reason is the addition of the eigenvalue $\lambda_5 = u = 0$), that is,

$$\tilde{\mathbf{M}}(\mathbf{Q}) = \begin{bmatrix} 0 & 1 & 0 & 0 & 0 & 0 \\ c^2 & 0 & \frac{A}{\rho}\psi_K & \frac{A}{\rho}\psi_{A_0} & \frac{A}{\rho} & 0 \\ 0 & 0 & 0 & 0 & 0 & 0 \\ 0 & 0 & 0 & 0 & 0 & 0 \\ 0 & 0 & 0 & 0 & 0 & 0 \\ 0 & \phi & 0 & 0 & 0 & 0 \end{bmatrix}.$$

It follows that for an arbitrary right eigenvector $\mathbf{R}$

$$\tilde{\mathbf{M}}\mathbf{R} = \lambda\mathbf{R},$$

which gives the algebraic system

$$\begin{cases} r_2 = \lambda r_1, \\ c^2 r_1 + \frac{A}{\rho}\psi_K r_3 + \frac{A}{\rho}\psi_{A_0} r_4 + \frac{A}{\rho} r_5 = \lambda r_2, \\ 0 = \lambda r_3, \\ 0 = \lambda r_4, \\ 0 = \lambda r_5, \\ \phi r_2 = \lambda r_6. \end{cases} \tag{B10}$$

Substituting $\lambda = 0$ in (B10), we first notice that $r_2 = 0$. After this latter substitution, system (B10) becomes

$$\begin{cases} r_2 = 0, \\ c^2 r_1 + \frac{A}{\rho}\psi_K r_3 + \frac{A}{\rho}\psi_{A_0} r_4 + \frac{A}{\rho} r_5 = 0, \\ 0 = 0, \\ 0 = 0, \\ 0 = 0, \\ 0 = 0. \end{cases} \tag{B11}$$

From the second equation of (B11) we can compute the value of one among r_1, r_3, r_4 and r_5 in terms of the others. Subsequently, we have four identities $0 = 0$, from which no information can be deduced. In this computation, by means of the second equation of system (B11), we will determine the value of r_5 with respect to r_1, r_3 and r_4, while these latter values

and also the value of r_6 will be assigned arbitrarily. By setting $r_1 = \beta$, $r_3 = \gamma$, $r_4 = \epsilon$, $r_6 = \delta$, for $\beta, \gamma, \epsilon, \delta \in \mathbb{R}$, arbitrary constants, we obtain

$$\mathbf{R}_0 = \begin{bmatrix} \beta \\ 0 \\ \gamma \\ \epsilon \\ \left[-c^2\beta - \frac{A}{\rho}\psi_K\gamma - \frac{A}{\rho}\psi_{A_0}\epsilon\right]\frac{\rho}{A} \\ \delta \end{bmatrix}.$$

This is a general form of a vector belonging to the subspace associated with $\lambda = 0$ for every choice of $\beta, \gamma, \epsilon, \delta, \in \mathbb{R}$. We then apply the generalized Riemann invariants method to this vector

$$\frac{dA}{\beta} = \frac{d(Au)}{0} = \frac{dK}{\gamma} = \frac{dA_0}{\epsilon} = \\ = \frac{dp_e}{\left[-c^2\beta - \frac{A}{\rho}\psi_K\gamma - \frac{A}{\rho}\psi_{A_0}\epsilon\right]\frac{\rho}{A}} = \frac{d(A\phi)}{\delta}. \tag{B12}$$

From the second term of (B12)

$$Au = const,$$

that considering $u = 0$, becomes

$$Au = 0.$$

From the equality between the first and the fifth terms of (B12) we obtain

$$\frac{dA}{\beta} = \frac{dp_e}{\left[-c^2\beta - \frac{A}{\rho}\psi_K\gamma - \frac{A}{\rho}\psi_{A_0}\epsilon\right]\frac{\rho}{A}},$$

that becomes

$$-c^2\frac{\rho}{A}dA - \psi_K\frac{\gamma}{\beta}dA - \psi_{A_0}\frac{\epsilon}{\beta}dA = dp_e. \tag{B13}$$

Considering the first and the third terms of (B12) coupled together and then the first and the fourth terms of (B12), we have that

$$\gamma dA = \beta dK, \quad \epsilon dA = \beta dA_0,$$

being c as in (13), we obtain

$$-c^2\frac{\rho}{A}dA = -\psi_A dA,$$

so (B13) becomes

$$-\psi_A dA - \psi_K dK - \psi_{A_0}dA_0 - dp_e = 0. \tag{B14}$$

Considering that

$$d\psi = \psi_A dA + \psi_K dK + \psi_{A_0}dA_0,$$

(B14) becomes

$$-d\psi - dp_e = 0,$$

from that, integrating, we obtain the second of (B9). From the equality between the first and the sixth terms of (B12)

$$\frac{dA}{\beta} = \frac{d(A\phi)}{\delta}, \tag{B15}$$

that leads to

$$\frac{dA}{A} = \left(\frac{\beta}{\delta - \beta\phi}\right)d\phi. \tag{B16}$$

β and δ are arbitrary, so from (B15) and (B16) the only consequence is that

$$A\phi \neq const, \qquad A \neq const, \qquad \phi \neq const.$$

□

Appendix C

Newton–Raphson Method

Here we present the Newton–Raphson method used to solve (42). The others are similar in structure, with the same tolerances. This method is written in Python language (Algorithm 1).

ALGORITHM 1 | The Newton–Raphson method to solve (42).

```
#initial values
Xstar=np.zeros(4)
Xstar[0]=aL
Xstar[1]=qL
Xstar[2]=aR
Xstar[3]=qR

for i in range(50):
    #fun=[f1,f2,f3,f4] is described in (42)
    fun=self.FuncStar(Xstar,QL,QR)
    #jf is the jacobian of fun
    jf=self.JacobFuncStar(Xstar,QL,QR)

    alpha = 1.
    for i2 in range(50):
        XstarA= Xstar - alpha*(scipy.linalg.
          solve(jf,fun))
        if XstarA[0]>0 and XstarA[2]>0:
            fAux=self.FuncStar(XstarA,QL,QR)
            if  (np.linalg.norm(fAux,np.inf)
              <np.linalg.norm(fun,np.inf)):
                break
            else:
                alpha *= 0.8
        else:
            alpha *= 0.8
    XstarOld= np.copy(Xstar)
    Xstar= Xstar  - alpha*(scipy.linalg.
      solve(jf,fun))
    if (np.abs(Xstar[0]-XstarOld[0])/
      ((Xstar[0]+XstarOld[0])/2.))<1e-6 and
    (np.abs(Xstar[2]-XstarOld[2])/((Xstar[2]
      +XstarOld[2])/2.))<1e-6:
        break
    if i==(49):
        print('Newton does not converge')
        exit(-1)
aSL=Xstar[0]
qSL=Xstar[1]
aSR=Xstar[2]
qSR=Xstar[3]
```